UNIVERSITA' DEGLI STUDI DI PADOVA

Dipartimento di Ingegneria Industriale DII

Corso di Laurea Magistrale in Ingegneria dell'Energia Elettrica

Titolo tesi

Space Vector Modulation applied to a split phase winding of a PMSM

Relatore:

Henk Huisman - Eindhoven University of Technology

Bolognani Silverio – Università degli Studi di Padova

Studente con matricola:

Andrea Martinello 1160020

Anno Accademico 2018/2019

Contents

Glossary

AC	alternating current. 8
AEV	all electric vehicles. 19
BEV	battery electric vehicles. 19
DC	direct current. 8
DOH	degree of hybridization. 10
EMF	electromotive force. 5
EPE	electromechanics and power electronics. 30
EV	electric vehicle. 5
HEV	hybrid electric vehicle. 9
ICE	internal combustion engine. 5
IPMSM	interior permanent magnet synchronous motor. 24
MMF	magnetomotive force. 28
MTPA	max torque per amper. 27
MTPV	maximum torque per volts. 31
PEV	plug-in electric vehicles. 19
PF	power factor. 34
PHEV	plug-in hybrid electric vehicles. 19
PM	permanent magnet. 8
PMS	power management strategies. 11
PMSM	permanent magnet synchronous motor. 24
PWM	pulse width modulation. 49
RMS	root mean square. 34
SOC	state of charge. 17
SPMSM	surface permanent magnet synchronous motor. 24
SVM	space vector modulation. 45
V2G	vehicle to grid. 8

Chapter 1

Introduction

1.1 Past, present, and future of electric vehicle

In recent years, more and more people have been hearing about hybrid and electric vehicles, always seen as an innovative and clean technology. Let's start by saying that it is not an invention of recent years, far from it. Actually, the idea of the electric car was born even before that of the internal combustion engine (ICE). In 1821, the British scientist, Michael Faraday concluded an experiment with which he proved one of the fundamental laws of electromagnetism that is how a magnetic field interacts with an electric circuit to produce an electromotive force (EMF), a phenomenon called electromagnetic induction. It is the fundamental operating principle of transformers, electrical motors, generators, inductors and solenoids. It seem that the first electric vehicle (EV) was built by a Hungarian engineer in 1828, such Ányos Jedlik, but it was little more than a prototype. In the same period the first electric locomotives were being studied but they had the same problem of the electric vehicles: the low autonomy. If in the railways the question was resolved brilliantly with the idea of the overhead contact lines, for the car there were no appreciable solutions, with the consequent spread of the ICE.

During the XIXth century many attempts were made and many car manufacturers devoted themselves to the development of an electric car, especially in the United States. However, the idea was soon abandoned, first of all because of the reduction of the fuel cost, since in those years large oil fields were discovered in Texas; second of all significant improvements were introduced for the ICE such as electric starter, water-cooling, clutch, and gear-shift system.

Nowadays the situation is changed and the world outlook is catastrophic to say the least, both with regard to the enormous demand for primary fuel that will exhaust the reserves which are already widely used with the technological progress since the industrial revolution, both for the alarming and worrying increase in polluting emissions and carbon dioxide which causes global warming. Some people think that global warming causes only phenomena such as heat waves, droughts, wildfires, but in general it causes more frequent extreme weather events that depend from region to region, so we also find hurricane, heavy rainfall with floods, and heavy snowfall. All this will change the earth's climate irreparably and there will be a massive extinction of plant and animal species. The largest source of greenhouse gas emissions from human activities in the world is from burning fossil fuels mainly for electricity, heat, and transportation as shown in Figure 1.1. When allocating emissions from electricity to consuming sectors, industry was the largest emitter followed by buildings, whose share increased from 8%

to 27% due to its strong reliance on electricity, and then transport with almost the 25%.

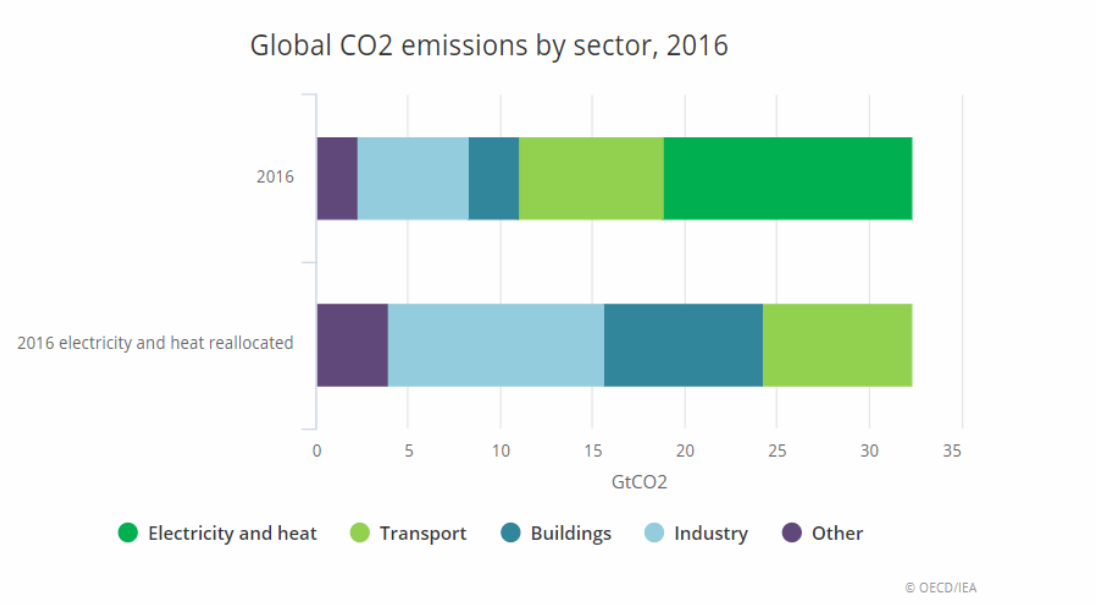

Figure 1.1: *Carbon dioxide emissions by sector in 2016* [1].

Emissions from transportation primarily come from burning fossil fuel for our cars, trucks, ships, trains, and planes, Figure 1.2. Over 90 percent of the fuel used for transportation is petroleum based, which includes gasoline and diesel.

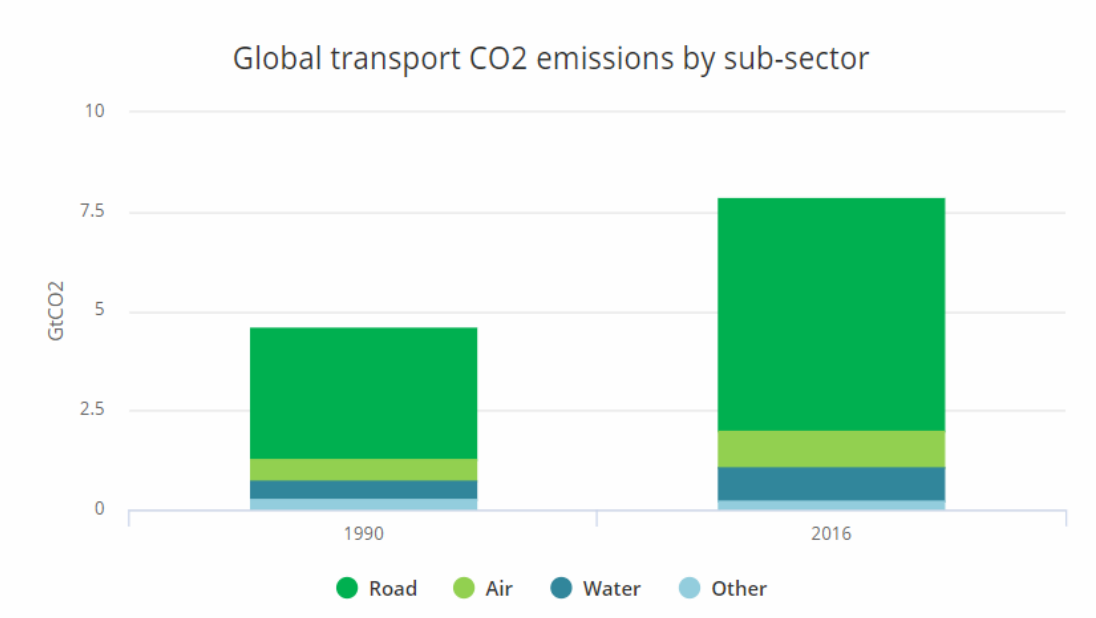

Figure 1.2: *Distribution of carbon dioxide emissions produced by transport sector* [1].

From these two figures we understand why it so important to gradually replace traditional vehicles with the electric ones, to reduce the(CO_2) emission. Obviously with the introduction of EV the emission of CO_2 won't become zero because the electricity must still be produced but will move the problem of pollution from densely populated

areas like cities to uninhabited ones. Moreover, we have to consider that electric motors have a higher efficiency compared to the ICE and that part of energy can be produced by renewable sources. In addiction to carbon dioxide, an ICE produces carbon monoxide (CO), nitrous oxides (NO_x), sulphur dioxide (SO_2), particulate matter (PM), and volatile organic compounds (VOC) [2]. CO inhibits the ability of the blood to carry oxygen, for this reason it is particular dangerous for people with heart disease. Moreover if it is inhaled in large quantities it causes permanent damage to the nervous system. NO_x reacts with ammonia, moisture, and other compounds to form nitric acid vapor that can penetrate deeply into the lung and damage it. Inhalation of NO_x increases the risk of lung cancer and can worsen respiratory diseases such as asthma, emphysema and bronchitis. In the presence of VOCs and sunlight NO_x reacts to produce ground level ozone and finally SO_2 emissions are a precursor to acid rain and atmospheric particulates that can influence the habitat suitability for plant communities, as well as animal life.

This issue has been addressed by world powers as a topic for the protection of our planet (November 2015, Paris), pushing car manufacturers to an exponential production of hybrid and electric cars, whose sales of its products is exptected to increase from now until 2030 as shown in Figure 1.3. Regulations will force and incentive producers to build and consumers to switch toward electrification over time, at least in China and Europe. In Europe, various countries are determined to phase out traditional combustion engines (diesel and gasoline), the UK and France from 2040, Norway potentially from 2025, and Germany from 2030-2040 [1], US will seek to meet regulatory requirements reducing from the current 95% to 66% by 2025.

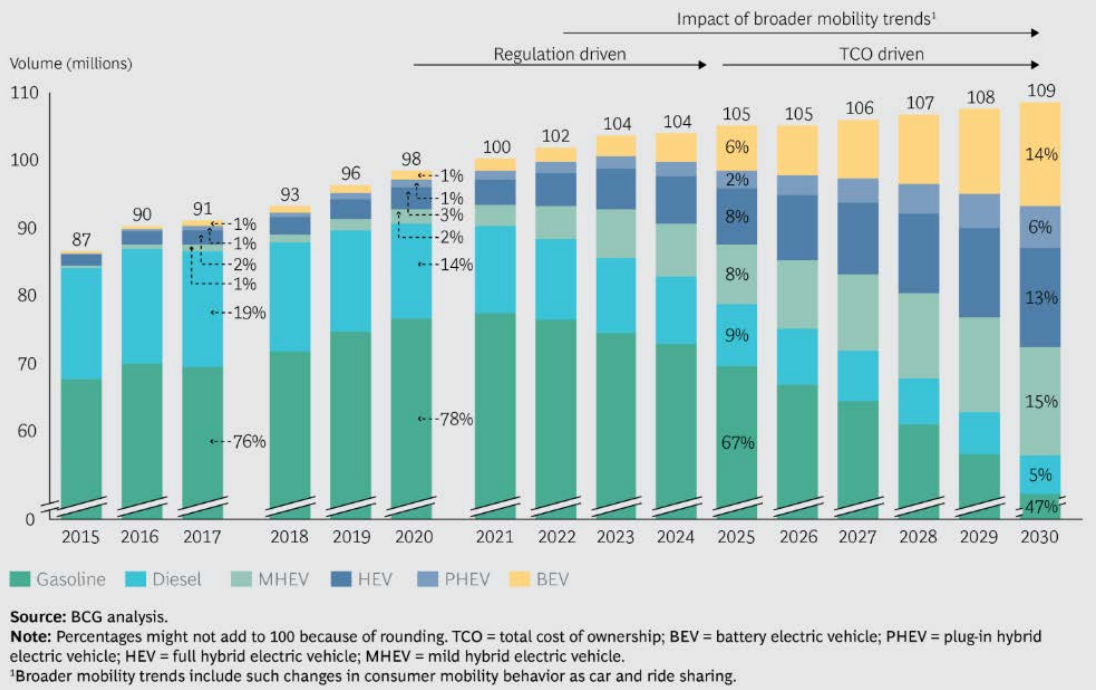

Figure 1.3: *Sales forecast of* EV *by 2030* [3].

As can be seen from the figure, traditional vehicles are not going to disappear (or even decline in importance) anytime soon as the majority of the road vehicles will also have an ICE. The outlooks indicate that pure ICE vehicles to decline in share from their current 95 percent of the global market to less than 50 percent by 2030. The trend for

each national and regional market (the US, Japan, Europe, and China, for instance) will be in the same direction, but the evolving mix of the traditional, hybrid, and electric vehicles will vary according to the relative cost of gasoline and electric energy, the number of kilometers that consumers drive in each region, and local regulations and incentives. Currently EV's cost isn't comparable to the cost of a traditional car mainly due to batteries' cost, so there is only a niche market based on supercars and high efficiency city cars, consequently it is very important to have government incentives. In fact, in 2016 after that Denmark and Netherlands cut them off there was a drastic decrease in sales.

There are several factors that must be developed for the electric car to succeed in the market, but the aspect that needs to be better defined is that of standardization of the charging and the interfaces, so as to allow the driver to be able to connect his/her car at any charge point. An e-boom could also pose a tough challenge for the existing electricity infrastructure and grids to handle, especially in countries using more electricity from renewable sources. Most national grids are currently ill equipped to handle a wider use of battery-powered vehicles and many countries lack the proper infrastructure to support recharging. Most countries in Europe have only a few thousand public charging point and they are mostly only slow-charging sources, which allow vehicle charging using common household lower voltage alternating current (AC) sockets and cables. Fast charging sources, on the other hand, deliver higher voltage direct current (DC), allowing for much quicker charging. However, this is more costly and more electricity is lost during charging [4]. A network of 120 kW charging poles, capable of recharging 50% of the model S battery in 20 minutes, is currently being installed by TESLA MOTORS in Asia, North America, and Europe [5]. With the introduction of millions of EVs in the market it will be possible to use batteries as storage elements to provide services to the network, the national grid will be able to draw power from car batteries at peak times as a way of balancing supply and demand, and at the same time, ensuring that the cars are fully recharged by the morning [4], bidirectional interaction between vehicle and network is called: vehicle to grid (V2G)

1.2 Electric and hybrid vehicles

EVs use one or more electric motors for propulsion, and an onboard electricity storage system as a source of energy.
The three main components of an electric car are: electric motor, controller and battery as shown in Figure 1.4. Nowadays three different types of electric motor are used in the market: DC brushless with top speed, AC induction with the best acceleration and permanent magnet (PM) motor . The controller takes power from the battery and passes it on the electric motor. The current is converted from the DC of the battery to AC, which is necessary to feed the motor. Battery aren't used only to power vehicles but also used for the functioning of wipers, light, ventilation, etc...

Electric cars look precisely like other normal vehicles outward, but for the lack of an exhaust system. However inward they are very different from each other [7]. They have apparently zero emission of pollutants, but they have been criticized as limited in range and of less environmental benefit than claimed. EVs are more efficient than traditional vehicle for several reasons:

1. the electric motor is directly connected to the wheels, so it consumes no energy while the car is at rest or coasting;

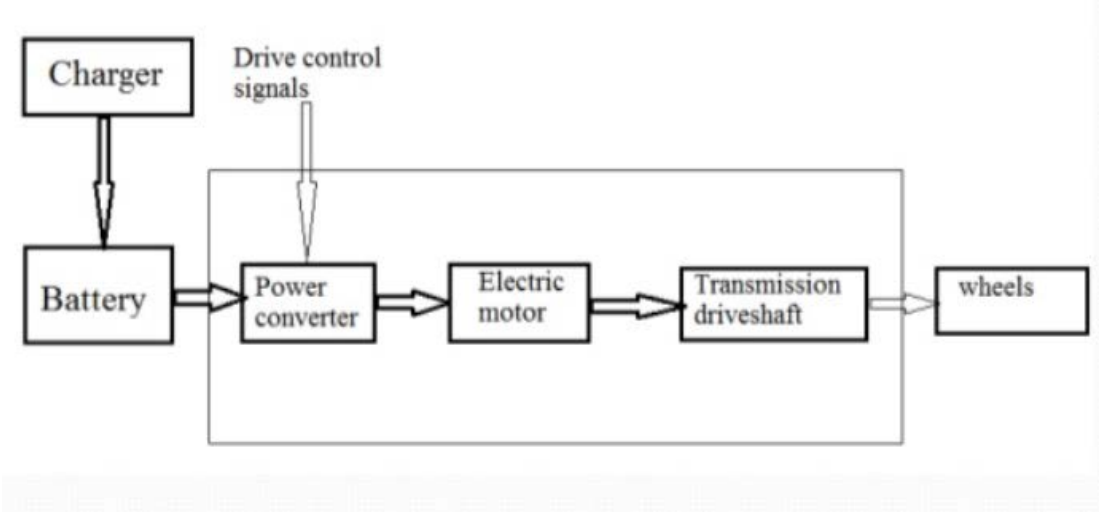

Figure 1.4: *Main components of an electric vehicle* [6].

2. part of the energy can be recovered by a regenerative braking system[1], a number of Tesla drivers have reported data using different data tracking apps. Model S drivers have reported recapturing as much as 32% of their total energy use while driving up and down downhill [8];

3. electric motors convert approximately 90% of the energy from the battery to mechanical energy while ICEs convert at most 33% of the chemical energy into mechanical energy;

4. significantly increased reliability of the electrical components compared to the mechanical ones, reduction of maintenance;

5. electric motors can be accurately controlled and provide high torque from rest, unlike internal combustion engines, and don't need multiple gears to match power curves, this means that gearboxes and torque converters are removed.

Nowadays the world is not ready yet for a diffusion of pure electric vehicles but we are witnessing the transition to hybrid electric vehicle (HEV). In general a hybrid vehicle is a vehicle that uses two different energy sources, we focus on HEVs that combine a conventional ICE system with one or more electrical machines. The main difference between HEVs and EVs is that the first can work also without an external battery recharge system, so it can be independent of charging infrastructure. Currently HEVs are a good alternative because they allow not to give up the comforts normally attributed to normal cars (first of all autonomy) with an increase in cost not too high but with advantages from the point of view of emissions that can be significant. To give some value, we get an improvement in consumption of about 40% compared to a traditional vehicle with an increase in costs of about 15%. Hybrid power system were conceived as a way to compensate for the shortfall in battery technology. Because batteries could supply only enough energy for short trips, an onboard generator,

[1]With regenerative braking the motors act as generators, which recharge the batteries. With normal friction brakes, energy is lost in the form of heat created by friction from braking. In addition to improving the overall efficiency of the car, regeneration extends the life of the braking system as its parts don't wear out as quickly.

powered by an ICE, could be installed and used for longer trips. Hybrids carry a much smaller battery load than EV and are therefore lighter and cheaper [9].

There are different types of HEVs on the market, which differ in their structure and the impact that the electric motor, installed as assist to the ICE, has on functioning. They can be classified according to the degree of hybridization (DOH) or according to the type of architecture used.
DOH is define like:

$$h = \frac{P_{em}}{P_{em} + P_{ice}}$$

Where P_{em} is the power of the electric motor and P_{ice} is the power of the internal combustion engine. Depending on DOH, we can find two different types of HEV:

- **Mild hybrid** is a vehicle that cannot be driven solely on its electric motor, because the electric motor does not have enough power to proper vehicle on its own. A mild hybrid is essentially a conventional vehicle with oversize starter motor, allowing the engine to be turned off whenever the car is coasting, braking, or stopped, yet restart quickly and cleanly. Accessories can continue to run on electrical power while the gasoline engine is off, and as in other hybrid design, the motor is used for regenerative braking [10]. As compared to full hybrids, mild hybrids have smaller batteries and a smaller, weaker motor/generator, which allows manufacturers to reduce cost and weight.

- **Full hybrid** is a vehicle in which there is a small power ICE, compared to the overall power of the car, which is used to increase the autonomy of the vehicle. In addition there is an electrical system that allows, regardless of the autonomy of the batteries, to cover the entire route. These vehicles have a split power path allowing greater flexibility in the drive train by interconnecting mechanical and electrical power, at some cost in complexity [11].

There are no existing rules that identify precisely this subdivision, so this type of classification is currently discussed, we prefer to classify HEVs based on their architecture: series, parallel, or series-parallel (power split). This subdivision is made according to the way in which power is supplied to the drivetrain: there are two macro blocks that constitute the HEV: *gen-set* and *trac-set*. If the two macro blocks are in the same shaft (single shaft) we have the series configuration while if they are in two different shafts (double shaft) we have the parallel configuration. *Gen-set* is made up by ICE, generator and charger while the *trac-set* is made up by converter, electric motor, and transmission. It is possible that some components are not present for instance the electric motor can also work as a generator and if we use a bidirectional converter this can also play the role of the charger.

- **Series:** the main advantage of this configuration lies in the fact that the ICE is not mechanically connected to the driving wheels, this isolates the engine from demand, allowing it to operate at the point of maximum efficiency or at the curve of high efficiency. The entire mechanical transmission between the ICE and the wheels is removed, (they have no clutch and gearbox) and replaced by an electric generator, some cable and controls, and electric traction motors as shown in Figure 1.5. The ICE and also the generator can be sized to deliver the average value of the traction power, for the net energy balance of the battery to be null,

a lower size of the ICE means lower losses in the engine. The motor, instead, is sized for the peak value of the traction power that may be appreciably higher than the average value.

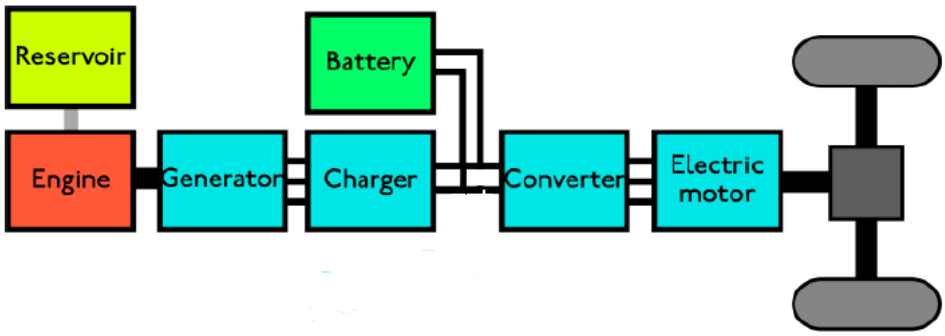

Figure 1.5: *Structure of a series-hybrid vehicle* [12].

Typically mechanical transmissions impose many penalties, including weight, bulk, noise, cost, complexity and a drain on engine power with every gear-change, on the other hand the energy produced by the engine undergoes many transformations: it starts as chemistry, mechanical, electrical (AC), electrical (DC), electrical (AC), and finally it arrives at the wheels. So even if the engine works at maximum efficiency, it is not so obvious that the overall yield is high.

There are two different power management strategies (PMS) which can be adopted for this configuration: the first consists in switching the ICE to charge the battery when it is depleted; otherwise it is off. When on, part of the ICE power goes to charge the battery, part to propel the vehicle. The ICE is operated at the point of maximum efficiency as shown in Figure 1.6.

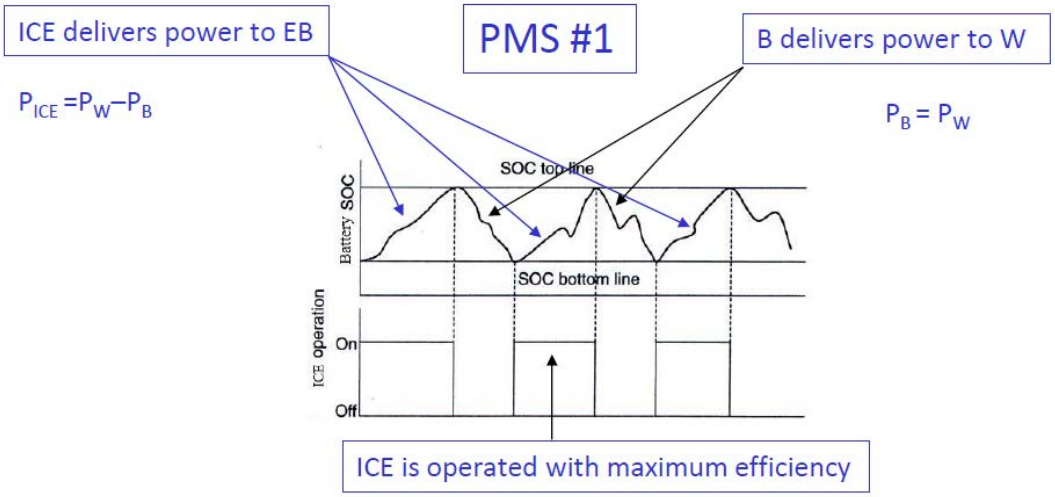

Figure 1.6: *First power management strategies* [13].

In the second PMS, the ICE is kept always on and delivers a constant power equal to the average traction power demand while the deficit/surplus power is provided by the battery. In this way it can be possible to reduce the size of the battery

and also costs. The ICE is operated at constant torque to get high efficiency, this process is also used for the parallel architecture.

In conclusion this configuration is not much used due to the costs, its needs of two electric machines (motor and generator) and a normal engine, in addition there is a somewhat large battery. It is suited for mid-heavy vehicles mainly travelling in urban areas, where the benefits of the full decoupling of the ICE from the wheels overcome the inconvenience of the multiple losses the various energy due to conversions. The series configuration has been applied to buses dedicated to the urban service within wide areas.

- **Parallel:** this configuration is obviously more used than the series one because it has only one electric machine sized to the average power and not to the peak power as in the previous case, and also the battery is smaller. However here, there is a mechanical connection between the engine and the wheels as shown in Figure 1.7, so the ICE can run only on a curve of high efficiency and not always at the maximum efficiency. Parallel hybrids can be categorized by the balance between the different motors which are providing motive power: the ICE may be dominant (engaging the electric motor only in specific circumstances) or vice versa, anyway current parallel hybrids are unable to provide electric-only or internal combustion-only modes. The ICE is sized to the averaged power and it has a smaller size compared to the engine of a normal vehicle that is sized for the peak power, but it is bigger than the ICE of a series configuration.

  The parallel architecture is suited for mid-light size vehicles travelling, they rely more on regenerative braking and the ICE can also act as a generator for supplemental recharging. They are used mainly on city roads where the powertrain is subjected to many acceleration and braking events and also along extra-urban routes, where the traction power varies in moderate ranges so that the engine can be run within or nearby its operating region.

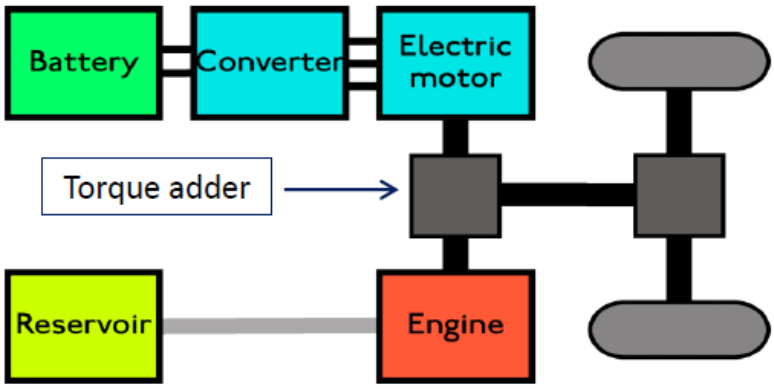

Figure 1.7: *Structure of a parallel-hybrid vehicle* [12].

- **Series-parallel**: This architecture, also called power split, has the benefits of a combination of series and parallel characteristics: overcomes both the limitations of the series configuration (no direct propelling of the vehicle from ICE), thus improving the efficiency; and the limitations of the parallel configuration (no fixed speed operation of ICE), which can be run at the optimal values of both

torque and speed in any driving condition. As a result, it is more efficient overall, because series hybrid tend to be more efficient at lower speeds and parallel tend to be more efficient at high speeds [11]. This vehicle is similar to a parallel hybrid but it incorporates two coupling devices: one is a power splitter that allows for power paths from the engine to the wheels that can be either electrical or mechanical; and one is a torque adder. In addition it has two electric machines like a series hybrid (one operates as a generator and the other one as a motor) as shown in Figure 1.8.

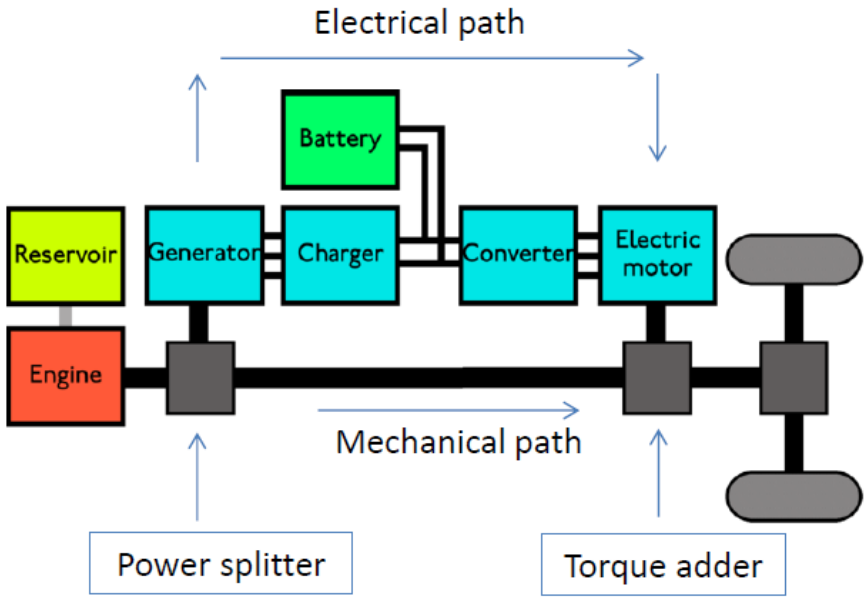

Figure 1.8: *Structure of a series-parallel hybrid vehicle* [12].

1.3 Longitudinal vehicle acceleration

The fundamentals of vehicle design involve the basic principles of physics, in particular Newton's second law, which describes what happens to a massive body when it is acted upon by an external force.

$$F = m\frac{dv}{dt} = ma \tag{1.1}$$

In a car several forces act on it and the resultant force governs the motion according to (1.1), the engine of the vehicle delivers the force necessary to move the vehicle forward. So it is important to understand which forces act on our car. When the car moves, it encounters resistive forces that try to retard its motion as shown in Figure 1.9.
The vehicle motion can be completely determined by analysing the forces acting on it in the direction of motion. The tractive force F_t in the contact area between the tires of the driven wheels and the road surface propels the vehicle forward. The tractive force is produced by the engine and transferred to the wheels by the transmission [15].

$$\text{Traction force:} \quad = \frac{1}{r_w}T_w \quad = \frac{1}{r_w}\eta_{gb}r_{gb}T_m \tag{1.2}$$

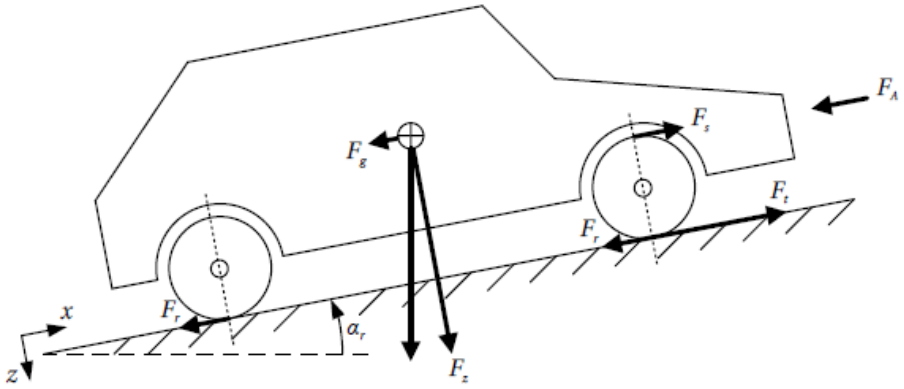

Figure 1.9: *Different forces that act on a vehicle* [14].

where T_w is the mechanical torque produced by the electrical machine, η_{gb} is the gearbox efficiency, r_{gb} is the gearbox ratio from the electrical machine to the wheel.

There are three types of traction resistance:

- Rolling resistance F_r
- Aerodynamic drag F_a
- Grading resistance F_g

The rolling resistance, sometimes called rolling friction or rolling drag, is the force resisting the motion when the wheel rolls on a surface. It is primary caused by the hysteretic deformation in the tire rubber. Factors that contribute to rolling resistance are the deformation of the wheels, the deformation of the roadbed surface, and movement below the surface. Additional contributing factors include wheel diameter, speed, load on wheel, surface adhesion, sliding, and relative micro-sliding between the surfaces of contact [16]. When the vehicle is stationary a force P is acting on the center of the wheel:

$$P = \frac{1}{4}gM \tag{1.3}$$

Where g is the gravity acceleration and M is the total mass of the vehicle pertinent to the wheel. The pressure in the contact patch between tire and ground is distributed symmetrically to the central line and the result ground reaction P_z is aligned to P, equal in magnitude and opposite in the direction as shown in Figure 1.10a. When the wheel is rolling, the leading half of the contact patch is loaded and the trailing half is unloaded. The presence of the hysteresis causes an asymmetric distribution of the ground reaction force as shown in Figure 1.10b. The pressure in the leading half of the contact area is larger than in the trailing half [17]. The two forces are not opposite like before, they have yet equal magnitude but they are applied on different points, as a result they create a torque called rolling resistance torque expressed as:

$$T_r = aP \tag{1.4}$$

where a is the distance between the forces and P is the normal load acting on the center of the wheel. The rolling resistance torque can be represented by a horizontal force

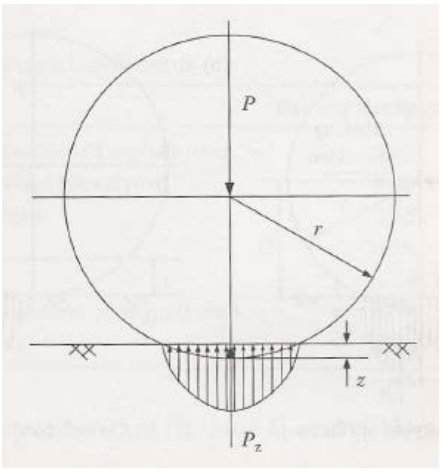

(a) *Weight distribution on a standstill tire*

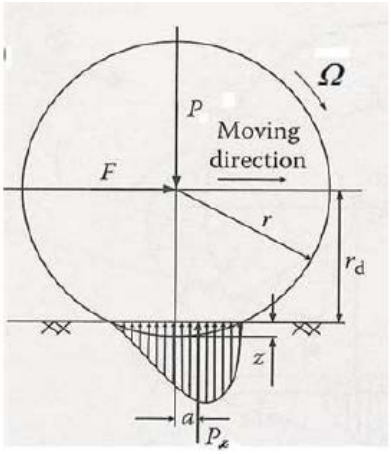

(b) *Weight distribution on a rolling tire*

Figure 1.10: *Difference in weight distribution on a vehicle* [13].

acting on the wheel center and opposing the wheel motion. The equivalent longitudinal force is called rolling resistance and has a magnitude of:

$$F_r = \frac{T_r}{r_w} = \frac{aP}{r_w} = f_r P \tag{1.5}$$

where f_r is called the rolling resistance coefficient. It depends on many variables: tread geometry, inflation pressure and material of the tire, roughness and material of the road, presence of liquids on the road and so on. For fuel saving, in recent years low-resistance tires for passenger cars have been developed with f_r less than 0.01, typical values on various roads are given in Table 1.1: The f_r varies with speed, the

Road condition	f_{ro}
Concrete or asphalt road	0.013
Rolled gravel road	0.02
Tar macadam road	0.025
Earth road	0.1-0.35

Table 1.1: *Rolling coefficient on various road* [13].

values in the table are valid for low speed. By experimental results, this coefficient is, with good approximation, a linear function of the speed. The following equation can be used for a passenger car on a concrete road, with acceptable accuracy for speeds up to 130 km/h:

$$f_r = f_{ro}\left(1 + \frac{V}{160}\right) \qquad \text{V in } km/h \tag{1.6}$$

Aerodynamic drag, or more simply air drag, is a force acting opposite to the relative motion of any object moving with respect to a surrounding fluid. This can exist between two fluid surfaces or a fluid and a solid surface as in our case. This force is formed by two components: skin friction and shape drag.
Air molecules close to the surface of the vehicle move almost at the same speed as the vehicle while air molecules away from the vehicle remain still. In between air molecules

move at intermediate values of speed. The difference in speed between two air molecules produces viscous friction and it is know as skin effect [13].
The second component is due to the shape of the vehicle. The forward motion of the car pushes the air in front of it resulting in a zone of high air pressure in front of the car. Correspondingly, the air behind the vehicle cannot immediately fill the space left by the forward motion of the vehicle, resulting in a zone of low air pressure at the back of the car. The resulting force is always directed from the region of higher pressure to the region of lower pressure, so it is in direction opposite to the movement. The name "shape" drag comes from the fact that this drag is completely determined by the shape of the vehicle body.
The aerodynamic drag is a function of the square of the speed:

$$F_w = \frac{1}{2}\rho A_d C_d \left(V - V_w\right)^2 \tag{1.7}$$

where ρ is the air density, A_f is the frontal area of the vehicle, C_d is the aerodynamic drag coefficient that characterizes the shape of the vehicle body, and V_w is the component of the wind speed along the vehicle moving direction. It has a positive sign when it is in the same direction as the moving vehicle and a negative sign when it is opposite to the vehicle speed.

Grading resistance is produced by the car's weight and it is always directed in the motion direction. This force either opposes to the forward motion (grade climbing) or helps the forward motion (grade descending). It is expressed as:

$$F_g = gM \sin\alpha \tag{1.8}$$

where α is the road angle.
The tractive efforts F_t are produced by the torque developed by the traction plant onboard the vehicle and are transferred through the transmission to the driven wheels. For the vehicle to move, the traction efforts must overcome the total traction resistance opposing the vehicle motion, given by the sum of three traction resistances:

$$F_{res} = F_r + F_w + F_g \tag{1.9}$$

According to (1.1), the vehicle acceleration can be written as:

$$\frac{dv}{dt} = \frac{F_t - F_{res}}{M_t} \tag{1.10}$$

where F_{res} is the total traction resistance and M_t is the total translational mass of the vehicle, which includes passengers, tank status and contribution of the translation equivalent mass of the inertias of the rotating elements (wheels):

$$E_k = \frac{1}{2}M_{eq}v^2 = \frac{1}{2}J\omega^2$$

$$M_{eq} = \frac{J}{r_w^2} \tag{1.11}$$

1.4 Battery

We have seen previously that the battery is one of the key components of electric and hybrid vehicles and it is the component with the highest cost, weight and volume.

Below will be given only a brief explanation about the batteries, more information can be found in [2]: battery consists of two or more electric cells joined together that convert chemical energy to electrical energy. The cells consist of positive and negative electrodes joined by an electrolyte. When connecting a load, the battery acts as an energy source and an electric current flows in the load connected to the battery terminals with the corresponding delivery of the stored chemical energy and the discharge of the battery. Delivery of chemical energy is due to a redox reaction that occurs spontaneously when a load is connected.
When connecting an electric energy source, the battery acts as a load and the current that is produced by the external source flows into the battery with a corresponding storage of chemical energy and the charging of the battery.

There are different types of batteries that are used in vehicles, at present these include lead acid, nickel iron, nickel cadmium, nickel metal hydride, lithium polymer and lithium iron, sodium sulphur and sodium metal chloride. There are also more recent developments of batteries that can be mechanically refuelled, the main ones being aluminium-air and zinc-air. Despite all the different possibilities tried, and about 150 years of development, a suitable battery which allows widespread use of electric vehicles (has still not yet been developed) [2]. However, there is an increased interest and activity, in the development of new electrochemical mechanisms, that may enhance the performance of future batteries, particularly among university research laboratories. From the electric vehicle designer's point of view the battery can be treated as a "black box", which is defined by some parameters to specify the performances and describe the operating condition, the most important are: efficiency, voltage (maximum, nominal, cut off), energy and power (specific and density), capacity, cost, self-discharge, commercial availability, life time and number of cycles, operating temperature and last but not least safety. Safety is one of the most important criterions for electric-car batteries especially for the health of the driver but not only, if there were a single battery fire, this could turn public opinion against electric mobility and slow down industry development for months or years. An increase of temperature could be caused by an overcharged battery, too high discharge rates or a short circuit. Therefore the vehicle needs a robust battery box with a very efficient cooling system to prevent the early stages of thermal runaway, precise state of charge (SOC) monitoring and cell discharge balancing. During normal use, overcharging is usually small and generates little hydrogen, which is very explosive, and it is dissipated very quickly trough a built in vent. When a battery is overcharged or when there is a short circuit, an explosive gas mixture of oxygen and hydrogen might be produced faster than it can escape from within the battery, leading to pressure build up and eventual to the explosion of the battery. Battery safety is indisputably a valid concern, it is useful to put this concern in context by recalling the significant safety challenges originally associated with ICE and with gasoline storage, which were largely overcome through improvements in design and engineering [18]. This basic knowledge is necessary both to understand the battery works and to understand the potential risks arising from a possible accident and the global impact of the use of battery chemicals on the environment. In fact, if electric cars will take hold in the next few years, we will have to face also the problem of battery disposal and recycling of used batteries will become increasingly important. In Europe the regulations, in addition to prohibiting[2] batteries containing a certain level

[2]Particular types of battery such as for military use of for space applications are excluded from the prohibition.

of mercury or cadmium, require precise methods of disposal. Recycling is just the last of the seven steps which made up the value chain of electric-car batteries:

- **Component production:** manufacture of anode and cathode active materials, binder, electrolyte, and separator.
- **Cell production:** production and assembly of single cells.
- **Module production:** configuration of cells into larger modules that include some electronic management.
- **Pack assembly:** installation of modules together with systems that manage power charging, and temperature.
- **Vehicle integration:** integration of the battery pack into the vehicle structure, including the battery car interface (plugs, connectors, mounts).
- **Use:** use during specified in vehicle battery lifetime.
- **Refuse and recycling:** battery reuse; deconstruction and cleaning preparatory recycling of material and component [18].

The first four steps are necessary because a single cell has low performance so many of them are connected in series to produce a reasonable voltage because when cells are connected in series, the battery voltage is the sum of the individual cell voltage while the capacity remains the same. Other ones are wired in parallel to reach the desired capacity because when they are connected in parallel the battery voltage is equal to the cell's voltage while the capacity is the sum of the cell's capacities. Traction batteries for electric or hybrid vehicles are usually specified as 6 V or 12 V but this voltage changes during operation. When the battery feeds a load, the voltage will drop while when the battery is being charged, the voltage will increase. The simplified equivalent circuit of a battery is showed Figure 1.11:

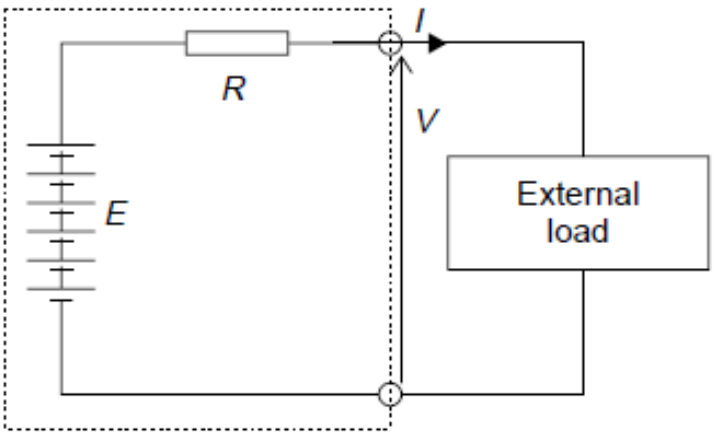

Figure 1.11: *Simplified equivalent circuit of battery composed of six cells* [2].

$$V = E - RI \tag{1.12}$$

where V is the terminal voltage, E is the EMF, R is the internal resistance and I the current delivered by the battery. In practice, E and R are not constant quantities

but depend on some parameters such as the SoC, the temperature and operating life. Generally (1.12) gives a fairly good prediction of the voltage. The E value can easily be determined by measuring the open circuit voltage while the measurement of the internal resistance requires an additional measure with a load connected to the battery. It is immediate to understand that the model of Figure 1.11 has little use for several reasons, including the fact that voltage E and internal resistance are constant. If a load is connected to the battery the voltage will immediately decrease to a lower value and this is not true because this variation takes time. Moreover, with this representation the battery has an infinite capacity and there is no way to obtain the SoC (problem common to many models). There are several ways to model a battery and these are done for several reasons for example many models are constructed to predict the effect of changing the thickness of the lead oxide layer of the negative electrodes of a sealed lead acid battery, other models make extensive use of fundamental physics and chemistry, other types are constructed to accurately predict the behaviour of a particular make and model of battery in different circumstances. However, all modelling of batteries is notoriously difficult and unreliable because they depend on parameters far harder to specify precisely, such as age and the way the battery has been used in the past [2]. In Figure 1.12 a possible battery model is proposed.

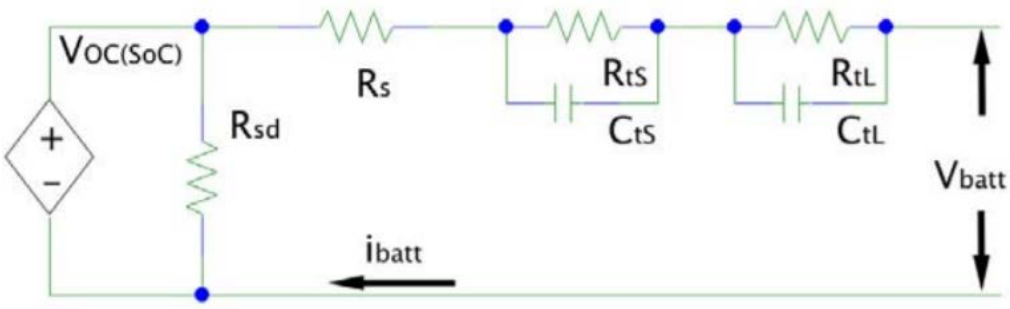

Figure 1.12: *Battery model*

Now in this model the battery's voltage (VOC) is a function of SoC, it has been inserted the resistance R_{sd} to take account of self-discharge, moreover RC networks have been added to simulate the response to transients.

To choose the right battery for a vehicle one must first choose the correct size according to the type of vehicle: vehicles that can charge their battery from the electricity grid are plug-in electric vehicles (PEV)s, a category that includes both plug-in hybrid electric vehicles (PHEV)s, of which we have already previously spoken, and all electric vehicles (AEV)s, also called battery electric vehicles (BEV)s. Then the designer will also need to decide on the specification and essential requirements of the vehicle. Is he/she, for example, designing the vehicle for speed, range, capital cost, running costs, overall costs, style, good handing, good aerodynamics, environmentally friendliness etc [2].
Of the batteries aforementioned, lithium ion (Li-ion) are too expensive, unless of course one is designing an electric racing car, with no expense spared, in which case this may be your first choice. For all other cases the choice narrows to lead acid, nickel metal hydride (NiMH) and sodium metal chloride. The lead acid battery is the most used battery in anything because it is not expensive, it performs reliably and it has a comparatively high voltage of about 2 V per cell. A factor to keep in mind is that this type of batteries

has an extremely low internal resistance, this mean that the drop in voltage is small. Lead acid batteries are the cheapest rechargeable batteries per kilowatt-hour of charge but they have a low specific energy so it is hard to see an AEV to use a lead acid battery, on the other hand they could be used in HEV which need only a limited amount of energy stored because they have an ICE. Currently, EVs are predominantly powered by either NiMH or Li-ion chemistry. A main advantage of NiMH batteries is that they can be recharged very quickly until 60% of the capacity in 20 mins but a cooling system is necessary making them more expensive than lead acid batteries. Of all the new battery systems NiMH is considered to be one of the most advanced and has been used in a range of vehicles including the Toyota Prius. The market volume of NiMH batteries is still small, but with quantity production the price will drop. The battery is considered to be one of the most promising for the future [2]. The alternative to NiMN are Li-ion batteries, they are very light and have a specific energy about three times greater than of lead acid batteries, this makes them an excellent choice for vehicles that require a high autonomy. NiMH is cheaper on a per-kWh basis than Li-ion, but Li-ion has higher energy density. Thus, NiMH is often used in HEV, while Li-ion is preferred in PEVs, where the battery capacity needs to be higher. Li-ion cells can be made with a variety of materials for the anode and cathode, with varying advantages in capacity, cycle life, safety, and cost [19], see Figure 1.13.

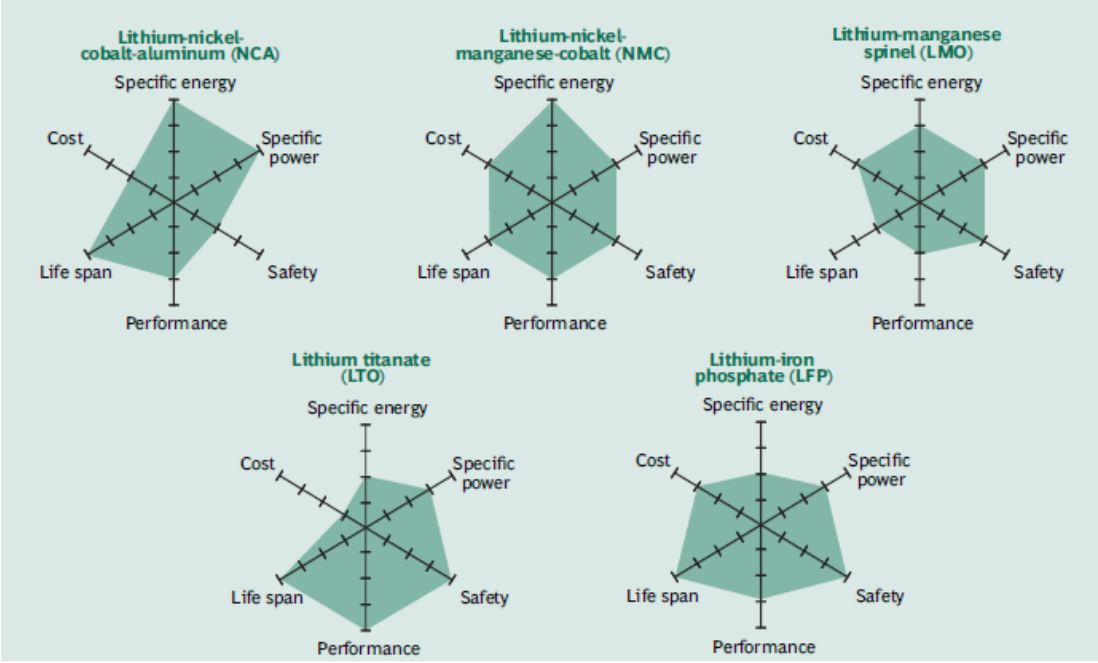

Figure 1.13: *Different types of Lithium ion batteries* [18].

In conclusion, for HEVs there are different types of batteries available and in recent years there have been massive improvements and several new developments are showing considerable promise. Nevertheless the specific energy of batteries, with the possible exception of zinc-air, is still extremely low see Table 3.1. There are no batteries that currently show signs of enabling pure electric vehicle to compete in both versatility and long range use with ICE vehicles [2]. However battery costs will decline steeply as production volumes increase. Individual parts will become less expensive thanks to experience and scale effects. Higher level of automation will further trim costs by increasing quality, reducing scrap levels, and cutting labor costs [18]. The production

related cost (excluding raw materials) could be reduced by 20% to 35% of each to the major steps in battery cell production. Currently about 25% of the battery costs are due to the cost of raw material and standard, which are independent of production volumes and expected to change modestly over time. AEVs will use Li-ion batteries, as will some 70% of the HEVs, the smaller and lower cost cars, will still have NiMN batteries popularized by first generation hybrid vehicle, such as Toyota Prius. On the basis of current estimates, the price of a battery pack for a midsize car will range from $7,600 to $10,700 in 2021. In this scenario, the price differential between BEVs and ICE vehicles in this category will decline to less than $5,000. BEVs would thus become cost competitive with ICE vehicles, especially considering tax incentives for the purchase of BEVs [20].

Battery type	Specifi c energy $Wh.kg^{-1}$	Battery mass kg, 75 km range	Battery mass kg, 150 km range	Battery mass kg, 225 km range	Battery mass kg, 300 km range
Lead acid	30	750	1500	2250	3000
NiMH	65	346	692	1038	1385
Li ion	90	250	500	750	1000
NaNiCl	100	225	450	675	900
Zn-Air	230	98	196	293	391

Table 1.2: *Example of distance travelled/battery weight for a typical car* [2].

Chapter 2

PMSM control

2.1 Split phase winding PMSM

When designing an EV the main objective of the designer is to maximize the autonomy of the vehicle according to a given battery size. This objective can be divided into two main points:

1. Minimize the energy required by the vehicle for a given driving cycle. An estimate of this energy can be given using the ECE15 cycle, which is used in Europe for the certification of the emissions of the light-duty vehicles in an urban environment. The speed along the cycle has been limited to 45km/h which is the maximum speed allowed by the rules for a city car [21]. The calculation of electric power demand along the ECE15 cycle, but it is valid in general for a given driven cycle, goes through the calculation of mechanical power that it can easy compute using (1.10) and the speed:

   $$P_m = Fv$$

   The profile of the electrical power demand P_e is compute by the following equation:

   $$P_e = \begin{cases} \dfrac{P_m}{\eta_t} + P_{aux} & \text{if } P_m > 0 \\ P_m \eta_b + P_{aux} & \text{if } P_m < 0 \end{cases} \tag{2.1}$$

   where η_t is the traction system efficiency, η_b is the regenerative braking efficiency and P_{aux} is the consumption of the electric auxiliaries of the vehicle such as lights, fan and so on. To get the electric energy, we need only to integrate the electric power:

   $$W_e = \int P_e dt \tag{2.2}$$

   Once the energy is known, it is also possible to estimate the car's autonomy, just discharge the battery using the profile just obtained.

2. Maximize the efficiency with which chemical energy(battery) is converted into mechanical (vehicle motion). The general issue in drive design for vehicle propulsion is the contradiction between the necessary low speed and high torque at the wheels and the arising high machine currents and resulting drive losses. This problem can be solved by means of a high gear ratio transmission to reduce the

torque requirement, but it additionally incorporates mechanical losses reducing the solution effectiveness [14].

In this thesis, an innovative approach is presented, an electric drive system which combines multiple torque versus angular velocity characteristics, in this way an electrical gearbox is obtained without having the disadvantages of the mechanical one: the weight of the machine is reduced, improve the reliability and the redundancy of the system, and there is an increase of efficiency. In order to do this a multi phase electrical machine is used which is fed by two full bridge inverter. During operation the configuration of the two inverters is varied as a function of the motor angular speed.

The electrical machine used is a permanent magnet synchronous motor (PMSM). Let's start with explaining what a PMSM is and how it works and then go into the details of our machine. The operating principle on which they are based is the same that we find in other electrical machines that is, the electromechanical conversion of energy. It is evident from the name itself, it has constructive and operating characteristics very similar to the normal synchronous motors with excitation winding. The characteristic that distinguishes them from ordinary machines is the fact that they have permanent magnet (PM) of hard ferromagnetic material that have a large hysteresis cycle and high residual magnetization, this property remains only below a certain temperature, called Curie temperature, above which the material behaves like a paramagnetic material. The electromechanical conversion occurs through to the interaction of the magnetic fields produced respectively by the PM and by the current flowing in the conductors, they are inside the stator slots and create a torque that bring into rotation the rotor, as in normal induction motors. This type of machine has a synchronous type of operation: their rotation speed depends on the electric frequency, in this thesis we will always refer to the motor operation, so there will be an electric input power and a mechanical output power. PM motors are increasingly used in the industrial field and are mainly intended for high performance drives, in which the particular design specifications justify their cost, high due to the presence of rare earth-based magnets, the most widespread are the Neodymium-Iron-Boron and the Samarium-Cobalt. There are two main types of PM motor as shown in Figure 2.1: surface permanent magnet synchronous motor (SPMSM) has the PM placed on the outer surface of the rotor, like the one used in the thesis, and interior permanent magnet synchronous motor (IPMSM), which has PM placed inside the rotor. We will not go into detail about the differences between these two configurations, but from the quick description just given you can immediately understand that SPMSM will be subject to more centrifugal forces that will tend to tear off the magnets from the rotor surface; while IPMSM, in addition to greater constructive complexity, it presents the problem of heat dissipation, therefore cooling channels are required. We will focus only on SPMSM motor and for the explanation it is supposed to have a model with linear behavior so saturation, temperature, and rotor position related parameter dependency are not taken into account. Generally, SPMSM motor have stator windings without a neutral wire, in this way the hypothesis of having at any moment the sum of the phase currents equal to zero verified:

$$i_a(t) + i_b(t) + i_c(t) = 0 \quad \forall t \tag{2.3}$$

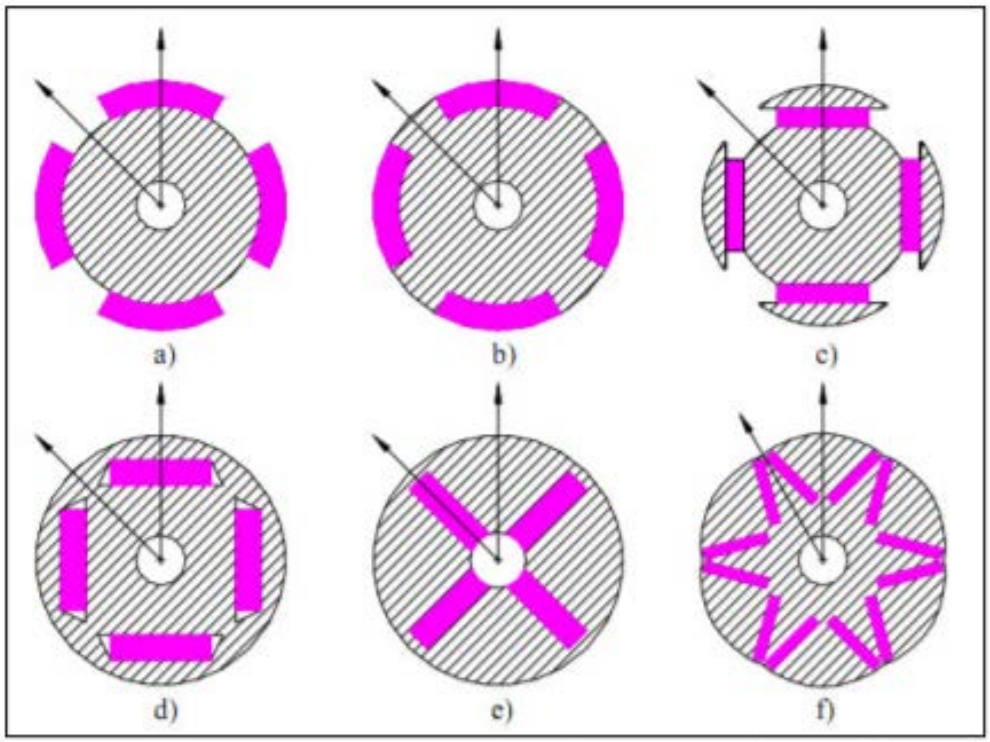

Figure 2.1: *Arrangement of magnets in radial flux machines* [22].

With the assumption made, the problem to be studied becomes linear and it is possible to apply the superposition principle, separating the contributions of the flux linkage, one due to the magnets (2.4) and the other due to the currents (2.5).

$$\begin{cases} \lambda_{a,pm} = \Lambda_{pm} cos(\theta_{me}) \\ \lambda_{b,pm} = \Lambda_{pm} cos(\theta_{me} - \frac{2\pi}{3}) \\ \lambda_{c,pm} = \Lambda_{pm} cos(\theta_{me} - \frac{4\pi}{3}) \end{cases} \tag{2.4}$$

where Λ_{pm} is the maximum flux linkage with each phase and Θ_{me} is the electrical angle[1] between the a-phase axis and the rotor position.

$$\begin{cases} \lambda_{a,i} = Li_a(t) \\ \lambda_{b,i} = Li_b(t) \\ \lambda_{c,i} = Li_c(t) \end{cases} \tag{2.5}$$

where L is defined as synchronous inductances: $L = L_{ss} + |L_M|$, L_{ss} is the self inductance of each phase and L_M is the mutual inductance between two phases.

[1]The electrical angle Θ_{me} is related to the mechanical position Θ_m from the relationship $\Theta_{me} = p\Theta_m$, where p is the number of pole pairs of the machine

Adding (2.4) and (2.5) we obtain:

$$\begin{cases} \lambda_a = Li_a(t) + \Lambda_{pm} cos(\theta_{me}) \\ \lambda_b = Li_b(t) + \Lambda_{pm} cos(\theta_{me} - \frac{2\pi}{3}) \\ \lambda_c = Li_c(t) + \Lambda_{pm} cos(\theta_{me} - \frac{4\pi}{3}) \end{cases} \tag{2.6}$$

Now using the voltage equation:

$$u = Ri(t) + L\frac{d\lambda(t)}{dt} \tag{2.7}$$

$$\begin{cases} u_a = Ri_a(t) + L\frac{di_a(t)}{dt} + e_a \\ u_b = Ri_b(t) + L\frac{di_b(t)}{dt} + e_b \\ u_c = Ri_c(t) + L\frac{di_c(t)}{dt} + e_c \end{cases} \tag{2.8}$$

These formulae can also be written using both a stationary reference, using Clarke's transformation (2.9), and using a rotor reference, using Park's transformation (2.10).

$$\begin{cases} u_\alpha = Ri_\alpha(t) + L\frac{di_\alpha(t)}{dt} - \omega_{me}\lambda_{\beta,pm} \\ u_\beta = Ri_\beta(t) + L\frac{di_\beta(t)}{dt} + \omega_{me}\lambda_{\alpha,pm} \end{cases} \tag{2.9}$$

$$\begin{cases} u_d = Ri_d(t) + L\frac{di_d(t)}{dt} - \omega_{me}Li_q \\ u_q = Ri_q(t) + L\frac{di_q(t)}{dt} + \omega_{me}Li_d + \omega_{me}\Lambda_{pm} \end{cases} \tag{2.10}$$

Multiplying both members of (2.10) respectively by $i_d dt$ and $i_q dt$ and summing the two equations we obtain an energy balance in the rotor reference frame:

$$(u_d i_d + u_q i_q)dt = (Ri_d^2 + Ri_q^2)dt + Li_d di_d + Li_q di_q + \omega_{me}\Lambda_{pm} i_q dt \tag{2.11}$$

For the sake of clarity some time dependencies have been omitted. The first member represents the electrical energy supplied to the motor during the time dt, the second member is composed by the energy transformed into heat in the winding's resistances, of energy stored in the magnetic field, and the last term represents the available mechanical energy. Remembering that the mechanical power can also be expressed as a product of the torque m for the mechanical velocity w_m. We must consider that to have a power conservation in the rotor reference we need a factor $\frac{3}{2}$.

$$m = \frac{3}{2} p \Lambda_{pm} i_q \tag{2.12}$$

The operation of the motor, considering the voltage and current limits, is easily described in a plane i_d i_q, as shown in Figure 2.2.

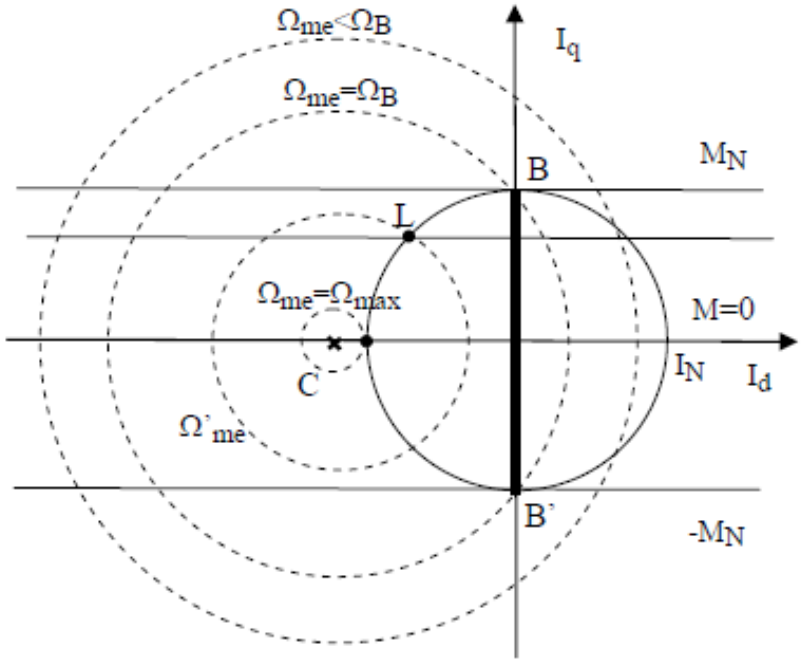

Figure 2.2: *Operating limits of a SPMSM* [23].

The dashed circles represent the voltage limit described by (2.13), while the circle in continuous line represents the current limit (2.14). The motor can only work in the intersection of two circles.

$$(\Omega_{me} L I_q)^2 + (\Omega_{me} L I_d + \Omega_{me} \Lambda_{pm})^2 \leq U_N^2 \tag{2.13}$$

$$I_d^2 + I_q^2 \leq I_N^2 \tag{2.14}$$

For low operating speeds, the voltage limit is very wide (the radius of the circumferences tends to infinity when the speed tends to zero) and therefore the current limit is more restrictive. Under these conditions it is convenient to operate the motor at a point in the BB' segment, depending on the required torque, in this way the torque is obtained with the minimum current absorbed and minimal losses for a given torque (max torque per amper (MTPA)). Above the speed Ω_B called base angular velocity, the available torque starts to decrease because there is less I_q component while the losses do not decrease because the I_d component increase. The value of Ω_B can be easy computed substituting $I_d = 0$ and $I_q = I_N$ into (2.13):

$$\Omega_B = \frac{U_N}{\sqrt{\Lambda_{pm}^2 + (L I_N)^2}} \tag{2.15}$$

After these considerations we can define the operating region of the motor as shown in Figure 2.3.

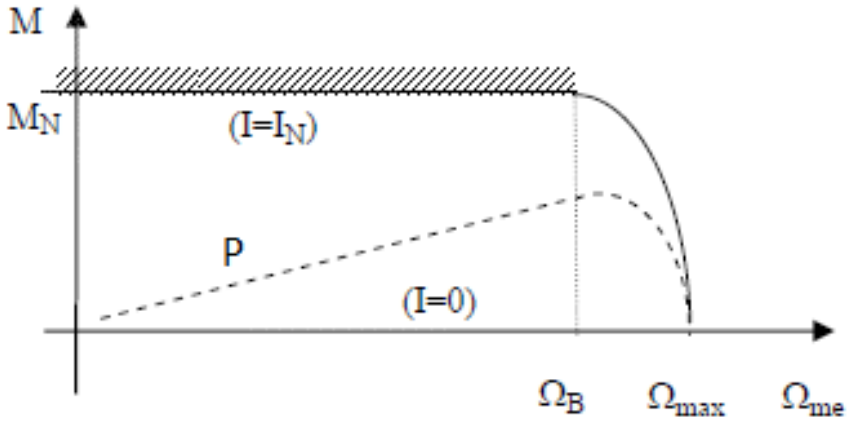

Figure 2.3: *Idealized electromagnetic output torque and power of a SPMSM versus the angular velocity* [23].

Nowadays, multiphase drives are used for high-power applications and can be employed in systems in which a high degree of reliability is required, which is necessary is some particular applications, such as in the naval propulsion, traction, and development of the concept of More Electric Aircraft in the aeronautic field. Multi-phase motor drives have many advantages with respect to their tree-phase counterparts. In particular, the load power can be split into multiple phases, leading to voltage source inverters having switching devices with limited power and current rating [24]. The fact of having several phases causes that the stator produces a field with lower harmonic content in multi-phase machines compared to three phases machines, which result in greater efficiency, moreover multiphase machines are less susceptible than their three-phase counterparts to time-harmonic components in the excitation waveform. Such excitation components produce pulsating torques at even multiples of the fundamental excitation frequency. In addition to the reasons just described, a multi-phase motor can be successfully exploited in different ways, such as increasing the electrical machine torque density, developing multi-motor drives, and improving the fault tolerant capability [25, 24], this combined with replacing the mechanical gearbox makes it an excellent choice for electric vehicles.

In the case of symmetric machines, it is possible to supply the individual phases through a single inverter with the same number of phase as shown in Figure 2.4a; or using an inverter for each phase as shown in Figure 2.4b, between the two configurations proposed only the second satisfies the criteria of fault tolerance which makes the use advantages of multi-phase machines in case of failure of the power supply system, and this is the configuration that is used to supply the machine in the EPE laboratory. Asymmetric multi-phase machines, on the other hand, allow the use of several independent multi-phase inverters of the same type because the stator consists of several configurations with isolated neutral as shown in Figure 2.4c. Although compared to the single-phase inverter configuration, there is a lower level of reliability but this structure allows the use of a well established technology [26].

The 6-phase motor available in the TU/e laboratory, is a custom designed SPMSM. It features a single layer concentrated winding layout, where every phase is comprised out of two coils that are wound around opposite stator teeth as shown in Figure 2.5. The two coil sets are identical, but physically shifted in space 180° from each other. Figure 2.6a shows the phasor representation of the magnetomotive force (MMF) for a

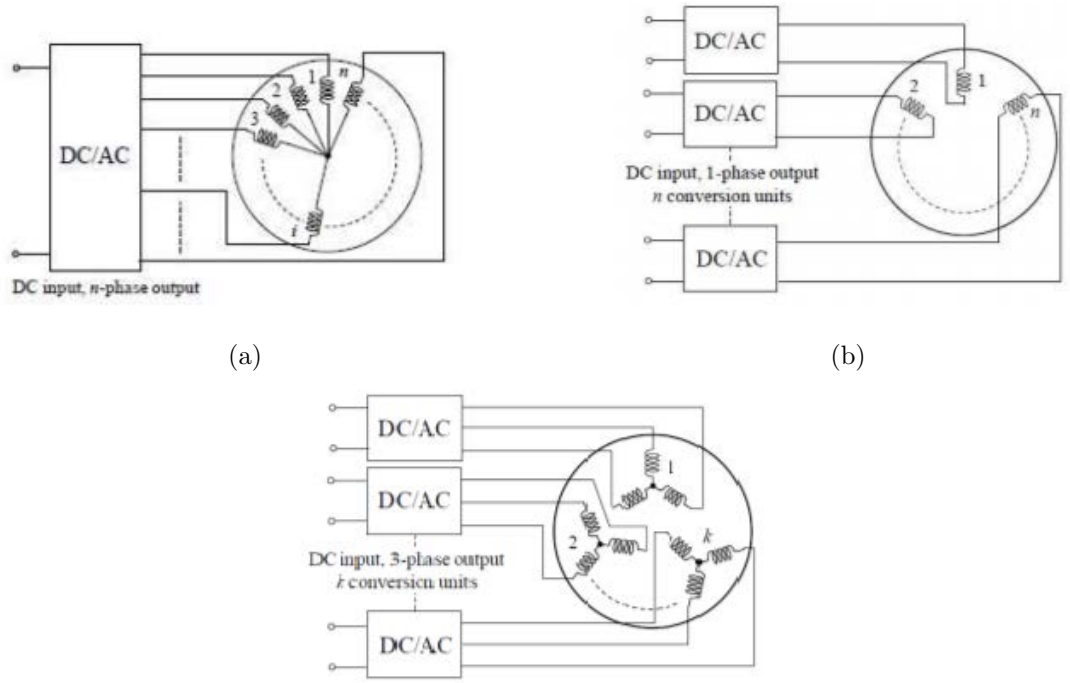

(a) (b)

(c)

Figure 2.4: *Multi-phase drives: possible configurations* [27].

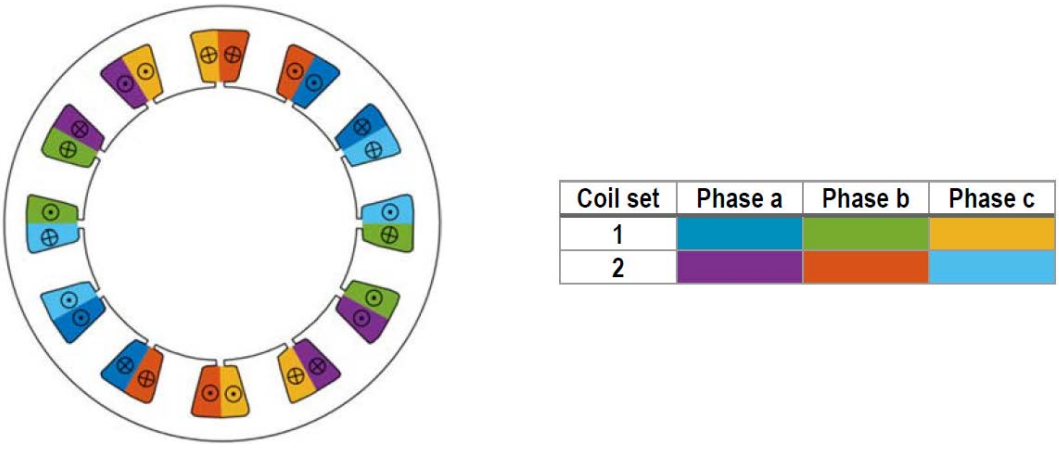

Figure 2.5: *The concentrated winding layout of multi-phases machine.Note that the rotor is omitted from the figure for readability* [28].

typical three phase system is shown, where the electrical angle between the phasors is 120°. In Figure 2.6b shows the representation of a general six-phase machine, with an electrical angle between the phasors of 30°, is shown. Figure 2.6c the representation of a double three-phase setup, as applied in this work, where the electrical angle between the phasors is again 120°, similar to the three-phase setup, [28]. The SPSM features no star point, meaning each phase has separate leads and is independent of the other phases. Disconnecting the neutral point enables additional control options, as the winding can be individually powered and common mode currents are possible alongside the usual

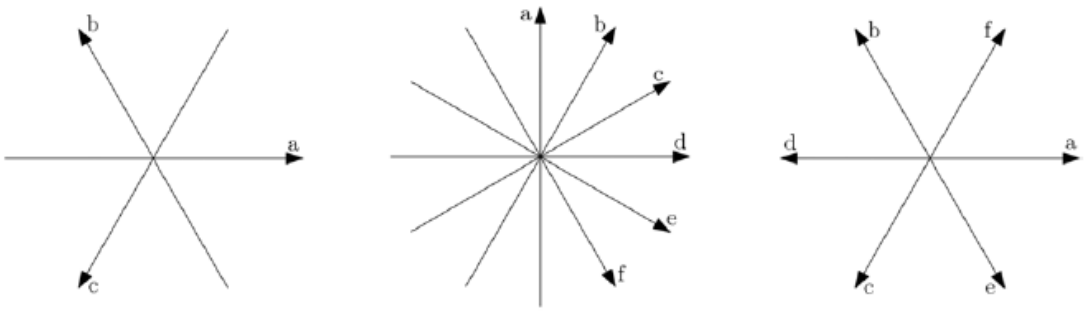

(a) (b) (c)

Figure 2.6: *Balanced phasor representation of the magnetomotive force of:* ***(a)*** *three-phase machine;* ***(b)*** *six-phase machine; and* ***(c)*** *double three-phase setup* [28].

balanced mode currents. Furthermore, the permanent magnets are fixed on top of the rotor, which results in negligible cogging torque and saliency [14, 28]. The work on this thesis consists in proposing a solution which extends the speed range of the machine, increasing the angular velocity ratio x_s defined as the ratio between the top angular velocity and the base angular velocity, considering rotation in equal direction.

$$x_s = \frac{w_{max}}{w_b} \tag{2.16}$$

As shown in Figure 2.3, an increasing x_s improves the time available to accelerate with nominal power. In other terms, for a given P and vehicle parameters, the fastest acceleration is achieved with the highest x_s [14]. In this work will be done referring to a single phase of the machine (RLE circuit), which can be divided according on the configuration used, a work similar to the one proposed below has been carried out in [14] where instead the complete circuit of the machine was used, furthermore in the appendix C, D, E, F there are measurements and parameters of the SPMSM present in the electromechanics and power electronics (EPE) laboratory.

2.2 Flux weakening

Flux weakening is the first method that is explained to increase the speed range, is the most used and the easiest to implement. As shown in Figure 2.2 and described by (2.13), (2.14) the operation region of the motor is the intersection of two circles. There is a particular case in which the speed range can be enhanced. For this to happen the circle's center of the voltage limit must be within the circumference that describes the current limit such as show in Figure 2.7. The circle's center in the I_d and I_q plane, has coordinate:

$$\begin{cases} I_{Cd} = -\dfrac{\Lambda_{pm}}{L} \\ I_{Cq} = 0 \end{cases} \tag{2.17}$$

which are the two components of the current, when the motor has the terminal in short circuit and the rotor is rotating. These equations are derived from (2.10), where: it has been imposed that the voltages were zero (short circuit condition) and the resistive

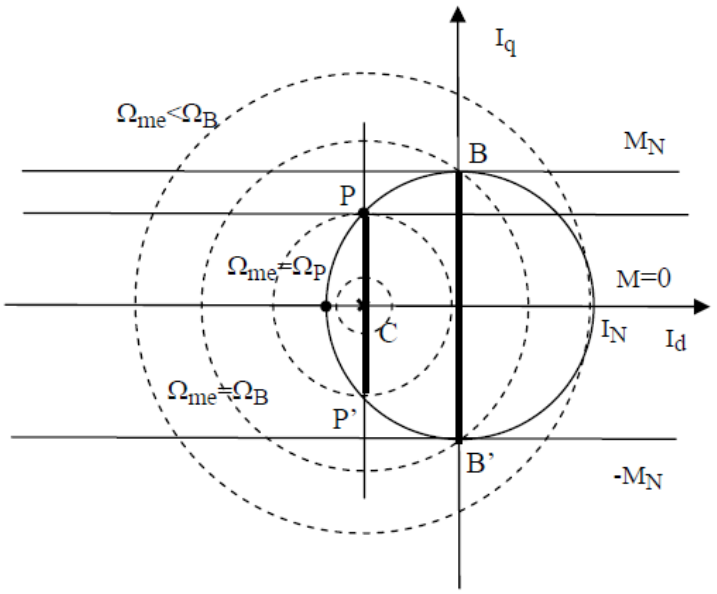

Figure 2.7: *Operating limits of a SPMSM with small short-circuit current* [23].

voltage drop has been neglected. In order for the voltage limit to be within the current limit it will sufficient that:

$$I_N > \frac{\Lambda_{pm}}{L} \tag{2.18}$$

The operation of the engine in this particular condition is the same as that previously described up to speed Ω_P, above which it is convenient to work in the PP' segment, that analogously to the BB' defines the region that ensures the maximum torque per volts (MTPV). In this case there is no speed limit and the operation of point C is ideally has at infinite speed, the operation of the machine is shown Figure 2.8: The top

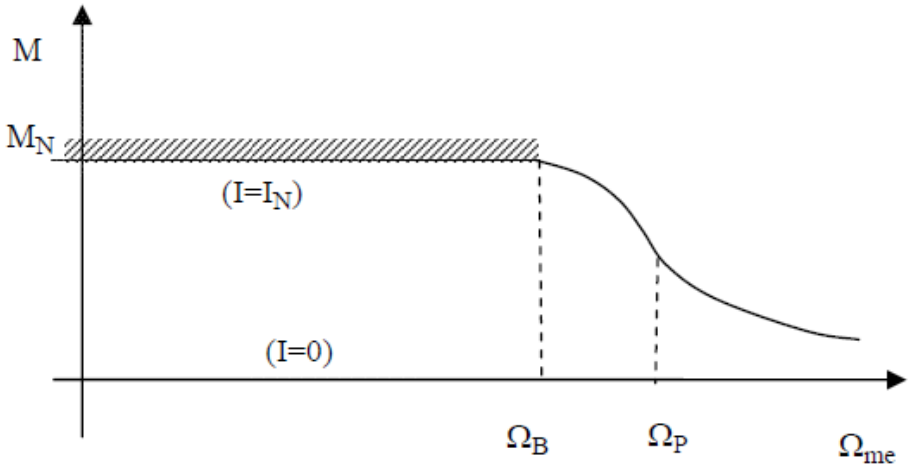

Figure 2.8: *Flux weakening operating region* [23].

angular velocity ω_t, is defined as the maximum speed that can be obtained with a drive system when applying flux weakening, could be theoretically infinite, as previously mentioned. Additionally, in [29], an extensive analysis of the underestimated influence of the winding resistance, R_{st} on ω_b and w_t is expounded [14]. The angular speed Ω_P

can be computed by substituting $I_d = I_{Cd}$ and $I_q = \sqrt{(I_N^2 - I_{Cd}^2)}$ into (2.13):

$$\Omega_P = \frac{U_N}{\sqrt{(LI_N)^2 - \Lambda_{pm}^2}} \tag{2.19}$$

In [14] an angular velocity ratio $x_s = 5$ using the PMSM present in the EPE laboratory is achieved increasing considerably the speed range. The main disadvantage of a high x_s is the reactive power produced by I_d. If during field weakening or regenerative breaking, for example, a voltage source inverter switching instance is missed, the drive is turned off to protect the semiconductor. As such, the excess energy generated in the electrical machine air-gap starts to increase the phase voltages [14]. When the line-to-line voltage exceeds the inverter voltage $e_{ll} > V_{inv}$, the anti-parallel diodes start to conduct current which generates a braking torque. To avoid this problem and protect both the people in the vehicle and the drive system, we must ensure that the peak EMF voltage $\hat{e}_q$, never exceeds the supply voltage of the applied configuration and remembering that usually the electrical machines have a wye connection $e_{ll} = \sqrt{3}e_q$.

2.3 Voltage range enhancement

The second method proposed is named voltage range enhancement and like the flux weakening it increases the speed range of the SPMSM. To do this two inverters are used, the first feeds the machine normally while the second adds a common mode current at the third harmonic to the fundamental to supply voltage of one inverter. Usually common mode currents are avoided because they increase the system losses and they decrease the overall efficiency. The result obtained is the same as flux weakening, that is to improve the torque versus angular velocity profile. The motivation for combining a fundamental frequency current with the third harmonic originates from the SVM principle, by adding a third armonic, the amplitude of the fundamental modulation signal is allowed to be increased above unity [14].

The voltage range enhancement principle is defined as a dual inverter machine drive concept with unequal inverter supply voltages to enlarge the fundamental frequency control operating range of the system [30]. To this end, the secondary side DC voltage is boosted to a higher level than the (battery) source powered primary side DC voltage. This is achieved by using the electrical machine magnetizing inductance as boost inductors. The intention is to power the electrical machine with the fundamental frequency balanced mode current, while transferring the power required at the secondary side using a third harmonic common mode current [14], the circuit used is shown in Figure 2.9. The same circuit as shown in Figure 2.9 is also used for the reactive compensation, the only difference is that in this case there is a connection between the primary supply midpoint $p0$ and the secondary supply side midpoint $s0$. In this way there is a clear separation between the two currents of the inverters in fact: the balanced mode current of the left inverter, can not flow through the ground connection because by definition the sum of per phase component is zero; on the other hand the common mode current of the right inverter has no return path. The only current that can flow between the two inverters is the common mode ground current i_g^{cm} as shown in Figure 2.9. Now, controlling i_g^{cm} it is possible to achieve the secondary

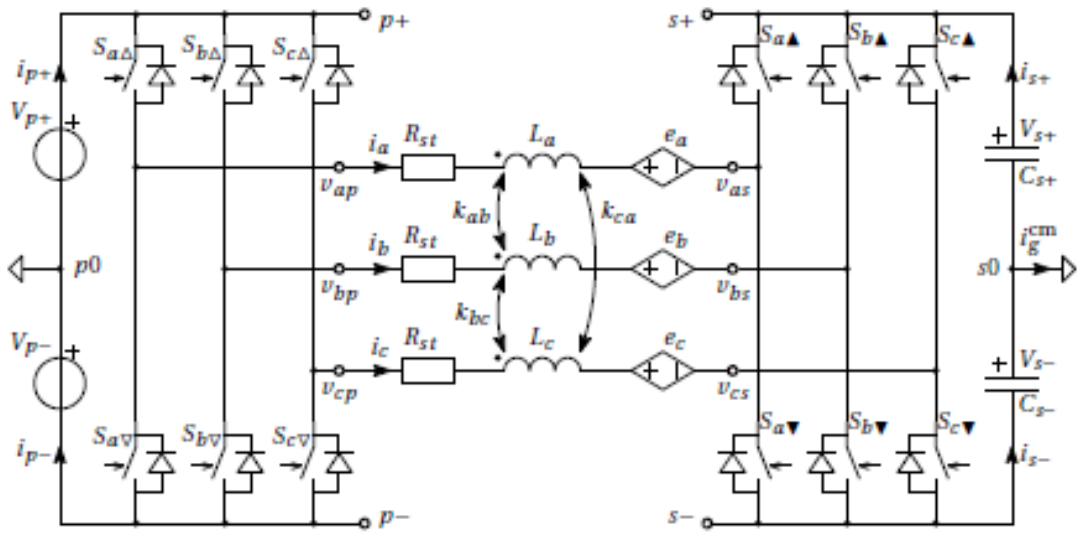

Figure 2.9: *Single winding per-phase voltage range enhancement, dual inverter topology with balanced primary side "p", and secondary side "s"* [14].

supply voltage V_s of a higher value than V_p, as such:

$$V_s = V_{s+} + V_{s-} \tag{2.20}$$

$$V_p = V_{p+} + V_{p-} \tag{2.21}$$

The magnetizing inductances of the electrical machine are used to carry out the boosting effect. Since this is applied to a common mode instead of a balanced mode, a net flow of energy from one inverter to the other is achieved. The two inverters compose a bidirectional full bridge DC-DC converter per phase to charge the secondary side capacitors C_{s+} and C_{s-}. Simultaneously with charging, the capacitors C_{s+} and C_{s-} are discharged by delivering active power to the electrical machine at the fundamental frequency [14]. As mentioned previously the aim of this solution is to extend the angular velocity range of SPMSM with a maximized system efficiency η_{sys}. The assumption made to achieve this are:

1. Regulate the fundamental frequency balanced mode spatial current vector magnitude to the torque producing q1 axis current, for instance:

   $$|\boldsymbol{i}_1^{bm}| = i_{q1}^{bm} \tag{2.22}$$

   thereby assuring fundamental frequency *mtpa* control [31].

2. Ensure that the primary and secondary side fundamental frequency spacial voltage vectors,$\boldsymbol{v}_{p1}^{bm}$ and $\boldsymbol{v}_{s1}^{bm}$ respectively, oppose each other in each working point to maximize the different voltage $\boldsymbol{v}_1^{bm}$, where

   $$\boldsymbol{v}_1^{bm} = \boldsymbol{v}_{p1}^{bm} - \boldsymbol{v}_{s1}^{bm} \tag{2.23}$$

   With the maximized voltage $\boldsymbol{v}_1^{bm}$, the maximum allowed EMF, and thus the maximum angular velocity is obtained.

3. Minimize the required third harmonic common mode current, $\boldsymbol{i}_3^{bm}$, for a demanded electromagnetic power, P_{em}, by ensuring that $\boldsymbol{i}_3^{bm}$ is in phase with the third harmonic secondary side inverter is avoided as illustrated with the unity power factor (PF) line, PF_{s3}^{cm}, in Figure 2.10. The combined power electronics and electrical machine losses are minimized as a result.

4. Regulate supply voltage V_s to a fixed level in order to achieve a power balance on the secondary side.

5. Maximize the combined spatial voltage vectors per side to minimize the required root mean square (RMS) current for a demanded P_{em} [14].

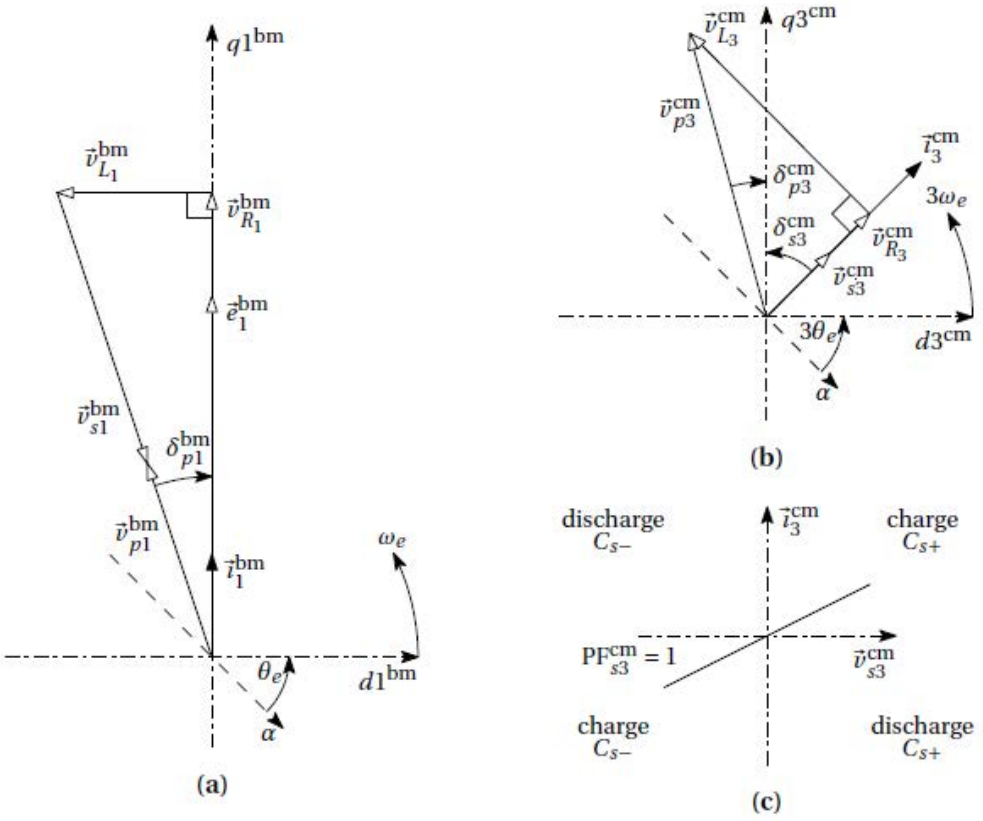

Figure 2.10: *Transformed relations in the (d,q) axis;* ***(a)*** *exemplifying balanced mode fundamental frequency quantity relations;* ***(b)*** *exemplifying common mode third harmonic quantity relations;* ***(c)*** *(dis)charge relation between the secondary side applied third harmonic spacial voltage vector,* $\boldsymbol{v}_{s3}^{bm}$*, and the third harmonic common mode spacial current vector* $\boldsymbol{i}_3^{bm}$*. The optimal situation complying with assumption n.3 and* ***(b)*** *is depicted.* [14].

In [14], the two different methods to extend the angular velocity range were applied to the machine in the TU/e laboratory and the results obtained were compared with each other. In general, the voltage range enhancement is a good alternative to field weakening above all for electrical machines that are unsuitable for field weakening.
In particular, by applying the two methods to the machine in laboratory, the voltage range enhancement concept is not as effective as field weakening, from the optimization and experimental verification it is concluded that an angular velocity ratio improvement of a factor 1.6 is obtained compared with a factor of 3.57 obtained by field weakening,

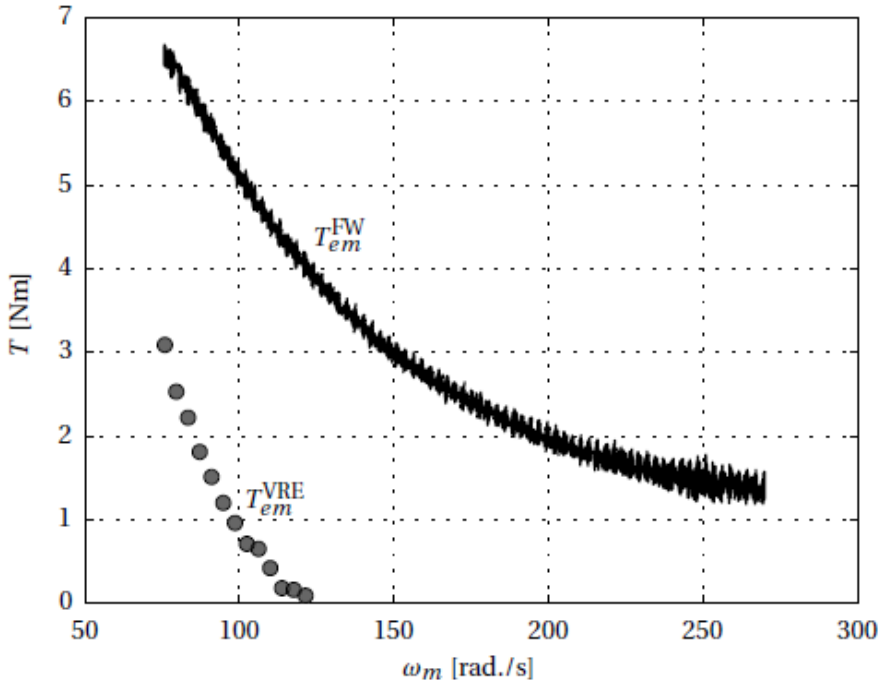

Figure 2.11: *Equal* RMS *current based comparison of the achievable electromagnetic torque,* T_{em}*, per indicated angular velocity range enhancement strategy* [14].

as shown in Figure 2.11. The nominal machine current level is not reached when applying voltage range enhancement due to the stringent assumption describe above. The assumption by which the concept operation can be relaxed to extend the current usage and improve the torque and angular velocity range according [14]. On the other hand, if the conditions are not observed, one of the advantage of this method, the minimization of the current strategy is lost with a consequent increase in losses and a decrease in the efficiency of the machine. Another advantage to consider in this method is that EMF voltage is not elevated to a level higher than the combined semiconductor breakdown voltage. This potentially avoids a system failure or shutdown in case of irregularities [14], a key feature in the automotive sector.

2.4 Dynamic drive configurations

This is the last method proposed to extend the angular velocity range and it is also the one that will be discussed later. At the base of this method is the variation of the power electronics circuit as a function of the machine angular velocity. The concept is very similar to the wye-to-delta transformation that it is applied in numerous applications to provide two fixed angular velocities from a grid connected induction machine, or to star an electrical machine [32], in this way in addition to an extension in the angular velocity range, an electrical variant to the mechanical gearbox is created because every winding configuration has a different base angular velocity. The presented ideas improve the angular velocity ratio x_s but at high angular speed the output power is limited due to the parallel configuration of the winding supplied by one half bridge. The total phase current is limited to the series connected level by the power electronics, halving the per winding current in parallel connected mode [14]. A possible solution to make better use

of the system would be to double the current of the inverters so that is was possible to feed the machine with the nominal current even during the series configuration, in this way the power electronics would be oversized and this leads to significantly switching losses in the series connected mode.
This method is applied to the machine shown in Figure 2.5, where each winding represents one phase half of the motor, the current can be distributed over the windings in any ratio. If the different windings of each phase are fed by the same current, magnitude and phase, the (produced torque T^u) per three phase winding set u which is closely related to the overall torque T_{em} according to:

$$T_{em} = N^{set} T^u \tag{2.24}$$

where N^{set} is the number of windings per-phase, in general it can be $N^{set} > 1$ but in our case $N^{set} = 2$. By increasing the number of windings per phase, different torque versus angular velocity combinations are obtained, just like when in a traditional vehicle the gear ratio is changed. In this way an increased machine power is obtained without resorting to a greater machine size or seen from another point of view it is possible to have the same machine power with a smaller motor, this means less space occupied by the machine, less weight, lower costs and an increase in the vehicle's autonomy. The price to pay for this increased angular speed range is a reduced efficiency when the motor works to high speeds because in a normal three phase machine the inverter uses only two switching legs while with this method four legs are used.
The per phase circuit of the N^{set} windings per phase topology is shown in Figure 2.12: This per phase circuit is therefore required three times to compose the complete power

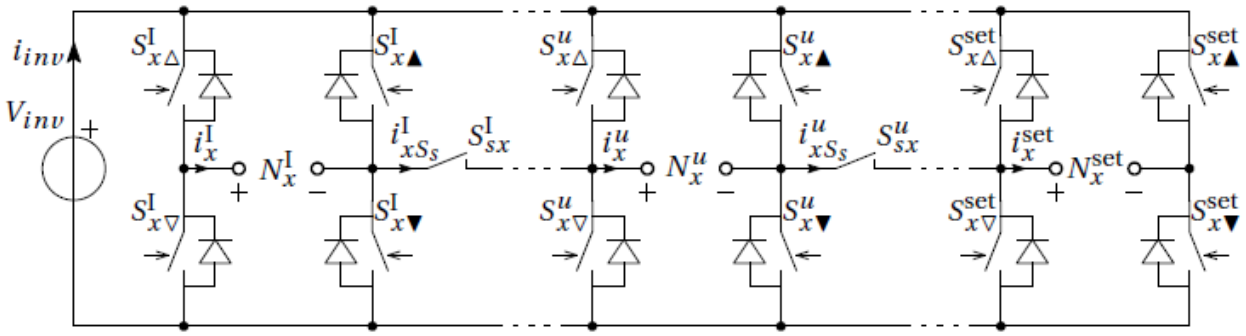

Figure 2.12: *Generalized N^{set} windings reconfigurable per phase topology to drive an electrical machine with the dynamic drive operation* [14].

electronics converter. The DC source voltage and current are indicated with V_{inv} and i_{inv}, respectively. Each full bridge converter is defined as a left half bridge leg (stroke triangle), and a right half bridge leg (filled triangle), each consisting of an upper switch (triangle points up), and a lower switch (triangle points down) [14]. The main disadvantage of the presented solution, as shown in Figure 2.12, is the number of switches (anti parallel connection between transistor and diode) compared with a conventional inverter. As previously mentioned, the circuit used has two winding per phase, so the circuit becomes the one shown Figure 2.13, which has far fewer components. The tendency to increase the number of semiconductor used in a power electronics converter is motivated with multiple arguments [33]:

- The system flexibility is improved, for example by multilevel [34], by interleaving

[35], or by altering between series or parallel connected outputs in a multiple modules DC-DC converter [36].

- With a dual inverter drive structure is possible reactive compensation, battery charging or voltage range enhancement .
- The system reliability is improved without adding redundancy.
- At lower output voltage levels, the switching losses are further reduced by scaling the number of switching elements with the angular velocity applying a series switch [14].

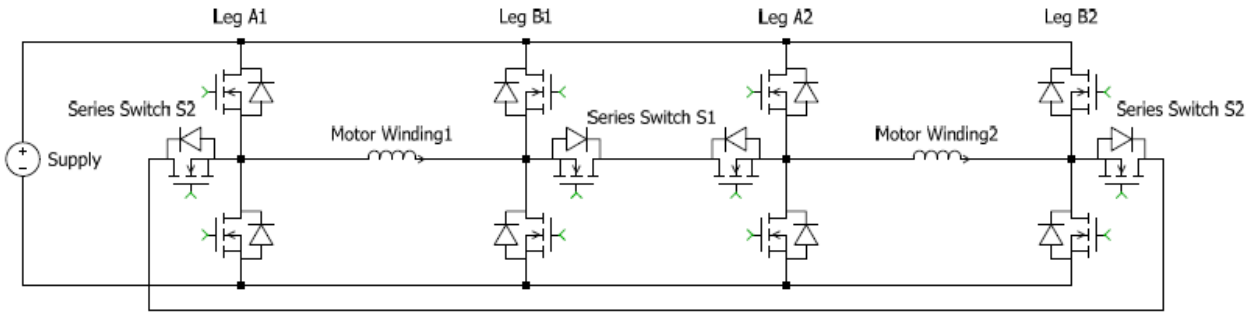

Figure 2.13: *Schematic view of the two phase halves in the dynamic configuration, with two series switches* [28].

As shown in the circuit of Figure 2.13, another pair of switches has been added, called $S2$, in this way it is possible to use both S1 and S2 during the series configuration so the thermal load is spread out more evenly and it is possible to increase the current. Another thing that can be observed from the circuit is that one MOSFET of each series switch has been drawn adjacent to a phase leg. This is a deliberate choice to allow constructing the power hardware as modularly as possible, and facilitates easy driving of the series switches by means of a bootstrapped power supply for their gate drivers [28]. The biggest advantage of winding reconfiguration is that by increasing the angular velocity and at the same time by maintaining a constant electromagnetic torque as shown in Figure 2.14b, the output power increases in contrast with what happens using a conventional gearbox. In [14] this method is applied to the SPMSM shown in Figure 2.5 and the absolute angular velocity range is improved by a factor 3.49. The dynamic drive configuration to allow to increase the speed range without using flux weakening that is very useful for EVs, avoiding problems for the safety of people in the vehicle and for the drive system, if there is a fault. Obviously, a method does not exclude the other, it is possible to go to exploit the advantages of both, the winding reconfiguration is used to stay in a region of constant torque for longer while increasing the speed and then field weakening can still be used to extend the angular velocity even further, as shown in Figure 2.14a.

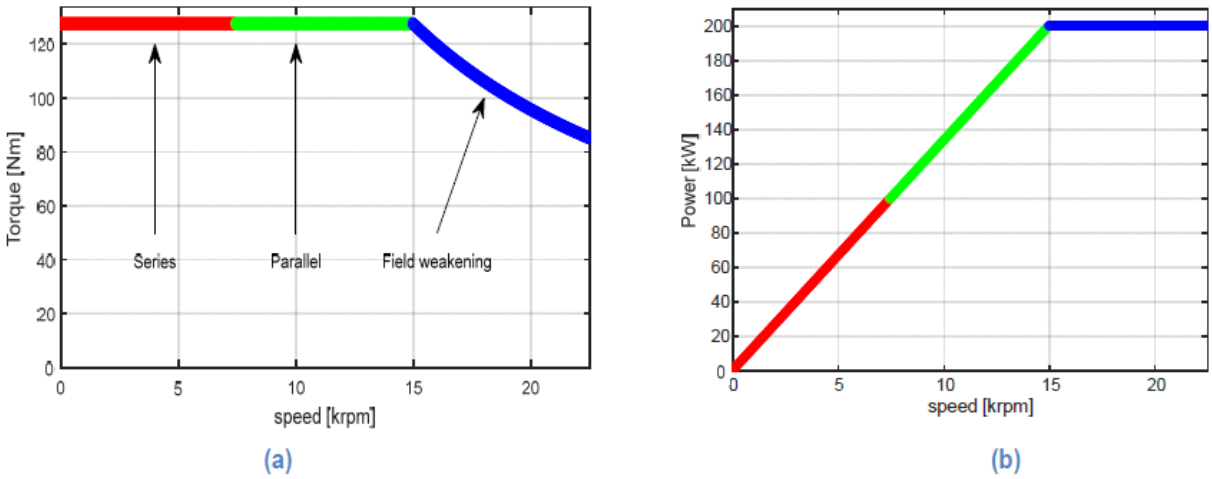

Figure 2.14: ***(a)*** *Torque vs speed and,* ***(b)*** *power vs speed characteristics, for the winding reconfiguration technique* [28].

Chapter 3

Voltage control using pre-calculated timing

3.1 Space Vector Modulation

To control the switches of the circuit shown in Figure 2.13, the SVM technique is used, not only for the series switches but also for the phase leg switches. Let's start by explaining what the SVM consists of and how it applies to a conventional 3-phase 2-level inverter. A tree-phase inverter as shown in Figure 3.1, to avoid short circuits of DC supply at no time must the switches in the same leg be turned on, this leads to eight possible inverter states that they can be represented by eight vectors of three components one for each phase, where it is indicated with 1 when the switch is closed and with 0 when the switch is opened.

Vector	A^+	B^+	C^+	A^-	B^-	C^-	V_{AB}	V_{BC}	V_{CA}	
$V_0 = \{000\}$	OFF	OFF	OFF	ON	ON	ON	0	0	0	zero vector
$V_1 = \{100\}$	ON	OFF	OFF	OFF	ON	ON	$+V_{dc}$	0	$-V_{dc}$	active vector
$V_2 = \{110\}$	ON	ON	OFF	OFF	OFF	ON	0	$+V_{dc}$	$-V_{dc}$	active vector
$V_3 = \{010\}$	OFF	ON	OFF	ON	OFF	ON	$-V_{dc}$	$+V_{dc}$	0	active vector
$V_4 = \{011\}$	OFF	ON	ON	ON	OFF	OFF	$-V_{dc}$	0	$+V_{dc}$	active vector
$V_5 = \{001\}$	OFF	OFF	ON	ON	ON	OFF	0	$-V_{dc}$	$+V_{dc}$	active vector
$V_6 = \{101\}$	ON	OFF	ON	OFF	ON	OFF	$+V_{dc}$	$-V_{dc}$	0	active vector
$V_7 = \{111\}$	ON	ON	ON	OFF	OFF	OFF	0	0	0	zero vector

Table 3.1: *Input table of switch positions with the corresponding vector* [37].

In three-phase systems, the output voltages define an orthogonal three-dimensional space, which results in a cube that contains the boundaries of all possible combinations of voltages that could be created. The simplified Clarke transformation is an isometric

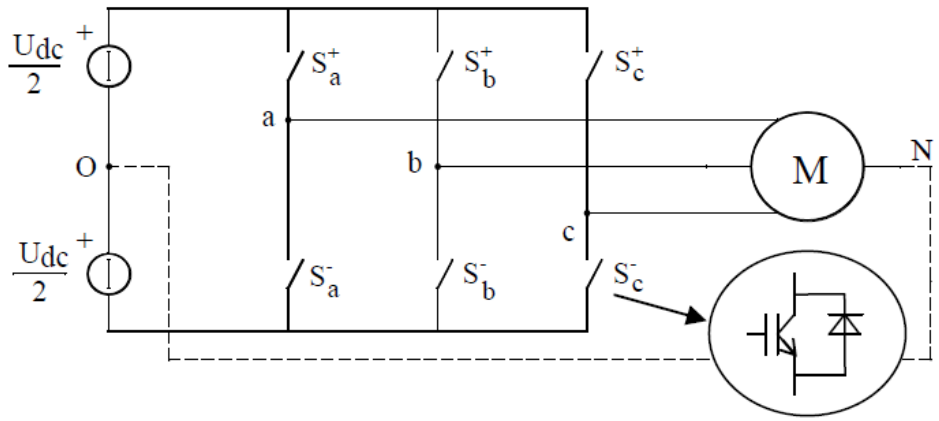

Figure 3.1: *Schematic representation of a three-phase inverter* [23].

projection of this cube on the $\alpha\beta$ plane [38].

$$\boldsymbol{X}_{\alpha\beta} = \begin{pmatrix} X_\alpha \\ X_\beta \end{pmatrix} = \frac{1}{3}\begin{bmatrix} 2 & -1 & -1 \\ 0 & \sqrt{3} & -\sqrt{3} \end{bmatrix} \begin{pmatrix} X_a \\ X_b \\ X_c \end{pmatrix} \qquad (with\ X = current\ or\ voltage) \quad (3.1)$$

Applying the definition of space vector (appendix), 6 of the 8 states are represented by six vectors of amplitude $\frac{2}{3}U_{dc}$ with 60 degrees between them, occupying the vertices of a hexagon centred in the origin of the axes in a $\alpha\beta\gamma$ plane, as shown in Figure 3.2. The two states 000 and 111, which correspond respectively to the configurations with all the lower and upper switches closed, are called zero vectors, and therefore occupy the origin of the axes of the complex plane. The reference vector V_{ref} is then synthesized using a combination of the two adjacent active switching vectors and one or both of the zero vectors. Various strategies of selecting the order of the vectors and which zero vector(s) to use exist. The selections tratégy will affect the harmonic content and the switching losses [37]. The expression of the generic active vector is given by:

$$\boldsymbol{u}_m = \frac{2}{3}U_{dc}e^{j(m-1)\frac{\pi}{3}} \qquad m \in [1..6] \quad (3.2)$$

In our case there are not only 2 switches per phase, but 10, even in here there are rules to prevent short circuits so the actual switches to be controlled are far fewer. The problem to be studied is very similar to SVM control of a matrix converter studied in [39]. Assume we want to generate an average voltage V_{ref} across the motor windings during a time interval with length T_s. This voltage can be generated by timed application of two active vectors and one or two zero vectors:

$$T_s V_{\alpha\beta} = T_0 V_{0,\alpha\beta} + T_1 V_{1,\alpha\beta} + T_2 V_{2,\alpha\beta} \quad (3.3)$$

The sum of the time intervals has to be equal to the cycle time T_s:

$$T_s = T_0 + T_1 + T_2 \quad (3.4)$$

Combine:

$$\begin{pmatrix} T_s V_{\alpha\beta} \\ T_s \end{pmatrix} = \begin{bmatrix} T_0 V_{0,\alpha\beta} & T_1 V_{1,\alpha\beta} & T_2 V_{2,\alpha\beta} \\ T_0 & T_1 & T_2 \end{bmatrix} \quad (3.5)$$

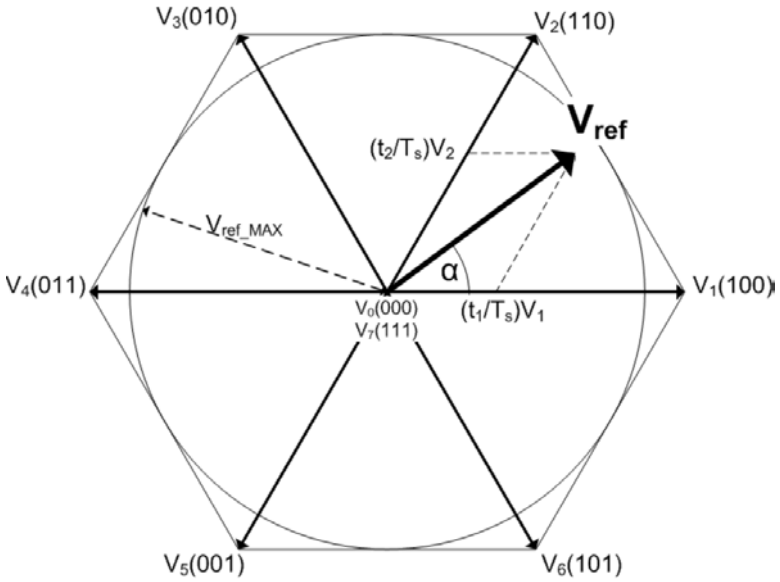

Figure 3.2: *All eight possible switching vectors for a three-leg two-level inverter using space vector modulation. An example V_{ref} is shown in the first sector. $V_{ref-MAX}$ is the maximum amplitude of V_{ref} before non-linear overmodulation is reached* [37].

Wanting to compute the times:

$$\begin{pmatrix} T_0 \\ T_1 \\ T_2 \end{pmatrix} = T_s \begin{bmatrix} T_0 V_{0,\alpha\beta} & T_1 V_{1,\alpha\beta} & T_2 V_{2,\alpha\beta} \\ 1 & 1 & 1 \end{bmatrix}^{-1} \begin{pmatrix} V_{\alpha\beta} \\ 1 \end{pmatrix} \tag{3.6}$$

In this way the times T_1, T_2 and T_0 are obtained, they are necessary to apply the respective vectors V_1, V_2 and V_0 (see Figure 3.2), in order to obtain the voltage V_{ref}.
A different solution was studied in [38], where it was implemented a various balancing control method for flying-capacitor, the circuit is shown in Figure 3.3

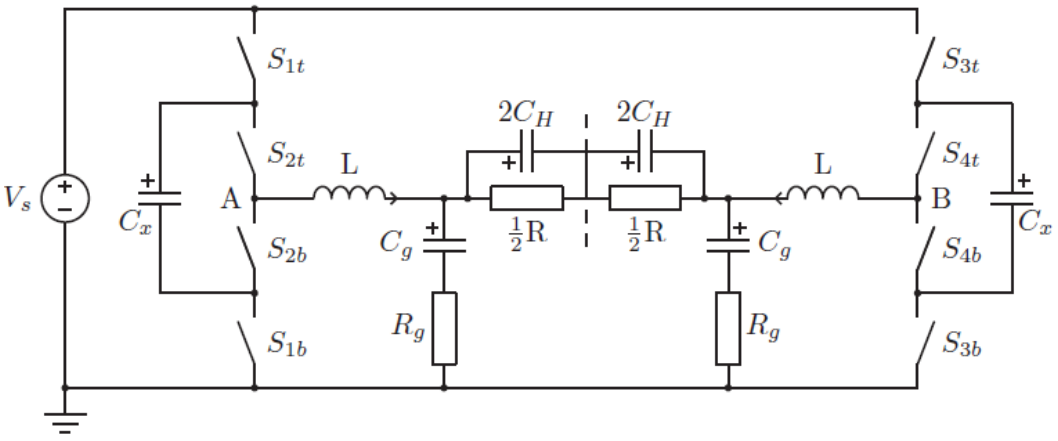

Figure 3.3: *Schematic of a full-bridge two-cell flying-capacitor amplifer* [38].

The flying-capacitor topology can be categorized in the family of multilevel converters in which some of the voltage levels are created by floating capacitors. The switch

devices are configured in such a way that the capacitors can be charged or discharged for a given voltage level [38]. For this circuit the PWM and control algorithm applied to the converter have two tasks. The first task is to create the output voltage by means of the volt-second principle, using a PWM cycle the average applied voltage is equal to the desired voltage. The second task is the balancing of the capacitor voltages by means amp-second principle, using a PWM cycle the average capacitor current should be zero [38]. The compensation of the capacitors can be implemented with two methods: the first consists of changing the duty cycle or the phase-shift; the second consists in computing the switching times and implementing a SVM.
Using the input voltage the output current to create a two dimensional space is possible to use also the zero vectors. In the new plane there are 4 state vectors:

$$\begin{aligned} \boldsymbol{v}_0 &= [-\frac{1}{2}V_s, 0]^T \\ \boldsymbol{v}_1 &= [-v_d, I_{out}]^T \\ \boldsymbol{v}_2 &= [v_d, -I_{out}]^T \\ \boldsymbol{v}_3 &= [\frac{1}{2}V_s, 0]^T \end{aligned} \tag{3.7}$$

where V_s is the DC supply voltage while the v_d is the output voltage. With these 4 vectors it is possible to define a vector diagram like the one in Figure 3.4

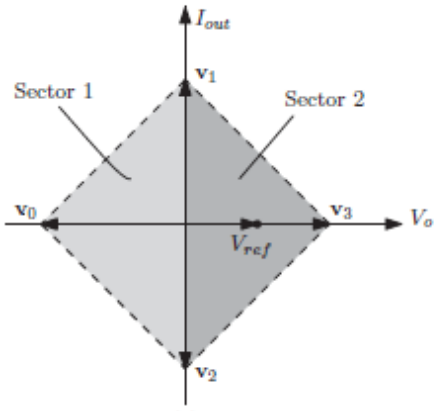

Figure 3.4: *Vector diagram in I-V plane* [38].

Once the plan is divided, proceed as in the normal SVM, each vector v_T defined as

$$\boldsymbol{v}_T = [V_{ref}, I_{ref}]^T$$

can be created using three of the four vectors of (3.7), the three vectors to use, will depend on which of the two sector lying v_T, for example if it lies on sector 1:

$$T_0\boldsymbol{v}_0 + T_1\boldsymbol{v}_1 + T_2\boldsymbol{v}_2 = T_s\boldsymbol{v}_T \tag{3.8}$$

The maximum possible vector which can be created is bounded, because the sum of the switching times cannot exceed the switching period. This result in [38]

$$T_0 + T_1 + T_4 = T_s \tag{3.9}$$

As an example the equations for sector 1 will be derived,

$$\begin{bmatrix} \boldsymbol{v}_0 & \boldsymbol{v}_1 & \boldsymbol{v}_2 \\ 1 & 1 & 1 \end{bmatrix} \begin{bmatrix} T_0 \\ T_1 \\ T_2 \end{bmatrix} = \begin{bmatrix} \boldsymbol{v}_T \\ T_s \end{bmatrix} \tag{3.10}$$

This can be rewritten into

$$\begin{bmatrix} T_0 \\ T_1 \\ T_2 \end{bmatrix} = \begin{bmatrix} \boldsymbol{v}_0 & \boldsymbol{v}_1 & \boldsymbol{v}_2 \\ 1 & 1 & 1 \end{bmatrix}^{-1} \begin{bmatrix} \boldsymbol{v}_T \\ T_s \end{bmatrix} \tag{3.11}$$

Using a different approach compared to conventional 3-phase 2-level inverter, the times to be used for the different configurations have been calculated in order to obtain the desired output voltage.

The last method presented to compute the times for the SVM configurations is explained in [39]. The basic idea is to construct switching sequences consisting of a number of different time intervals and switching vector which start and end at a zero vector. If 5 intervals are used per sequence, the fixed cycle time will be denoted by T_x can be written by [39]:

$$T_x = T_1 + T_2 + T_3 + T_4 + T_5 \tag{3.12}$$

Next step is to write the output voltage as a function of input voltage:

$$\boldsymbol{V}_{rst} = \begin{pmatrix} V_r \\ V_s \\ V_t \end{pmatrix} = S \begin{pmatrix} V_R \\ V_S \\ V_T \end{pmatrix} = SV_{RST} \tag{3.13}$$

and the same for the current

$$\boldsymbol{I}_{rst} = \begin{pmatrix} I_r \\ I_s \\ I_t \end{pmatrix} = S^t \begin{pmatrix} I_R \\ I_S \\ I_T \end{pmatrix} = S^t I_{RST} \tag{3.14}$$

where in the matrix S there are the entries expressing the switch state (1=closed, 0 open) corresponding to the positions as shown in figure Figure 3.5. The two equation systems of equations just written are very similar to those that were obtained for the normal SVM, the only thing that changes is the matrix S. Considering the average values of the output variables we obtain:

$$V_{rst,av} = \frac{1}{T_x}(T_1S_1 + T_2S_2 + T_3S_3 + T_4S_4 + T_5S_5)V_{RST} \tag{3.15}$$

$$I_{rst,av} = \frac{1}{T_x}(T_1S_1^t + T_2S_2^t + T_3S_3^t + T_4S_4^t + T_5S_5^t)I_{RST} \tag{3.16}$$

which can be rewritten as:

$$\begin{pmatrix} V_{\alpha,av} \\ V_{\beta,av} \\ R_W I_{A,av} \\ R_W I_{B,av} \end{pmatrix} = \frac{1}{T_x} \begin{bmatrix} TS_2V_{RST} & TS_3V_{RST} & TS_4V_{RST} \\ TS_2^t R_W I_{rst} & TS_3^t R_W I_{rst} & TS_4^t R_W I_{rst} \end{bmatrix} \begin{pmatrix} T_2 \\ T_3 \\ T_4 \end{pmatrix} \tag{3.17}$$

where the contribution related to the zero vector is zero and is been added an impedance weighting R_W to obtain numerical values in the same range. There are 4 equations with 3 unknowns so an optimal solution can be found:

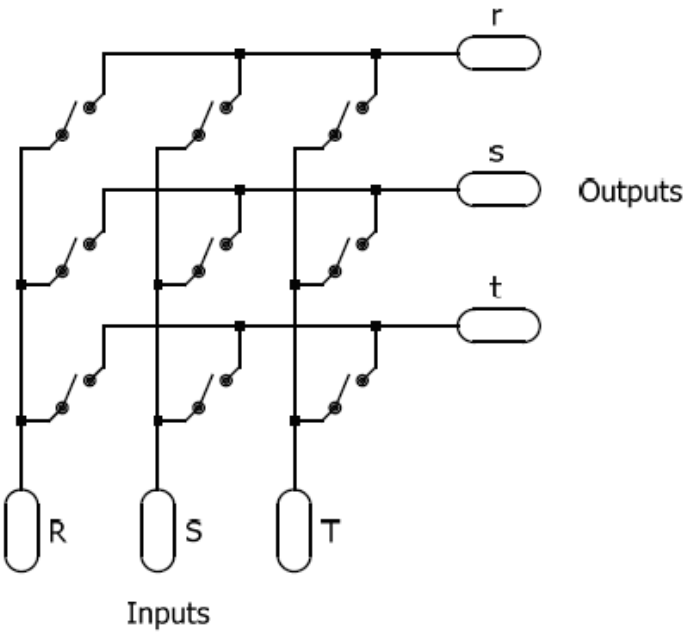

Figure 3.5: *Schematic of 3x3 direct matrix converter* [39].

$$\begin{pmatrix} T_2 \\ T_3 \\ T_4 \end{pmatrix} = T_x \begin{bmatrix} TS_2 V_{RST} & TS_3 V_{RST} & TS_4 V_{RST} \\ TS_2^t R_W I_{rst} & TS_3^t R_W I_{rst} & TS_4^t R_W I_{rst} \end{bmatrix}^+ \begin{pmatrix} V_{\alpha,av} \\ V_{\beta,av} \\ R_W I_{A,av} \\ R_W I_{B,av} \end{pmatrix} \tag{3.18}$$

where the $()^+$ indicates the Moore-Penrose pseudo-inverse of the matrix that is a generalization of the inverse matrix and it satisfies some but not necessarily all the properties of a standard inverse matrix. This inverse is found as follows:

$$A^+ = (A^t A)^{-1} A^t \tag{3.19}$$

In our case, due to symmetry, in a period there are only two unknown timing T_1 and T_2 respectively for the series configuration and for the parallel configuration. The main difference with the SVM applied to matrix converter is that with the method used, zero vectors cannot be used. In (3.11) does not appear the Moore-Penrose pseudo-inverse but the normal inverse matrix this is due to being able to use zero vectors, in this way there aren't incompatible set points (corresponding to a difference between input and output power) for the average voltages at the output and currents at the input of the converter [28], as was the case with the previous method.

3.2 Overview of the project

In the previous chapter several methods for extending the speed range were presented, each with its own peculiarities, with its own advantages and disadvantages. Now the method of reconfiguration that was previously analyzed from the general point of view, will be explained in detail. The simplified circuit used is the one shown in Figure 2.13, where the DC-link capacitors are omitted from the schematic for readability. The legs are switched using silicon IGBT's while MOSFET's are used, as shown in Figure 3.6a,

to switch between series and independent configuration. The MOSFET's are used since the switching is not frequent in this setup and therefore the conduction losses are minimized [40]. This is not the only solution, the other option is to create a bidirectional switch using an anti-parallel connection of two reverse blocking IGBT's, as depicted in Figure 3.6b. The favoured solution depends on the application, the main advantage of using MOSFETs is that they have a low on-state resistance, they therefore have low losses at low RMS current. The two series switches are used to change the configuration

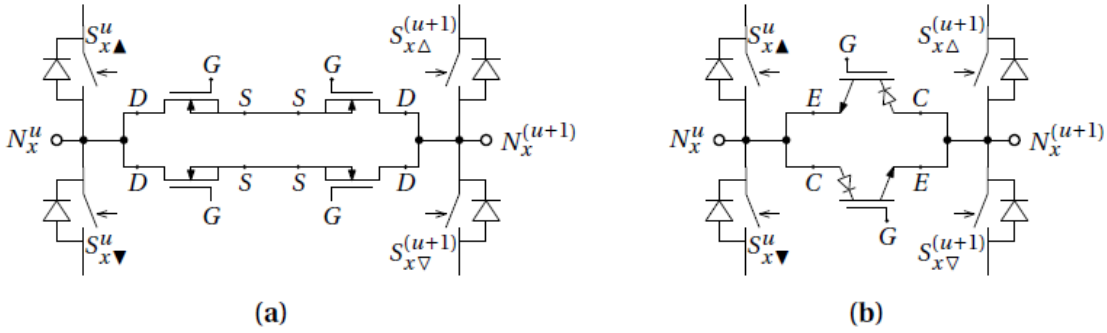

Figure 3.6: ***(a)*** *anti-series connected dual leg* MOSFET *based,* ***(b)*** *anti-parallel connected reverse blocking* IGBT *based* [14].

of the system from the series operation to independent (also called parallel, even though strictly speaking the windings are not in parallel) operation. The reconfiguration of windings can theoretically be done at arbitrary moments, actually to follow specific voltage or current waveform, the exact moments of the passage from one configuration to another must be calculated. For every operating cycle the circuit passes through four stages: "parallel", "series1", "parallel", and "series2", shown respectively in Figure 3.7, Figure 3.8 and Figure 3.9; where the difference between "series1" and "series2" is which of the two switches $S1$ or $S2$ is used. In practice, due to symmetry, in some cases only half of these stages need to be addressed, so for example only "parallel", "series1".
In the series1 configuration the switch $S1$ must be closed while the switch $S2$ must be open, vice versa for the series2 configuration. In the circuit the supply voltage is represented by a DC voltage source so with constant value, it does not take into account that the supply characteristic changes for example because of battery SOC.
From the circuit shown in Figure 3.8 it can be seen that during the independent configuration two switches are used for each half winding for a total of four therefore during the period of time that this configuration is used the losses switching will be double. The aim of this work will be to calculate the optimal times within an operating cycle for which the different configurations will have to be maintained in this way, there will also be the opening times of the S1 and S2 switches, finally for each configuration the optimal choice of opening/closing of the other switches must be found in order to obtain the desired output characteristics. To command the switches the space vector modulation (SVM) technique will be used but this is not the only option that can be used, at TU/e some students are implementing different approaches and in the following paragraph some will be presented.
Once obtained the time of each configuration and the optimal combination of switches will need to design a feedback control system so that the whole system is stable, the quantity to be controlled can be both the voltage applied to the SPMSM and the current. In our case it was decided to control the current because it is closely linked with

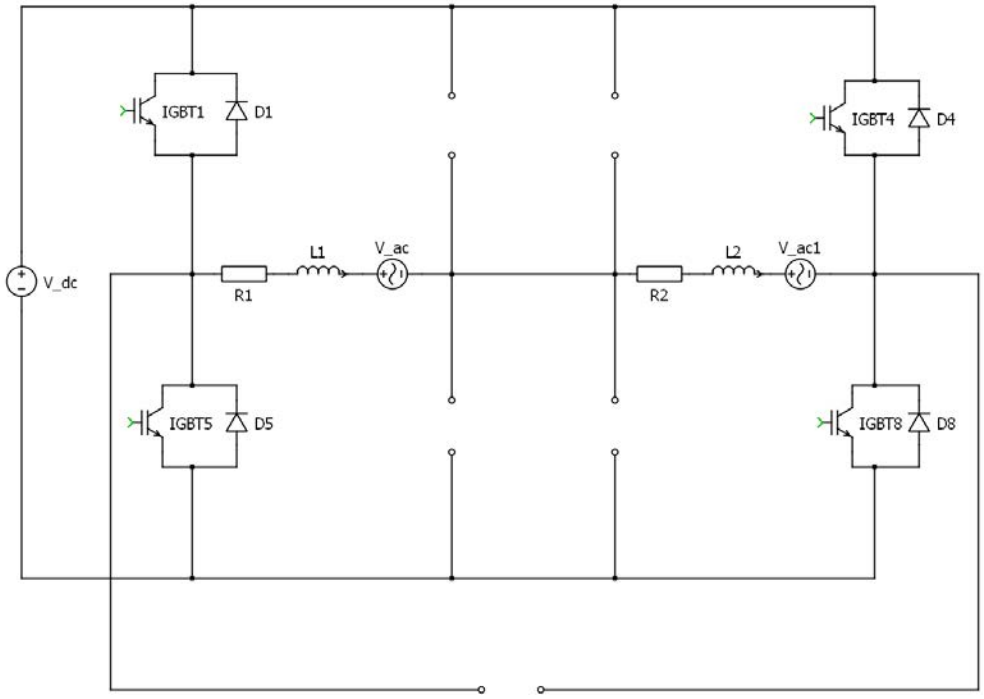

Figure 3.7: *Schematic view of the two phase halves of a single winding connected in series1.*

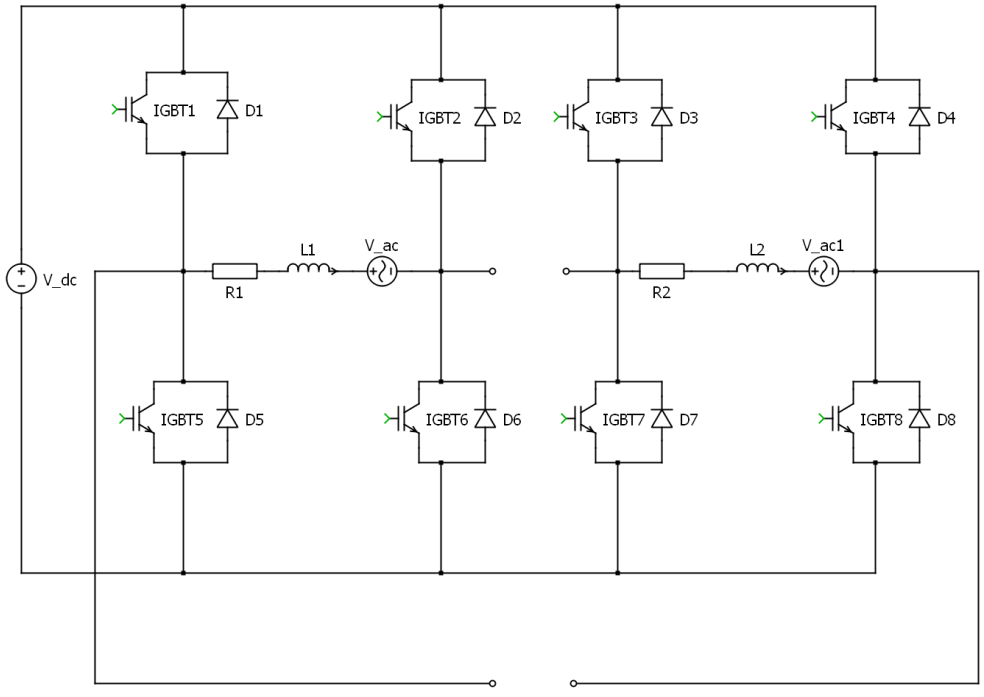

Figure 3.8: *Schematic view of the two phase halves of a single winding connected in parallel.*

the torque of the machine and also to avoid problems related to current unbalance in the two half winding during the passage from series to independent configuration. The calculation of the time and the best combination of the switches will be made using MATLAB and a second part made in SIMULINK consisting of the inverter, the current control, and the simplified functionality of the motor, it has been used a series

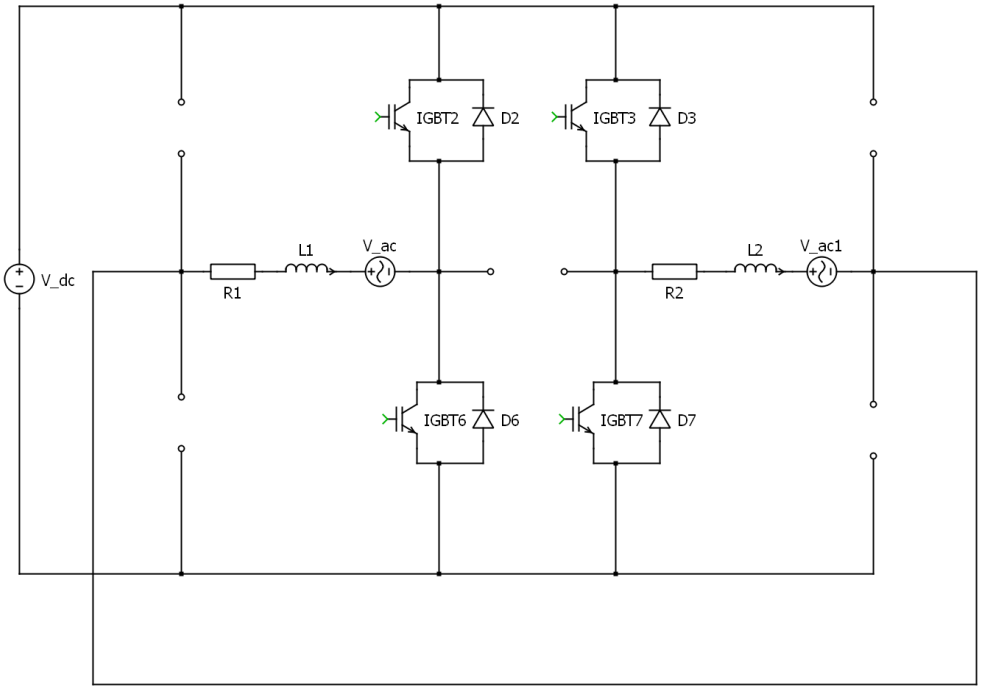

Figure 3.9: *Schematic view of the two phase halves of a single winding connected in series2.*

connection of an inductor, resistance, and voltage source. Initially the part of the inverter and the motor was made in SIMULINK but then it was preferred to use PLECS, a software tool for system level simulation of electrical circuits, commercial software 100% compatible with SIMULINK and MATLAB which has several advantages, the most important being: firstly, it yields systems that are piecewise-linear between switching instants, (thus resolving the otherwise difficult problem of simulating the non-linear discontinuity that occurs in the equivalent-circuit at the switching instant). Secondly, to handle discontinuities at the switching instants, only two integration steps are required (one for before the instant, and one after). Both of these advantages speed up the simulation considerably [41]. The last step is to use an interface between the physical components and create a controller in MATLAB, a dSPACE microlabbox is necessary. The scheme made in SIMULINK refers to the equivalent one-phase scheme so it is not possible to test directly on the six-phase motor, to simulate the back-EMF a one-phase transformer will be used while an inductor can be used separately to emulate the winding inductances.

3.3 Different types of reconfiguration

The most straightforward method to use the dynamic reconfiguration is to use the actual motor speed to switch over from series to parallel operation or vice-versa. With increasing motor speed, the back-EMF of a PMSM rises accordingly. Above a certain (pre calculated) speed, it is assumed that series operation is no longer possible and, hence the parallel mode is activated. A very simplified representation (for one phase only) of the operation is shown in Figure 3.10 [28]:
As it can be seen from the figure, when the modulation index, related to the speed of the machine, exceeds 1 the configuration is changed from series to parallel, the index decreases which makes it possible to continue increasing the speed. Although very

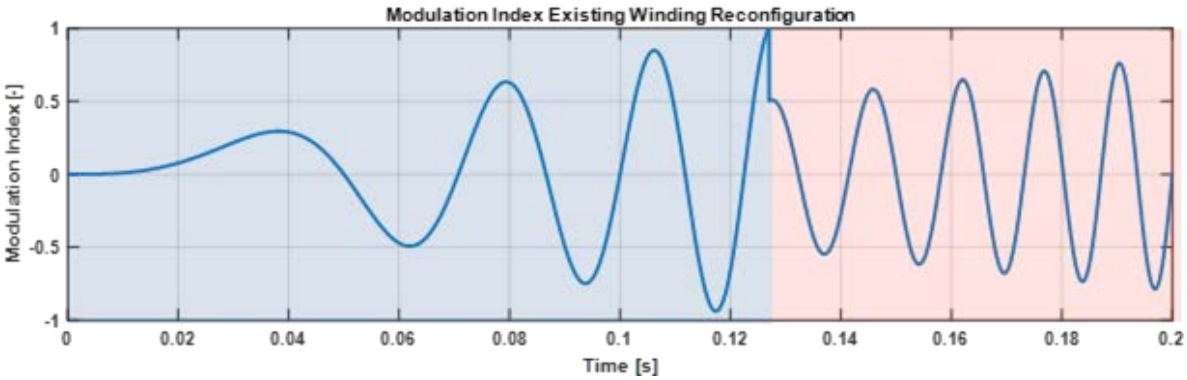

Figure 3.10: *Simplified representation of velocity-based winding reconfiguration* [28].

simple to implement this method has several disadvantages:

- The voltage produced by the inverter is the sum of the back-EMF and the voltage drop over the winding. The DC supply can vary considerably because depending on battery characteristics.
- The condition that allows to change configuration from series to parallel, actually does not just depend on the speed of the motor but also on the load or torque that is produced.
- Above the switch-over speed, the windings are continuously driven in the "parallel" configuration, although this is only really necessary during the peaks of the inverter voltage. Hence the losses in the inverter circuit increase more than absolutely necessary [28].

A method that allows to reduce the losses introduced by the long times of the parallel configuration and at the same time increase the velocity range consists of switch over from one series to parallel configuration only when the modulation index exceeds one. The difference from the previous method is that when the modulation index drops below one, the windings can be connected again in series. The process is illustrated by Figure 3.11.

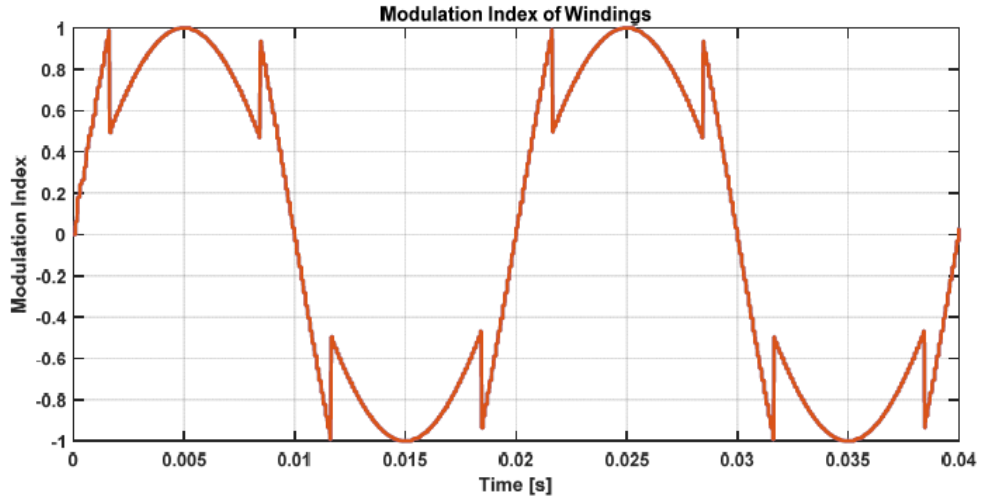

Figure 3.11: *Reconfiguration of windings by modulation index* [28].

Unlike Figure 3.10 where once the index equal to 1 has been reached, the parallel configuration was maintained, here is maintained until the modulation index drops below the hysteresis threshold, in our case fixed at 0.5. In this way it is not necessary to use the parallel configuration beyond the necessary, the series connection is used for about $\frac{1}{3}$ of the time, leading to a considerable reduction in switching losses. On the other hand, the series switches are more used than in the other method but they toggle only few times per cycle so the switching losses will be low compared to the other switches. The shape of the modulation index signal is depicted in Figure 3.12:

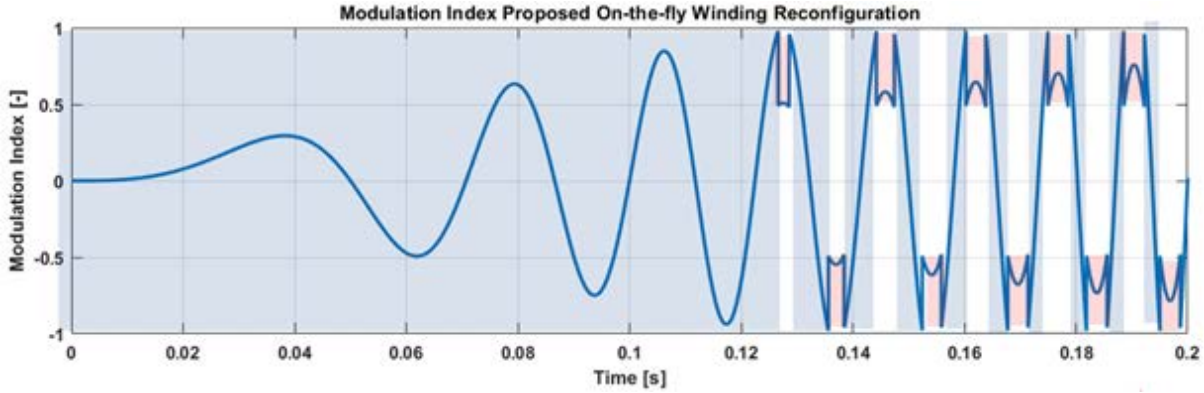

Figure 3.12: *Simplified representation of modulation index-based winding reconfiguration, the red parts indicate the time spent in independent mode and blue the time spent in series mode* [42].

The last method presented before going to the one used in this work consists in using pulse width modulation (PWM) for the series switches, this essentially brings two benefits:

1. A more equal distribution of losses between the phase leg switches so it is possible to increase the current rating.

2. A more equal distribution between the phase leg switches and series switches, problem of the previous method, also this as the previous point allows to increase the current rating.

This method uses a current controller with a modulation index as output and gate control based on the switching of the winding. The difference compared with a conventional current control is that the first half winding and the second one have the same current during series operation because one of two switches S1 or S2 is closed, while the current could be different in the two half winding, due to differences in inductances, during the parallel configuration so it is necessary to balance the load current between both windings. For this reason the controllers that are being used in this system are sum and difference controllers, since the sum controller can always be used to control the current through the windings, in series or independent mode, and the difference controller can regulate the difference in current between the windings when in independent mode [42].

3.4 Project execution

The approach used for the calculation of the times of the different configurations is that used for the matrix converter then using the the Moore-Penrose pseudo-inverse of the

matrix but nothing makes it necessary to use this method also the other explained above are valid. As mentioned previously, the problem to be studied is symmetrical, therefore it is possible to study only the transition from the series1 to parallel configuration because the transition from parallel to series2 is similar. Given a certain input variable to follow which may be a voltage or a current, it is necessary to search among all the possible configurations of the two inverters, the optimal one. There will be an optimal configuration for the phase leg switches for the series configuration that will have to remain for a time T_s and an optimal configuration of the phase leg switches for the parallel configuration that will have to remain for a time T_p where:

$$T_k = T_s + T_p \tag{3.20}$$

where T_k is half of total period because only half of the total problem is being studied. The first step will therefore be to compute all the possible configurations of the phase leg switches of the two inverters and then decide on a criterion according to which to choose the best one. In the following study all the possible configurations will be taken into consideration, it could also be continued with a reduced number, for an effective exploitation of the two inverters in this way it is also possible to balance the losses of the inverters. Referring to the circuit of Figure 3.12, for the series1 configuration there are 4 possible configurations, simultaneous closing of the switches: S_1 and S_8; S_4 and S_5; S_1 and S_4 and finally S_5 and S_8 (where with S_X mean the switch constitute by the antiparallel of the $IGBT_x$ and of the D_x diode), other configurations have been neglected because they lead to the DC-bus short circuit. Now referring to the parallel circuit of Figure 3.1 there are 16 possible configurations, for the sake of clarity all 16 possible combinations will not be explained, the procedure to be followed is analogous to the one done for the series1 circuit only that now there are two inverters. To consider all the possible combinations during the time T_k it is necessary to put together both those of the series configuration and those of the parallel configuration, obtaining a total number of configurations equal to 64. The next step is to create a matrix that takes into account the closing/opening of all the switches, so that it was possible to relate the DC-bus voltage to the output one, as done for the matrix converter.

When considering the possible combinations of the voltages of the two configurations, there are two substantial differences:

1. **The voltage value:** in the series configuration there are voltage values equal to $\pm\frac{1}{2}U_{dc}$ or zero voltage, the latter case is represented in Figure 3.13; while for the parallel configuration it still has the zero voltage value but the other values are double $\pm U_{dc}$.

2. **Windings' connection:** in the series configuration the two half windings are closely related, the voltage in a winding is identically equal to the other, pair of equal values are obtained, for example $(\frac{U_{dc}}{2};\frac{U_{dc}}{2})$; $(-\frac{U_{dc}}{2};-\frac{U_{dc}}{2})$ and finally (0,0). For the parallel configuration the voltage present in a winding is independent of that present in the other, in fact there are 16 combinations.

Taking into consideration the above clarification just made it is possible to write the voltage of the two half windings, as follows:

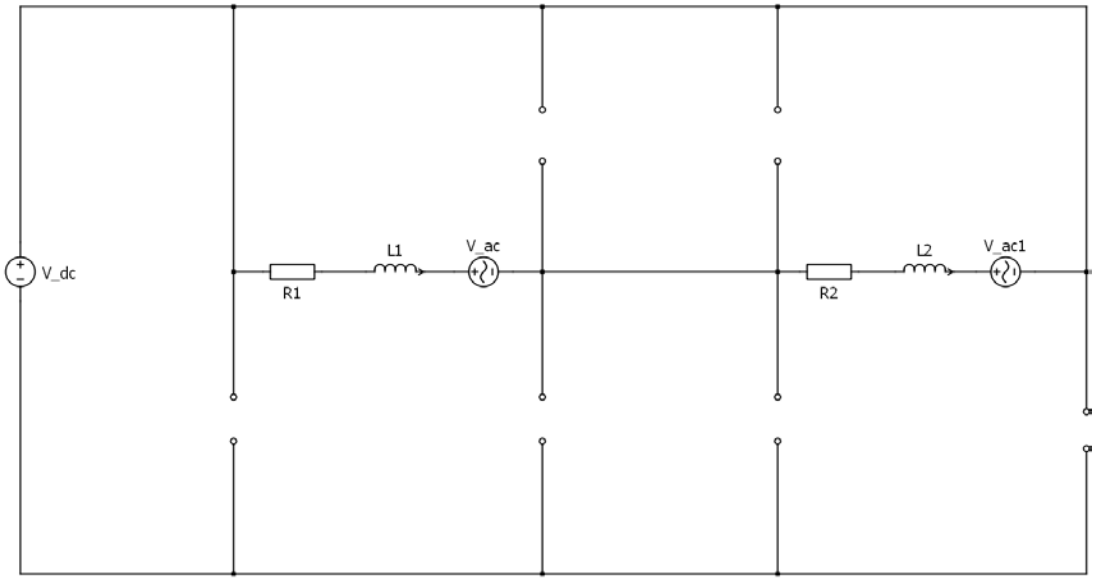

Figure 3.13: *Configuration in which the two windings have zero voltage, as can be seen the switches T_1, T_4 and the switch to allow the series configuration are closed .*

$$\begin{pmatrix} \boldsymbol{U}_1 \\ \boldsymbol{U}_2 \end{pmatrix} = \pm 1/0 \begin{pmatrix} \frac{U_{dc}}{2} \\ \frac{U_{dc}}{2} \end{pmatrix} \frac{T_1}{T_k} + \begin{pmatrix} \pm 1/0\, U_{dc} \\ \pm 1/0\, U_{dc} \end{pmatrix} \frac{T_2}{T_k} \pm 1/0 \begin{pmatrix} \frac{U_{dc}}{2} \\ \frac{U_{dc}}{2} \end{pmatrix} \frac{T_3}{T_k} + \begin{pmatrix} \pm 1/0\, U_{dc} \\ \pm 1/0\, U_{dc} \end{pmatrix} \frac{T_4}{T_k} \tag{3.21}$$

Where the time for the series configurations T_s is divided into two, T_1 for the series1 configuration and T_3 for the series2 configuration; the same is done for the parallel one T_p that is divided into T_2 and T_4. Obviously the (3.20) it is still valid so:

$$T_k = T_1 + T_2 + T_3 + T_4 \tag{3.22}$$

Using (3.21) is possible to obtain the voltage of the two half windings in a period, this value is given by the contribution of all 4 different configurations, directly proportional to the time that this configuration is maintained in a period. The symbol $\pm 1/0$ is a compact way, to indicate that the value considered could be $\pm U_{dc}$ or 0 depending on how the switches are closed, note that during the series configuration the symbol is inside the brackets while during the parallel configuration it is outside, this is due to the fact that during the parallel times $\boldsymbol{U}_1$ is independent from $\boldsymbol{U}_2$ while during series times the values must be equal so it is possible to take the symbol out of the brackets. As mentioned several times, only half of the period will be consider so (3.21) it becomes:

$$\begin{pmatrix} \boldsymbol{U}_1 \\ \boldsymbol{U}_2 \end{pmatrix} = \pm 1/0 \begin{pmatrix} \frac{U_{dc}}{2} \\ \frac{U_{dc}}{2} \end{pmatrix} \frac{T_1}{T_k} + \begin{pmatrix} \pm 1/0\, U_{dc} \\ \pm 1/0\, U_{dc} \end{pmatrix} \frac{T_2}{T_k} \tag{3.23}$$

In this equation the unknowns are not the two voltages but rather the two times T_1 and T_2 for which the two configurations must be applied, so (3.23) must be rewritten. The first approach used is to add a new equation for the times $T_m = T_1 + T_2$. So (3.23)

becomes:

$$\begin{pmatrix} \boldsymbol{U}_1 \\ \boldsymbol{U}_2 \\ 1 \end{pmatrix} = U_{dc} \begin{bmatrix} \pm 1/0 & \pm 0.5/0 \\ \pm 1/0 & \pm 0.5/0 \\ 1 & 1 \end{bmatrix} \begin{pmatrix} \frac{T_1}{T_m} \\ \frac{T_2}{T_m} \end{pmatrix} \tag{3.24}$$

$$\begin{pmatrix} T_1 \\ T_2 \end{pmatrix} = \frac{T_m}{U_{dc}} \begin{bmatrix} \pm 1/0 & \pm 0.5/0 \\ \pm 1/0 & \pm 0.5/0 \\ 1 & 1 \end{bmatrix}^+ \begin{pmatrix} \boldsymbol{U}_1 \\ \boldsymbol{U}_2 \\ 1 \end{pmatrix} \tag{3.25}$$

where the two times were obtained using the Moore-Penrose pseudo-inverse of the matrix. This method does not lead to an effective solution because zero vectors have not been excluded and as seen the method of Moore-Penrose pseudo-inverse of the matrix cannot be used with zero vectors. This procedure is valid if the I-V plane method is used. For the solution of the equation system a very similar procedure is used with some small changes. Starting from (3.23):

$$\begin{pmatrix} \boldsymbol{U}_1 \\ \boldsymbol{U}_2 \end{pmatrix} = U_{dc} \begin{bmatrix} \pm 1/0 & \pm 0.5/0 \\ \pm 1/0 & \pm 0.5/0 \end{bmatrix} \begin{pmatrix} \frac{T_1}{T_m} \\ \frac{T_2}{T_m} \end{pmatrix} \tag{3.26}$$

Where it is possible replace $T_2 = T_m - T_1$ and obtain:

$$\begin{pmatrix} \boldsymbol{U}_1 \\ \boldsymbol{U}_2 \end{pmatrix} = U_{dc} \begin{bmatrix} \pm 1/0 & \pm 0.5/0 \\ \pm 1/0 & \pm 0.5/0 \end{bmatrix} \begin{pmatrix} \frac{T_1}{T_m} \\ \frac{T_m - T_1}{T_m} \end{pmatrix} \tag{3.27}$$

In this way the problem to be studied is passed from a system of two unknowns or from a single vector unknown to a single scalar equation, where the only unknown is T_1. With some simple mathematical passage from (3.27) it is possible to compute T_1:

$$\begin{pmatrix} \frac{\boldsymbol{U}_1}{U_{dc}} \\ \frac{\boldsymbol{U}_2}{U_{dc}} \end{pmatrix} = \begin{bmatrix} \pm 1/0 & \pm 0.5/0 \\ \pm 1/0 & \pm 0.5/0 \end{bmatrix} \begin{pmatrix} 1 \\ -1 \end{pmatrix} \frac{T_1}{T_m} + \begin{bmatrix} \pm 1/0 & \pm 0.5/0 \\ \pm 1/0 & \pm 0.5/0 \end{bmatrix} \begin{pmatrix} 0 \\ 1 \end{pmatrix} \tag{3.28}$$

$$T_1 = \left[\begin{bmatrix} \pm 1/0 & \pm 0.5/0 \\ \pm 1/0 & \pm 0.5/0 \end{bmatrix} \begin{pmatrix} 1 \\ -1 \end{pmatrix} \right]^+ * \left[\begin{pmatrix} \frac{\boldsymbol{U}_1}{U_{dc}} \\ \frac{\boldsymbol{U}_2}{U_{dc}} \end{pmatrix} - \begin{bmatrix} \pm 1/0 & \pm 0.5/0 \\ \pm 1/0 & \pm 0.5/0 \end{bmatrix} \begin{pmatrix} 0 \\ 1 \end{pmatrix} \right] T_m \tag{3.29}$$

The result of the first square bracket is a vector of dimension 1x2 while the second square bracket gives a 2x1 vector, multiplying them the result is actually a scalar. After calculating the time T_1 using (3.29) is simple to compute T_2, remembering that $T_2 = T_m - T_1$ with T_m know. By this method it is possible to calculate the times to be applied to the two different configurations based on the voltage required on the two windings, therefore effectively a voltage controlled system is being implemented, it will be explained later how to change the method to obtain a current controlled system. The equation (3.29) must be resolved for each possible configuration of the two inverters, 64 times in total; this is done by changing the two matrices that take into account which switches are closed. Not all the solutions obtained from this resolution are valid,

in fact it is necessary to exclude all the solutions which have negative values of T_1 or T_2. Actually, these solutions have not been neglected in the script in order not to lose too many potentially useful solutions, it has been preferred to adapt the unacceptable solution to the nearest limit case. For example, if one of the two times T_1 or T_2 was negative the relation $T_m = T_1 + T_2$ means that one of the two times is greater than T_m and this is not acceptable. To accept these solutions too, this value has been set equal to T_m and the negative time equal to zero in to respect: $T_m = T_1 + T_2$. In the script, a vector called $\boldsymbol{t}$ of size 64x2 was created that took into account the times of each combination. This vector has been replaced in the following equations:

$$\begin{pmatrix} \boldsymbol{U}_{1real} \\ \boldsymbol{U}_{2real} \end{pmatrix} = U_{dc} \begin{bmatrix} \pm 1/0 & \pm 0.5/0 \\ \pm 1/0 & \pm 0.5/0 \end{bmatrix} \begin{pmatrix} \frac{T_1}{T_m} \\ \frac{T_2}{T_m} \end{pmatrix} \tag{3.30}$$

The formula (3.30) is the same as (3.24), the difference is that in the latter, the given voltage values were used to compute the times while in (3.30) the calculated times are entered to obtain the voltage values that are actually applied in the two motor windings during each of the 64 combinations. Obviously the discrepancy between the given value and the one actually applied must be as small as possible, ideally tending to zero. A very simple scheme that clearly summarizes what has been done is presented below: As shown in the diagram, is done for all 64 combinations and then among all

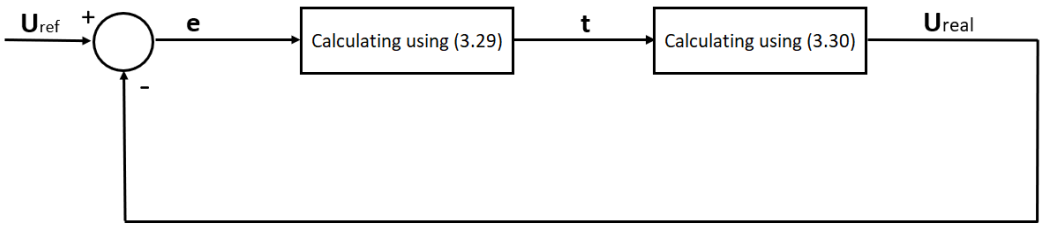

Figure 3.14: *Simple scheme that summarizes the voltage control, in the scheme* $\boldsymbol{U}$*,* $\boldsymbol{t}$ *and* $\boldsymbol{e}$ *are vector of two components.*

the possible configurations it was chosen the one that minimizes the error between the given voltage and the voltage that actually applied in the two motor windings. As shown in Figure 3.14, it is necessary to compare each time, two voltage values between them, therefore the calculation of the error will not be a simple algebraic difference but a vector difference. It is possible to find the minimum error among all possible combinations minimizing the norm function of the error vector. The calculation of the 64 positions with the respective matrices, whose elements are 0; 0.5 and 1, were made using a MATLAB script, as shown in Figure 3.15:

```
Q=[0 0 1 1];
P=[0 1 0 1];
r=Q-P;
s=(Q-P)/2;
    for y=1:4
    for w=1:4
    for z=1:4
        S12(L,:)=[Q(w),P(w)];          % switches 1,2 during T1
        S34(L,:)=[Q(y),P(y)];          % switches 3,4 during T1
        S56(L,:)= not([Q(w),P(w)]);    % switches 5,6 during T1
        S78(L,:)= not([Q(y),P(y)]);    % switches 7,8 during T1
        SS14(L,:)=[Q(z),0,0,P(z)];     % switches 1,2,3,4 during T2
        SS58(L,:)=[not(Q(z)),0,0,not(P(z))]; %switches 5,6,7,8 during T2
        B=[r(w),s(z);r(y),s(z)];
        A(1:2,j:j+1)=Udc*B;
    C=[r(w),s(z);r(y),s(z);1/Udc,1/Udc];
    t1=pinv(B*[1;-1])*(U/Udc-B*[0;1])*Tk;
```

Figure 3.15: *Part of the entire script, used for calculating the 64 matrices linked to the switches' position, which defines the voltage applied in the two half windings.*

First, two vectors called "P" and "Q" have been defined and they will be used to create all the matrices. Starting from these two vectors, two more have been obtained, to go to differentiate the values equal to 1 for the parallel configuration and the values equal to 0.5 for the series configuration. To cycle all the values within the matrix that in the script is called "B", 3 for loop were used, each of 4 iterations for a total of 64. These 3 indices change the component of the vectors "r" and "s", defined starting from "Q" and "P", so as to obtain the desired matrix. The "B" matrix is made by 0,1,0.5 which will be useful to compute the times of the two different configurations through the use of the Moore-Penrose pseudo-inverse of the matrix which in MATLAB is calculated using the "pinv" command. For the project it is not important to have only the time but also the position of the switches for each configuration so that it is then possible to extract this information from the script and control the two inverters. To define the position of the 8 switches for each of the 64 configurations the two vectors "Q" and "P" previously defined were used. In the script, the name of the switches were differentiated during the parallel configuration by calling them with a single "s" from the one during the series configuration, calling them with a double "s" while the switch number specifies which switch is working, number that can be found in Figure 3.8. For the parallel configuration there are 16 different combinations, this means that they can be studied using only 2 of the 3 indexes of the for loop, the last one will be used for the 4 combinations of the series configuration. During the parallel configuration, the eight switches have been divided and controlled in pairs so it is not necessary to control every one of the eight switches. Actually, the switches of each leg must never be closed at the same time, therefore they can be controlled using logical complement, further simplifying the control of the eight switches. During the series configuration having only 4 combinations, things are further simplified, in addition to controlling the switches in the same inverter's leg in logical complement, the four central switches of the two inverters always open are not used, as shown in Figure 3.7, and for this reason

they are set to zero. Inside the loop, the switching of the central switch allows the configuration to be changed, this because the switch changes its state once the time has elapsed. In the script, in addition to the concerning part the calculation of the switching time and the definition of the states of the switches, there is the calculation part of the error and the choice of the minimum. The input requires only 4 parameters, as shown in Figure 3.16: the two voltages on the two half windings coming from the control loop, the T_m time and the bus voltage U_{dc}, these two known a priori. In

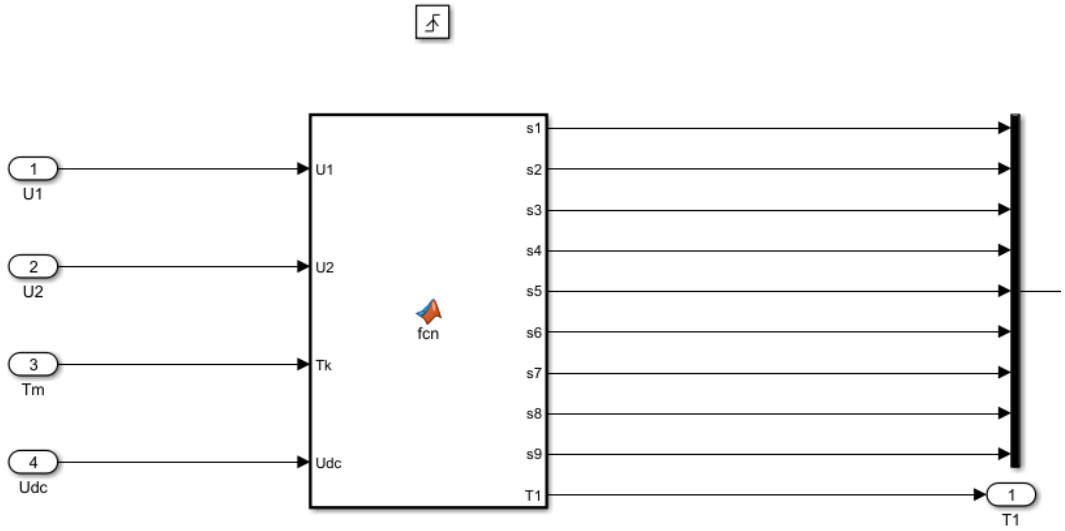

Figure 3.16: *Input and output of the* MATLAB *script*

Figure 3.16 there are 9 signals representing the states of the nine switches, including the one for change from series to parallel. Each signal is a vector of two components, the first returns the state of the switch during the parallel configuration and the second component the status of the switch for the series configuration. The signals are then sent to a selector, shown in Figure 3.17, which allows to choose all the first components of the nine vectors or all the second components; the choiche will be based on a logic built on time T_1, shown in Figure 3.18. Using a clock's frequency of $100\mu s$, also used to define the computation of the switch states, a constant value is integrated to obtain a ramp. This ramp is then compared with the time T_1, if the ramp is greater than T_1, a switch selects the first nine values of the switches vector state and maintains this configuration during the time T_1; if the ramp is smaller than the T_1 value, the switch select the second nine states of the vectors and this combinations is maintained for the time T_2 or better for the time $T_2 = T_m - T_1$ because the time T_2 is never calculated directly, this is shown in Figure 3.19 or more in detail in Figure 3.20. Figure 3.20 shows the change in configuration, moreover the values assumed by the functions have been inserted, in this way it is possible to verify that the time for which the parallel configuration is really T_1 and it is equal to $70\mu s$ and that effectively the sum of the time for which the series and the parallel configurations persist is equal to the imposed value of $100\mu s$.

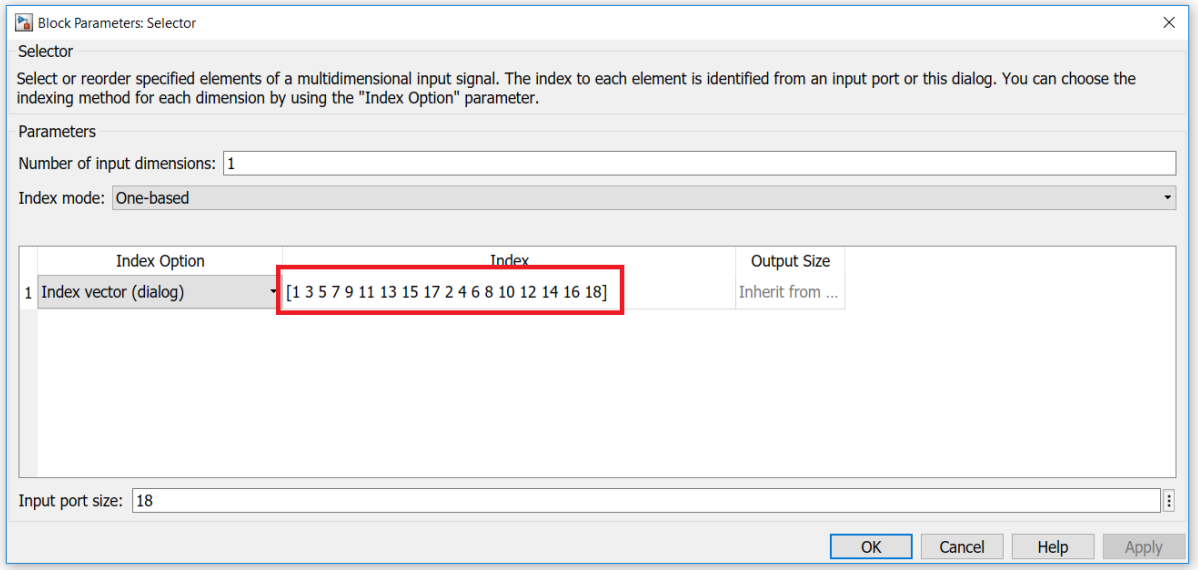

Figure 3.17: *Selector that shows how to choose all the first components or all the second ones of the 9 switches' state.*

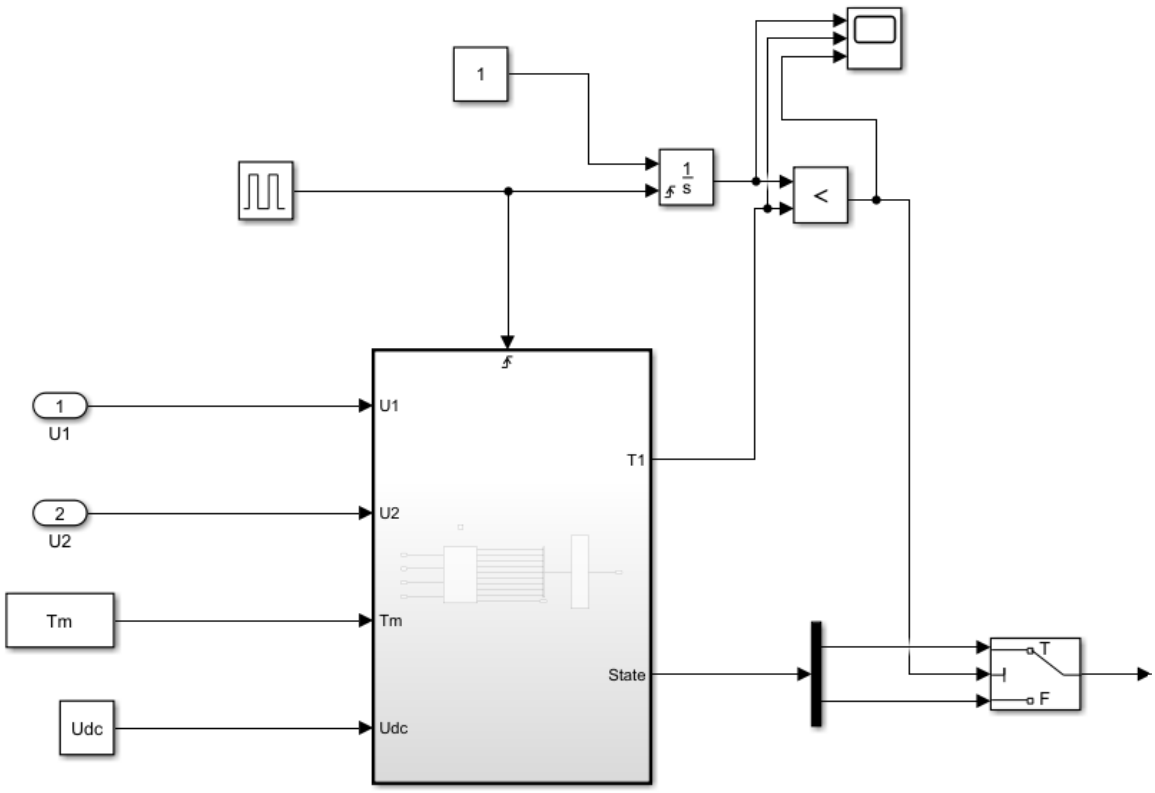

Figure 3.18: *Logic based on T_1, with which the two inverters are controlled selecting the appropriate signals to be given to the switches.*

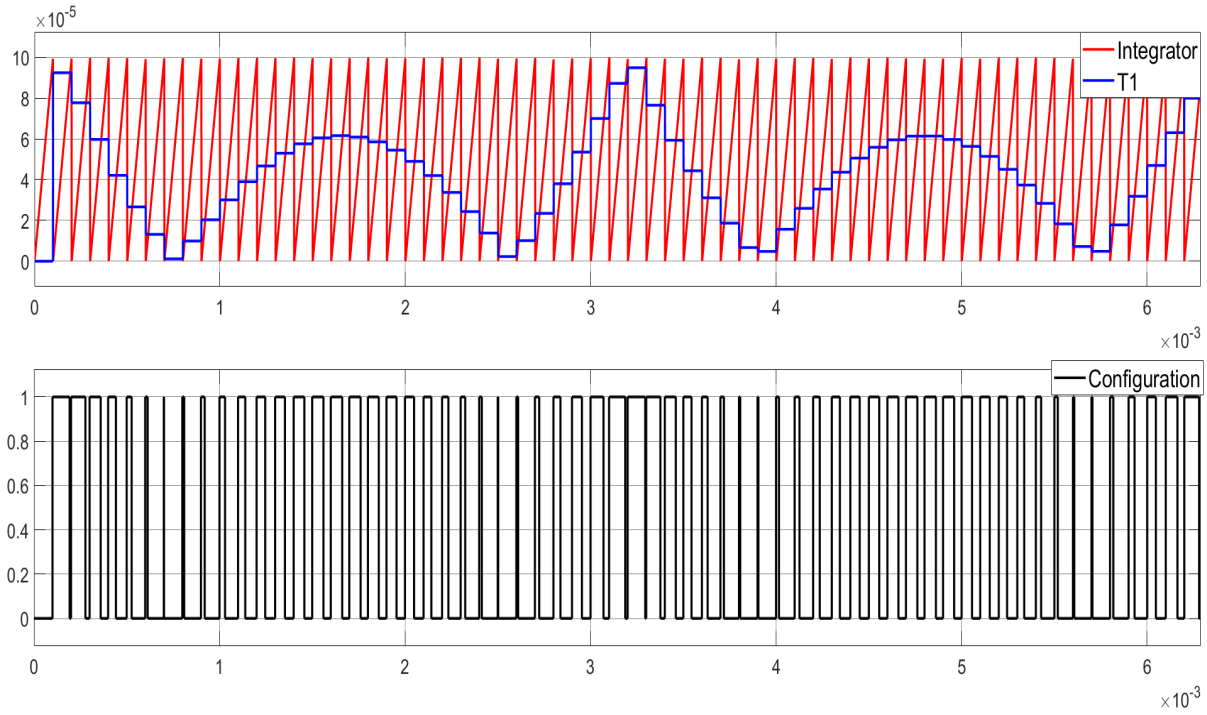

Figure 3.19: *T_1 time is compared with a ramp signal to define the transition from parallel configuration to series configuration.*

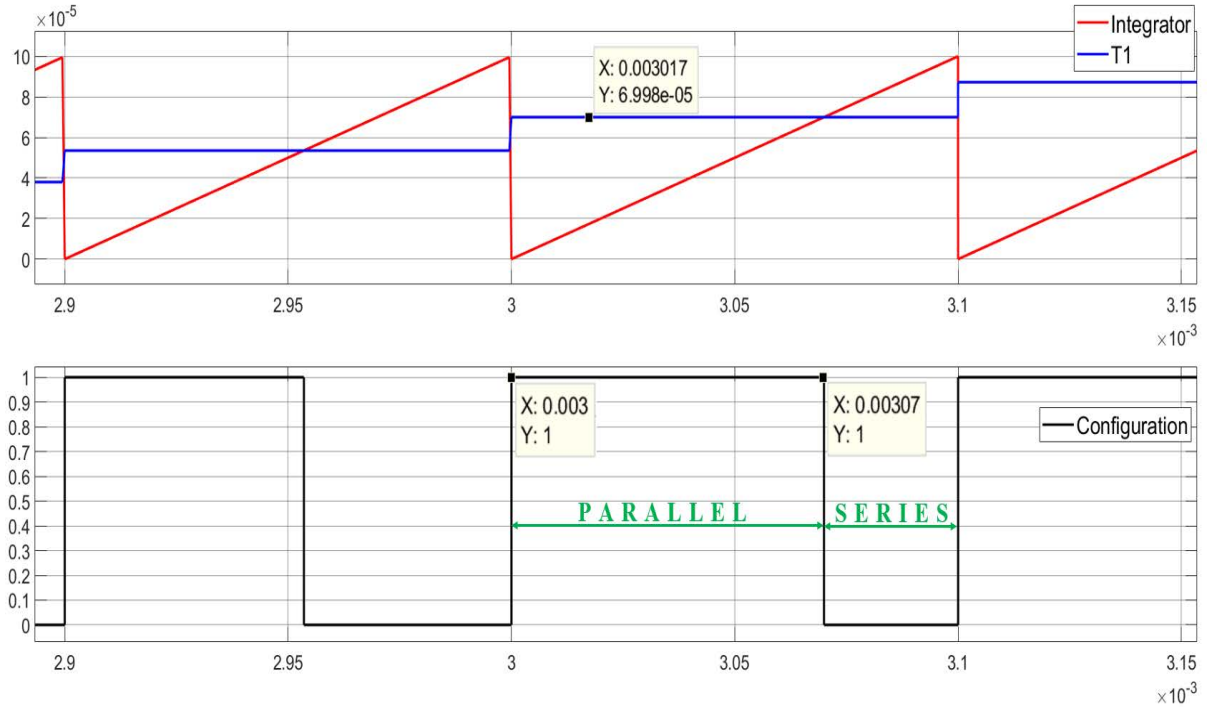

Figure 3.20: *The figure shows in greater detail the passage from the parallel configuration to the series configuration as soon as the ramp exceeds the T_1 value.*

At this point the switch states generated by the matlab script can be sent to the two inverters designed with PLECS.

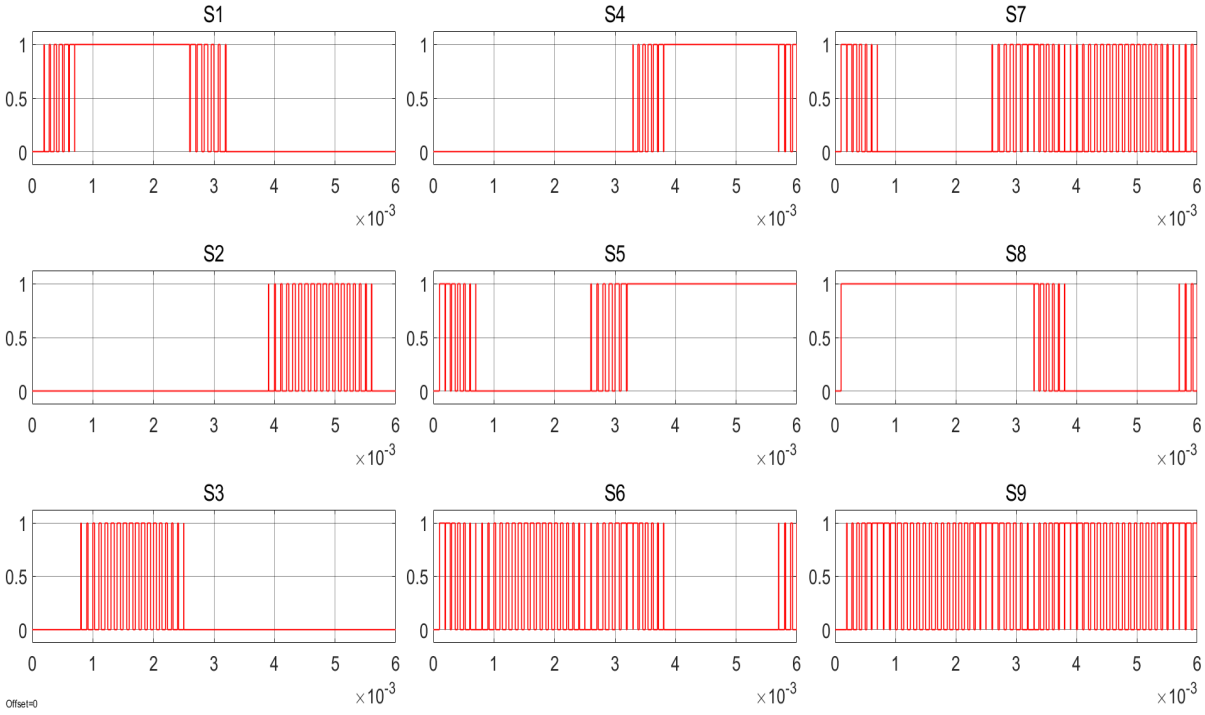

Figure 3.21: *Signal command of the 9 switches.*

Figure 3.21 shows the 9 signals of the switches, where the ninth is the one for the configuration change. From the figure it is possible to find that the switches of the same leg of the inverter vary with a logical complement as actually written in the script, like for example S1 and S5 or S2 and S6. A verification that everything works correctly is to verify that the ninth switch is open when the ramp is greater than T_1, as shown in Figure 3.22.

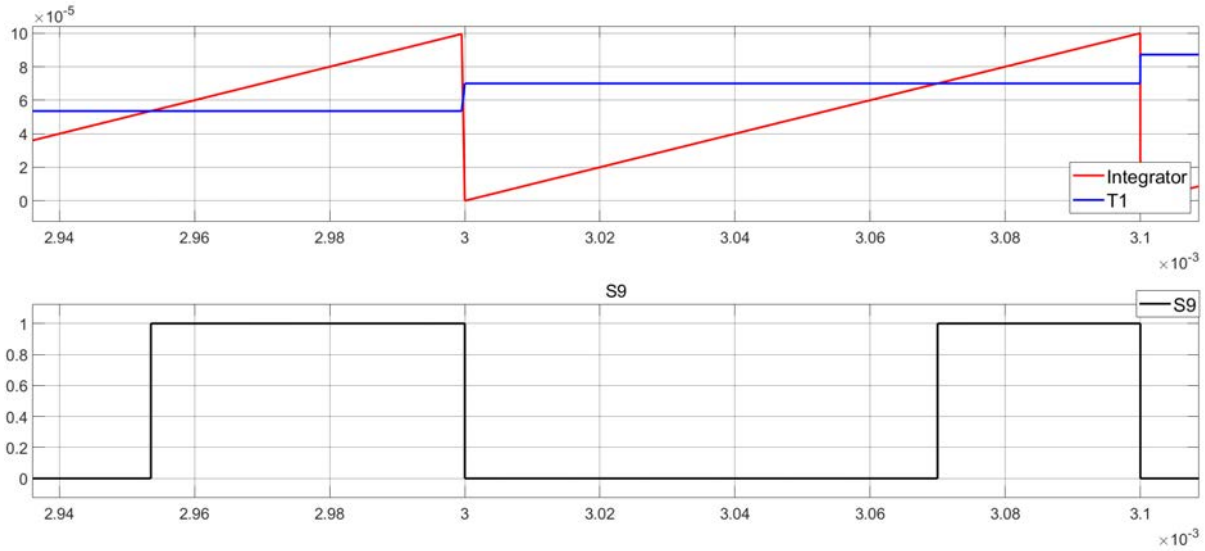

Figure 3.22: *Verification of exact command to the switch dedicated to the configuration change.*

Another aspect that can be noticed in Figure 3.22 is that not all the switches are used in the same way, some of them switch more than others. This is an aspect not to be overlooked when designing a control system, especially in the automotive sector. The fact that some switches work more than others, leads to an increase in temperature in these devices and an early deterioration of the switches. It would be possible to limit this discrepancy in the use of the switches, correcting the cost function. The cost function is at the base of predictive control. It uses the fact that only a finite number of possible switching state can be generated by a static power converter, as in our case, and that models of the system can be used to predict the behavior of the variable for each switching state. The cost function is the method that will be evaluated for the predicted values of the variables to be controlled, some expamples are current control, torque control, power control, etc [43]. In this project it was initially thought only for a current control and then adjusted. The method of choosing the best configuration to be used initially thought based only on the norm, worked correctly but for some specific current value it gave more switching than necessary ones. Below are set out the images of the simulations made initially only using the norm as the criterion of choice for the best configuration.

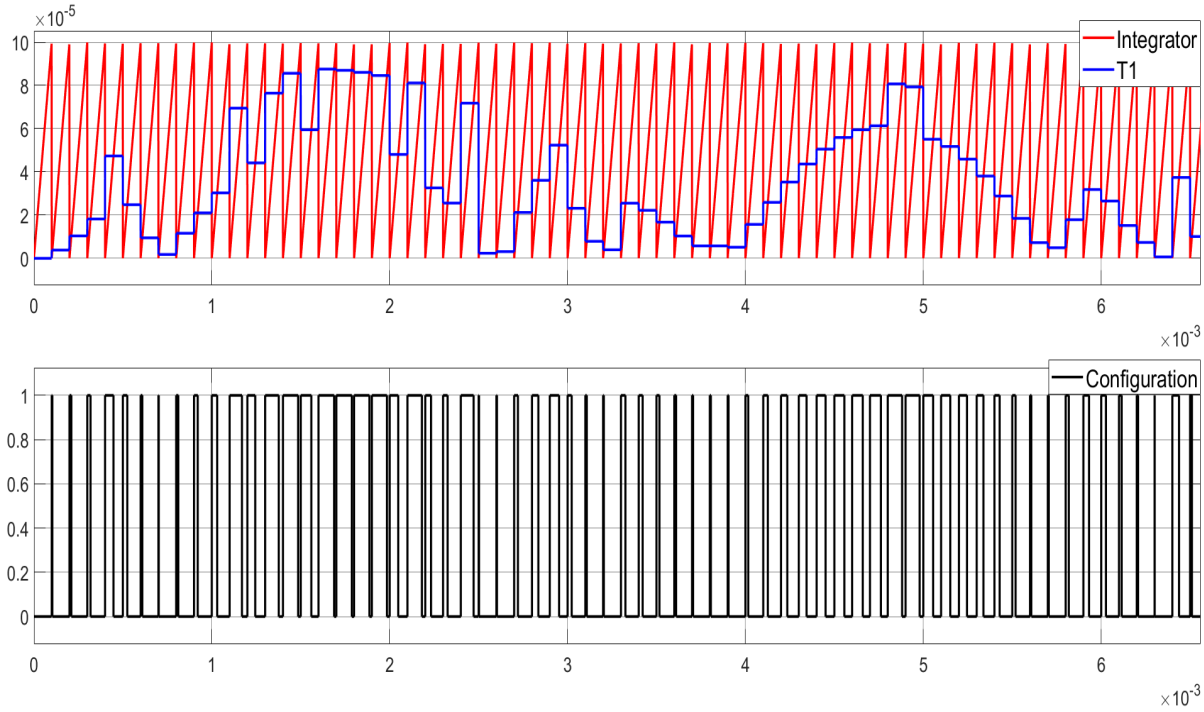

Figure 3.23: T_1 *time is compared with a ramp signal using only the criterion of the norm.*

Comparing Figure 3.23 with Figure 3.19, it is evident that in some moments the time T_1 assumes anomalous values. From the point of view of the average output current value and the minimization between the imposed value and the assumed value of the motor, this method is correct but the switches assume different positions from those assumed in the previous instance with a consequent increase in switching frequency and in the losses as shown in Figure 3.24. This problem occurs because when the script computes the norm between the imposed current value and the one assumed by the i-th combination, it can happen that several combinations have the same error and the script randomly chooses which combination to use, not caring about which

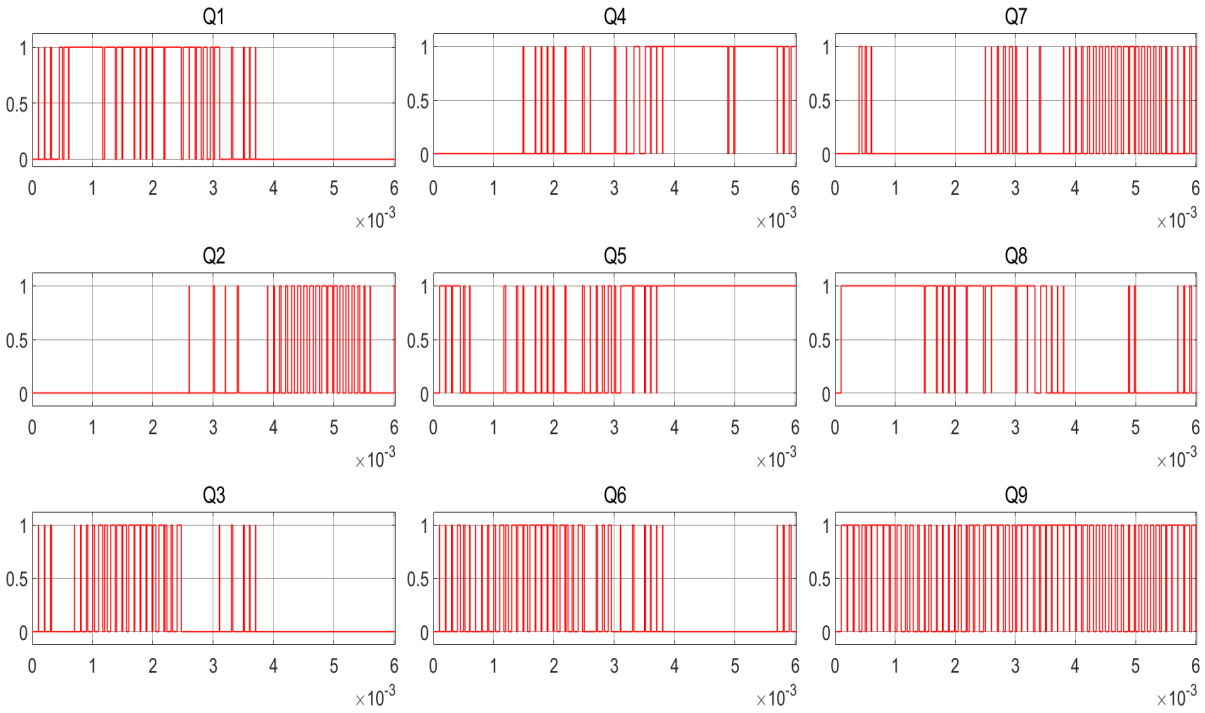

Figure 3.24: *Signal command of the 9 switches using only the criterion of the norm.*

combination is assumed in the previous instant. From Figure 3.24, it can be seen that given a sinusoidal current value as input, the choice of combination chosen by the script is not the same for every cycle and it is noted by the fact that the T_1 waveform is not periodic unlike what happened in Figure 3.21. This happens only when the result of the norm of many combinations give the same value, the following case is taken as example.

Data
T_m=10
U_1=5.8
U_2=5.8
U_{dc}=10

Case 1	
Errors	Combinations
1,26E-15	41
1,26E-15	43
1,26E-15	44
2,51E-15	42
1,131371	3
1,131371	7
1,131371	11
1,131371	15
1,131371	19
1,131371	23
...	...

Case 2	
Errors	Combinations
1,60E-09	43
4,80E-09	41
4,80E-09	44
5,87E-09	42
1,414214	3
1,414214	7
1,414214	11
1,414214	15
1,414214	19
1,414214	23
...	...

Table 3.2: *Comparison of the choice of combinations between the criterion of the norm (Case 1) and the criterion of the cost function (Case 2).*

The tables show that in the case in which the norm is used the calculated error is the same for configurations 41,43 and 44. Having the same error at the end of the average value which of these three is chosen it is irrelevant, and in the case in question, fell on the combination 41. It must be considered that the error of the combination 42 is greater than the other 3, but in practice it is equivalent. Using the cost function the indeterminacy on which configuration to choose is solved and now the best solution is the 43. The discrepancy on the error is due to the fact that now besides the norm another term has been added to the formula and this term must be multiplied by an appropriate weighting factor. Now, the cost function for calculation of the error is of the type:

$$e = ||\boldsymbol{x}^* - \boldsymbol{x}^p|| + \lambda \Big[||t_1(\boldsymbol{U}_1 - \boldsymbol{U}_{1inv})|| + ||t_2(\boldsymbol{U}_2 - \boldsymbol{U}_{2inv})|| \Big] \tag{3.31}$$

Where the first terms is the norm, used also for the case 1; λ is the weighting factor; the last one is a term that varies with the area under the function. U_{xinv} is the voltage value that is applied by the inverter to the motor winding, so for example $U_{dc} = 10V$ the U_{xinv} can be equal to $0; \pm 10$ and ± 5 using the series configuration. The concept will be better explained using the voltage output waveforms.

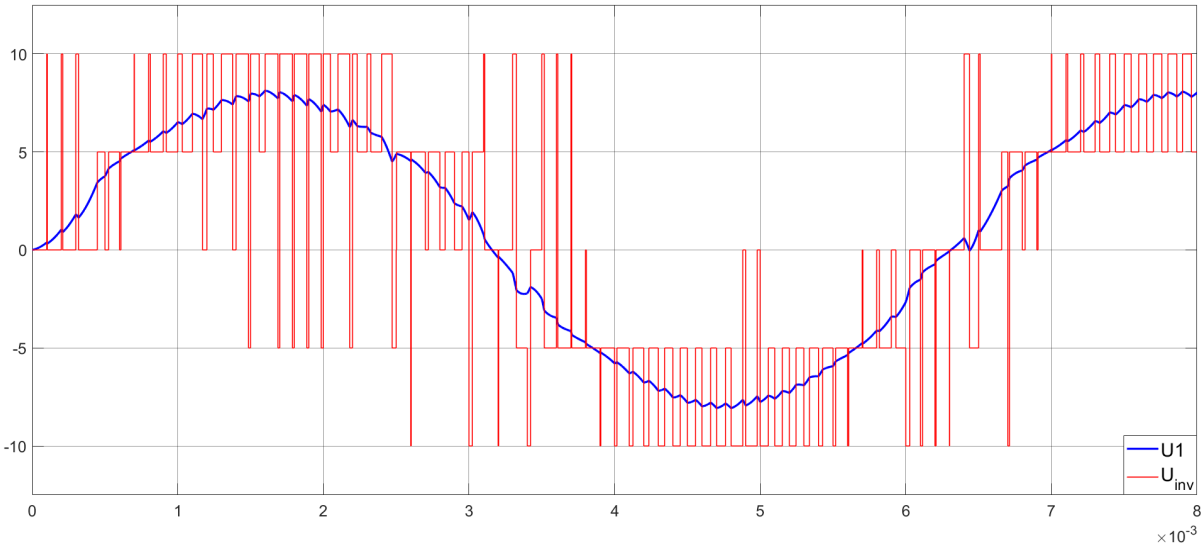

Figure 3.25: *Output voltage using the norm criterion*

The voltage waveforms both in Figure 3.25 and in Figure 3.26 follow the sine wave given in input. Using only the norm, the script in some cases, to obtain a certain average value, prefers to switch to the parallel configuration with higher voltage values than the series $\pm 10V$ and keep it for a shorter time compared to using the series configuration, consequently there are unnecessary configuration changes. The second term that has been added to the (3.31), consist in making the difference between the input value (blue line) and the inverter value (red line) and then multiplying it by the time for which this voltage is maintained. The subscript "2" does not refer to the second half winding but it refers to the voltage and to the time during the series configuration. It is important to point out that the aim of the cost function is to minimize the difference between input and output waveform. In fact it is also possible to modify the cost function so that it minimizes the switching frequency or the losses in the switches, maybe at the expense of other parameters. What has been done has served to optimize the choice of

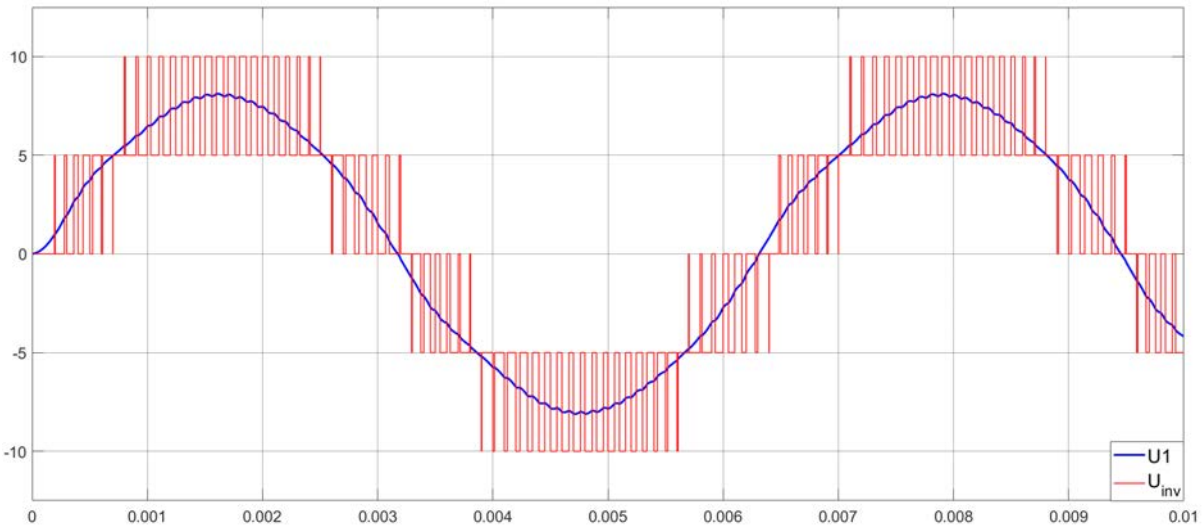

Figure 3.26: *Output voltage using the cost function criterion.*

the configuration and has resulted in a reduction in the switching frequency but this cost function was not aimed at reducing the switching frequency.
The output waveforms of the two half windings are the same because the control system is the same for both, for this reason it was decided not to show the second waveform.

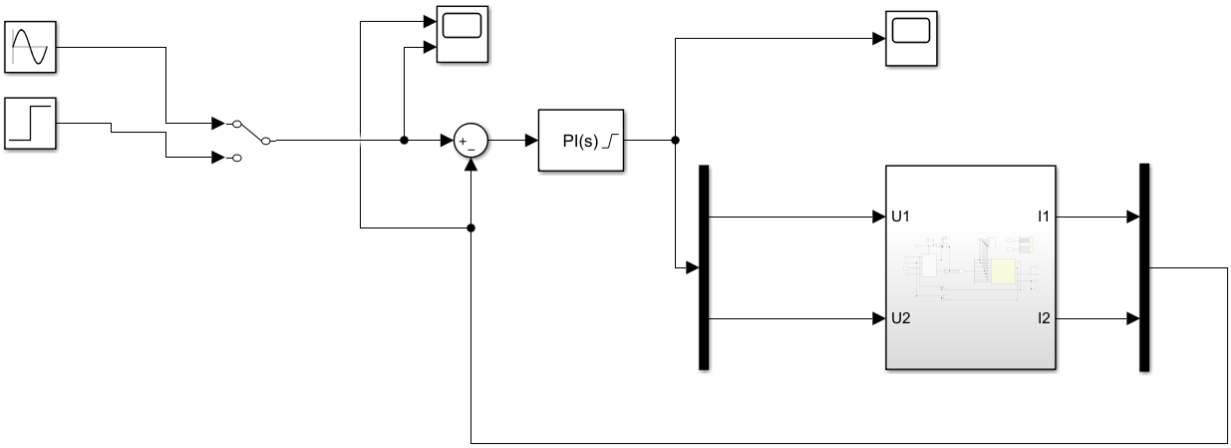

Figure 3.27: *SPMSM control system.*

The control system consists in a simple PID feedback controller and it is identical for both windings. The anti- windup has also been inserted so as to limit the output and not supply the motor with current or voltage values that could damage it. Having set the anti-windup at the same value as the DC bus, i.e 10V, if this value is exceeded the waveform would be cut off, as shown in Figure 3.30:
After several attempts the PID controller parameters were found:

- $K_i = 5500$
- $K_p = 0.1$

- $K_b = 2000$

With this values it is possible to obtain a control which is able to follow the input waveform well with rapid response times.
The project can work both with a current control and with a voltage control, initially it was started with a voltage control, which gave some problems during the parallel-to-series configuration transition, because the current on the series o f the two half windings was not perfectly equal. The motor was simulated with both a sinusoidal waveform and its step response.

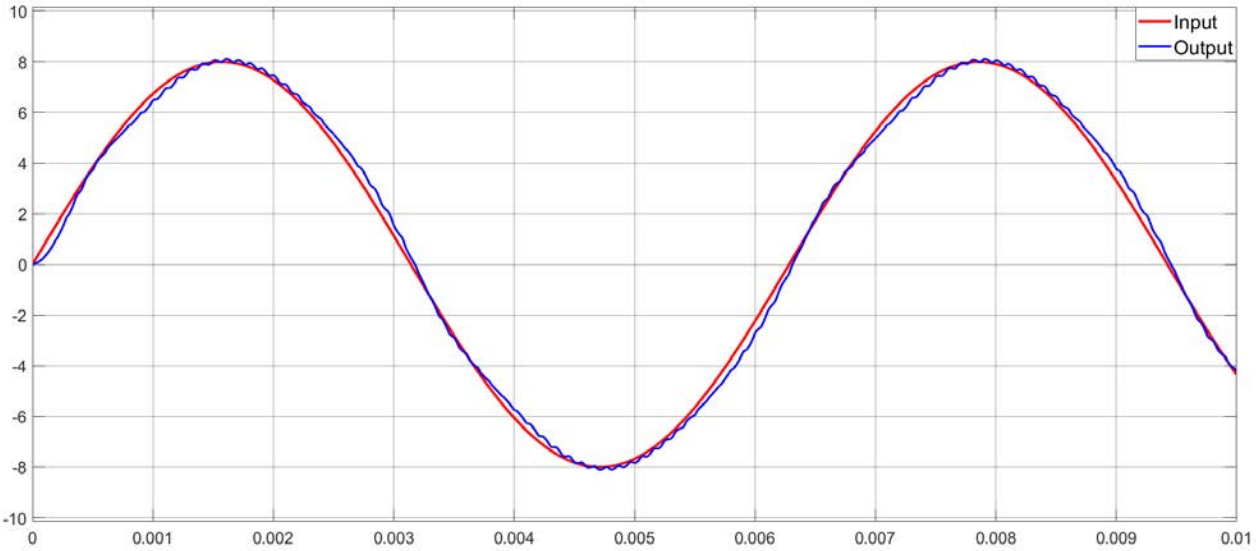

Figure 3.28: *Response of the* PID *feedback controller to a sine wave.*

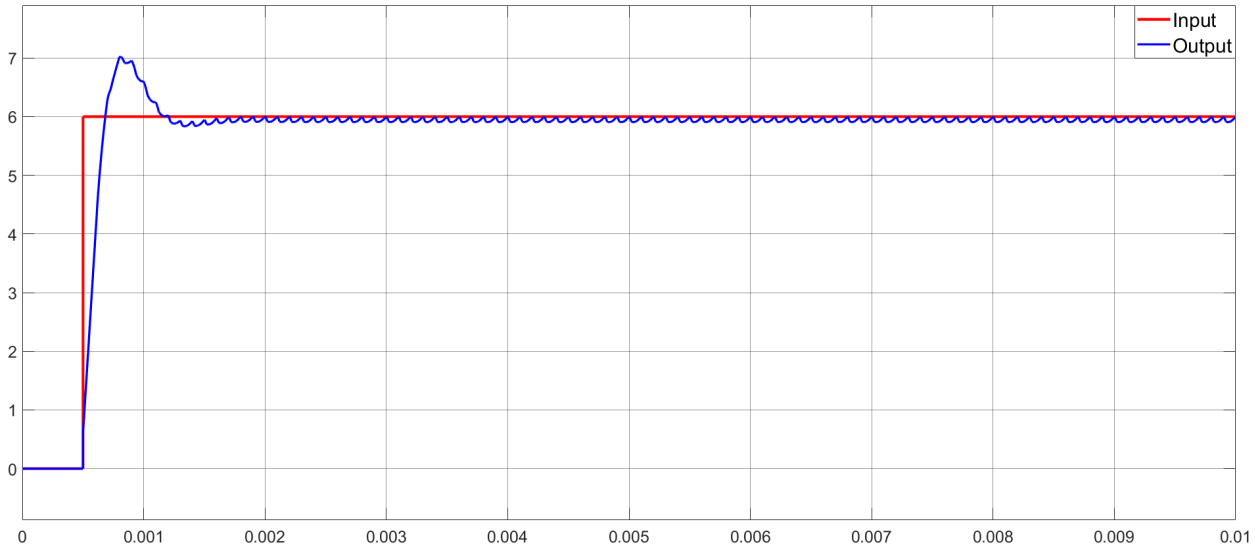

Figure 3.29: *Response of the* PID *feedback controller to step function.*

The last step is to use an interface between the physical components and create a controller in MATLAB, a dSPACE microlabbox is necessary. The occurrence of some

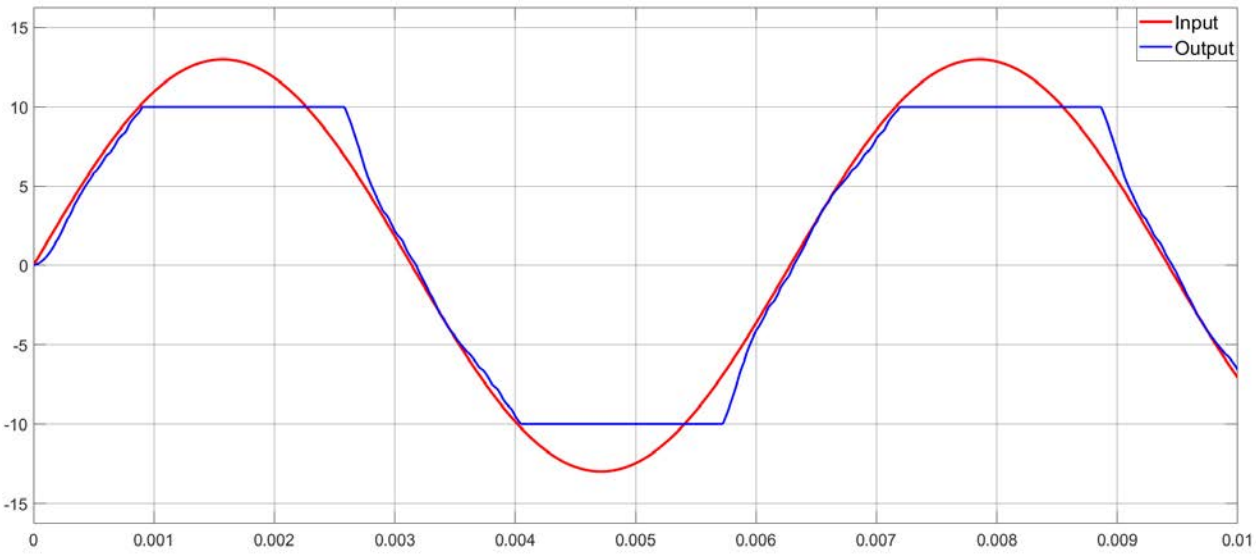

Figure 3.30: *Use of anti windup.*

problems and the lack of time did not allow this last step, so it was not possible to verify the results of the simulation on the motor present in the laboratory. The SIMULINK scheme as it was designed could not be used directly by DSPACE. The MATLAB function for the calculation of the best configuration took too long and it would not have been possible to use it for the motor control. The block with the MATLAB function with the three for loop had to be replaced by only SIMULINK blocks that did the same operation. First of all, the three for loop had to be converted from 4 iterations each into a single for loop of 64 iterations. So the calculation of the configurations seen in Figure 3.15 becomes that of Figure 3.31.

```
for y=1:64
S12(L,:)=[Q(fix((y-1)/4)+1-4*fix((y-1)/16)),P(fix((y-1)/4)+1-4*fix((y-1)/16))];
S34(L,:)=[Q(fix((y-1)/16)+1),P(fix((y-1)/16)+1)];
S56(L,:)= not([Q(fix((y-1)/4)+1-4*fix((y-1)/16)),P(fix((y-1)/4)+1-4*fix((y-1)/16))]);
S78(L,:)= not([Q(fix((y-1)/16)+1),P(fix((y-1)/16)+1)]);
SS14(L,:)=[Q(y-4*fix((y-1)/4)),0,0,P(y-4*fix((y-1)/4))];
SS58(L,:)=[not(Q(y-4*fix((y-1)/4))),0,0,not((y-4*fix((y-1)/4)))];
```

Figure 3.31: *Compute of the 64 matrices linked to the switches' position, using a single index.*

In Figure 3.32 there is only the part for the calculation of the combinations, then there is also the part for the Moore-Penrose pseudo-inverse of the matrix and finally the part for the cost function. The cyan and red signals are the known parameters, the green and orange signals are the states of the switches respectively for the parallel and series configuration, while the yellow signals are used for the calculation of the Moore-Penrose pseudo-inverse of the matrix. To find the best solution with this method, the state of the switches at all zeros and the relative error at 100 are initialized, a very large value

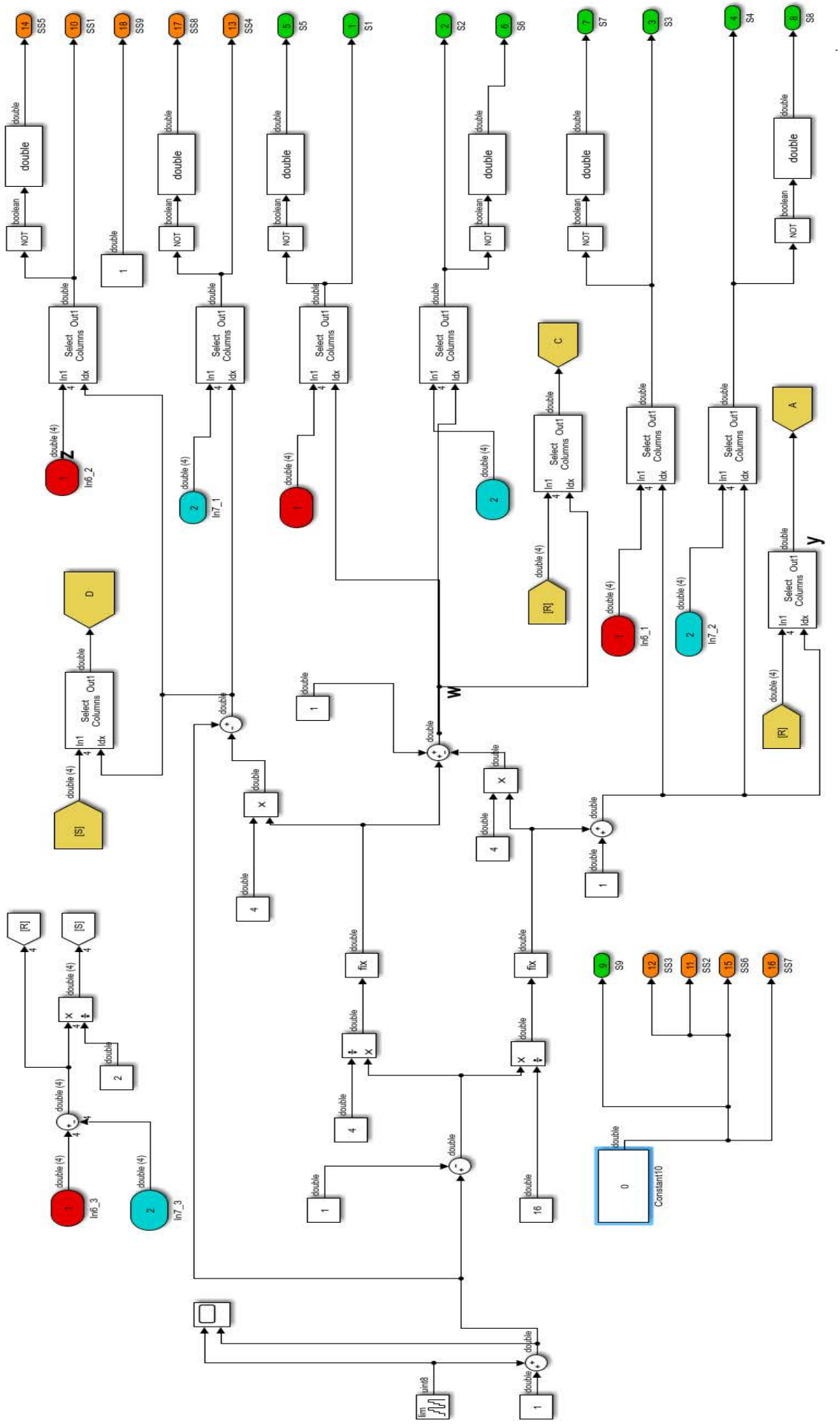

Figure 3.32: *Compute of the 64 combinations using only* SIMULINK *blocks.*

that will be impossible to obtain. From time to time the states of the switches will be calculated and the relative error compared with the previous one, the first is 100, if the error is smaller than the previous one, the combination is overwritten otherwise the previous value is maintained. At the end of the 64 iterations the best combination and the smallest error are obtained, as shown in Figure 3.33. These data are then used in the general scheme of Figure 3.34, which is the same used also for the MATLAB script.

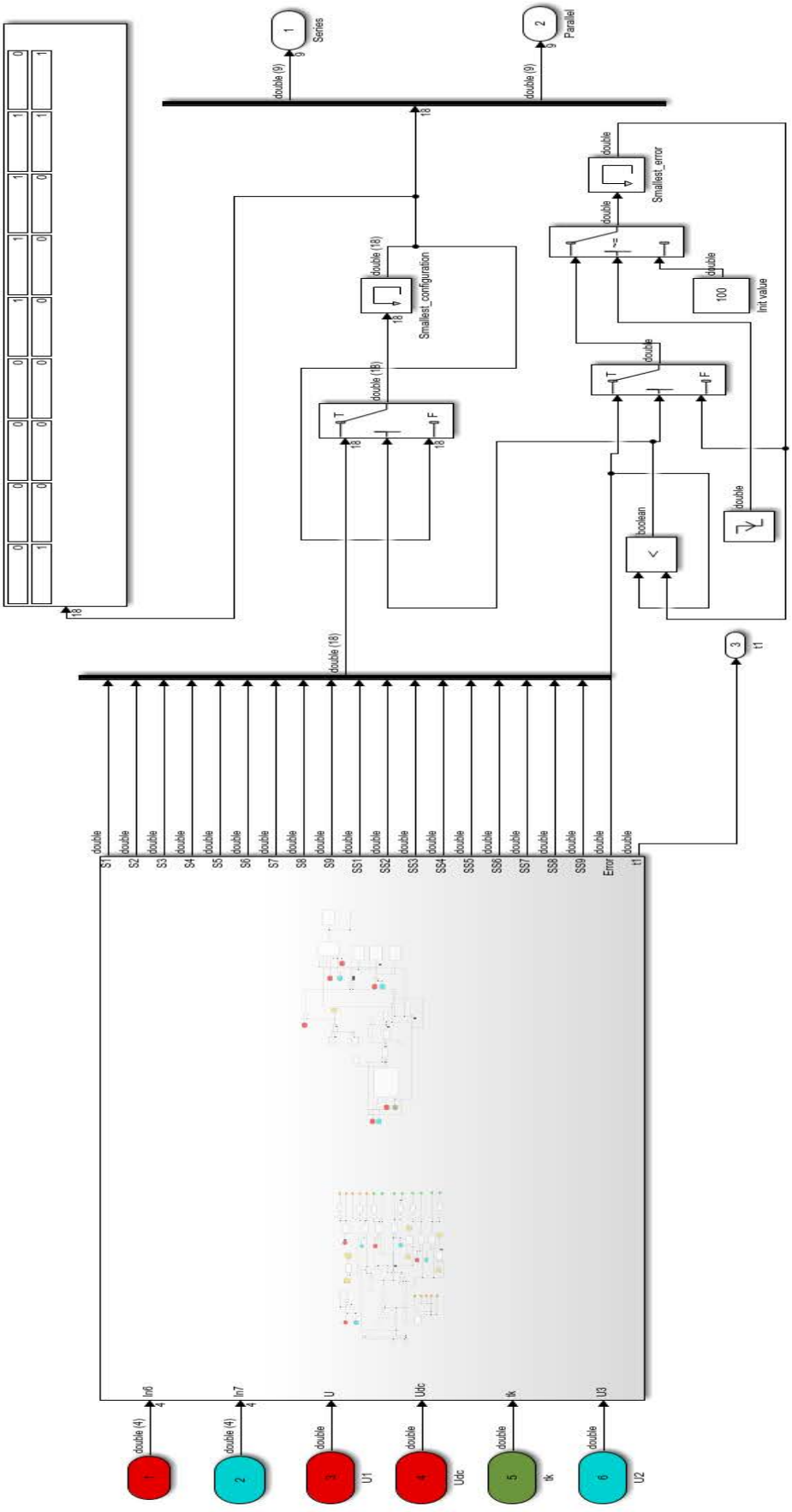

Figure 3.33: *Compute of the 64 combinations using only* SIMULINK *blocks.*

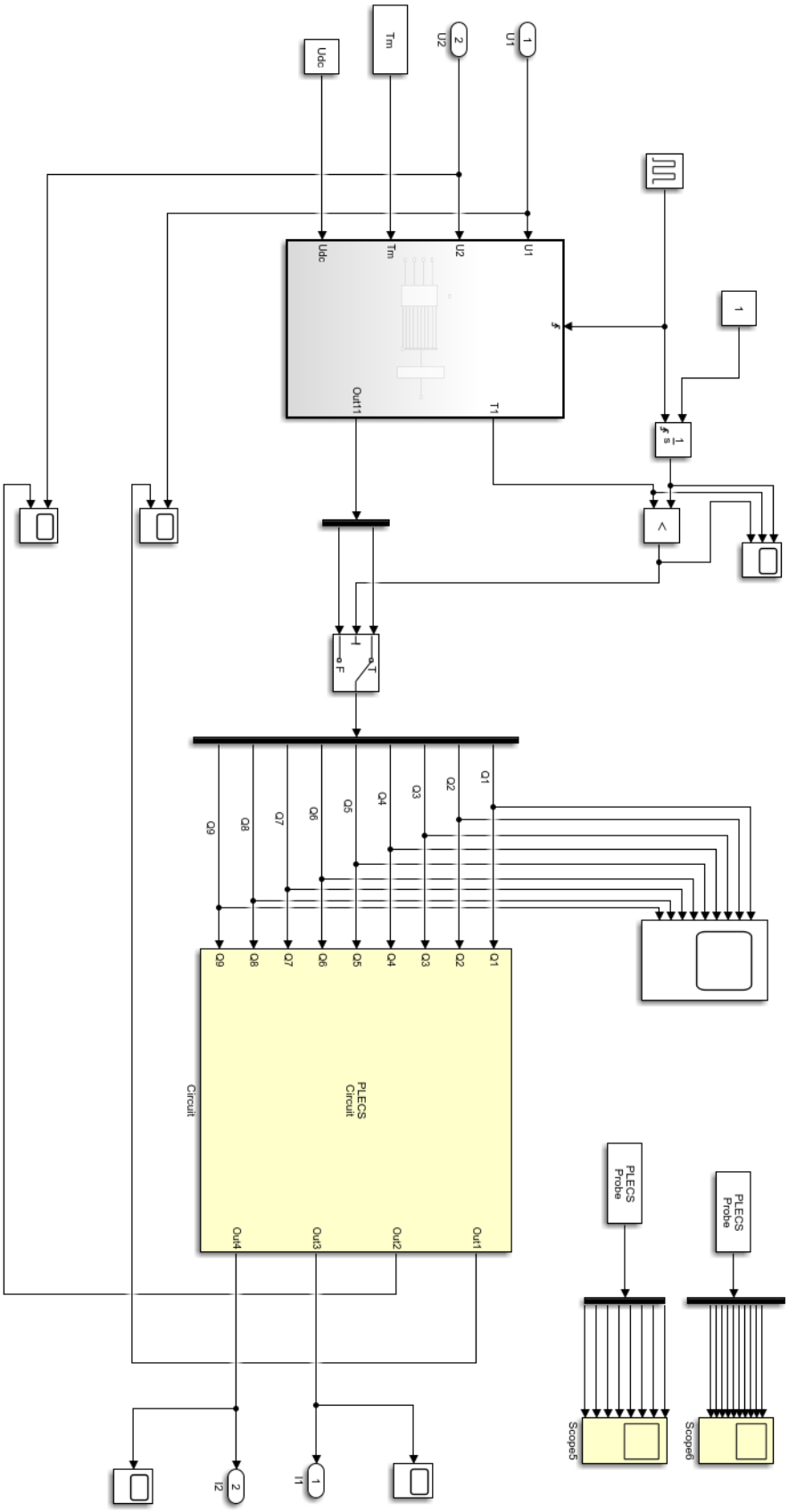

Figure 3.34: *General* SIMULINK *scheme.*

Chapter 4

Conclusion

In this thesis, an unconventional solution is presented to extend the angular velocity range of a SPMSM. The advantages and disadvantages of this technique were presented and it compared with other techniques that allow to increase the velocity range such as flux weakening and the voltage range enhancement. In this work it was necessary to model the operation of the motor and its driving circuits in detail. Given the circuit and the control technique to be used, it was necessary translate the problem into a system of equations that could be easily implemented and solved by software such as MATLAB and SIMULINK. It has been realized a control method for a single winding pair (intended to be implemented three times for a six-phase motor), allowing dynamic switching between windings in series and windings in an independent configuration. This method (which can be classified as infinite control set model predictive control) is based on a model of the motor behavior, that is used for predicting the circuit behavior one switching cycle ahead time. Doing so, the best of all 64 possible switching configurations with the associated timing can be obtained. The waveforms have been reported both of how the control system follows the given reference, and of how the switches are controlled. In this way it was possible to demonstrate that it is possible to increase the velocity range of the motor without losing the control features that present the other conventional methods.
The initial target was to also implement the thus obtained solution in a rapid prototyping system and to drive a test circuit to verify the operation in practice. Due to the realization of the intended test hardware being substantially delayed, this part of the assignment has unfortunately not been realized, as confirmed by Professor Huisman's letter. Possible future developments for this work could be to study the thermal behavior of the two inverters and of the motor and adjust the cost function so that it takes into account not only a given reference but also the thermal losses, switching frequency etc. Finally, it might give a different weight to individual contributions, based on economic aspects, thus choosing the best solution at lowest price.

List of Figures

List of Tables

Bibliography

[1] Carl Berrisford, Rolf Ganter, Kevin Dennean, and Sally Dessloch. Smart mobility. *Long Term Investment*, October 2017.

[2] James Larminie and John Lowry. *Electric vehicle technology explained*. John Wiley & Sons, 2012. Cited on pages 14, 15, 16, 18,and 19.

[3] Xavier Mosquet, Hadi Zablit, Andreas Dinger, Gang Xu, Michelle Andersen, and Kazutoshi Tominaga. The electric car tipping point. `https://www.bcg.com/publications/2018/electric-car-tipping-point.aspx`, January 11, 2018. Cited on page 5.

[4] Driving to an electric future? `https://www.eea.europa.eu/signals/signals-2017/articles/driving-to-an-electric-future`, August 2017. Cited on pages 5 and 6.

[5] Inc Tesla Motors. `http://teslamotors.com`. Cited on page 5.

[6] `https://www.slideshare.net/dasaramutt/electric-and-hybrid-vehicles`. Cited on pag 7.

[7] How electric cars work. `https://www.conserve-energy-future.com/howelectriccarswork.php`. Cited on page 6.

[8] Micah Toll. Regenerative braking: how it works and is it worth it in small evs? `https://electrek.co/2018/04/24/regenerative-braking-how-it-works/`, April 2018. Cited on paged 6.

[9] The Gale Encyclopedia of Science. Electric vehicles. `https://www.encyclopedia.com/science/encyclopedias-almanacs-transcripts-and-maps/electric-vehicles`, Retrieved December 28, 2018. Cited on page 7.

[10] Wikipedia. Hybrid electric vehicle. `https://en.wikipedia.org/wiki/Hybrid_electric_vehicle#cite_note-GreenMild-16`. Cited on page 8.

[11] Chukwulenwenwa John Orie and Queendalline Ijeoma Nwatu. Challenges of energy saving crisis as a panacea to hybrid electric vehicle (hev). *Mediterranean Journal of Social Sciences*, 2(6):12, 2011.

[12] Wikipedia. Hybrid vehicle drivetrain. `https://en.wikipedia.org/wiki/Hybrid_vehicle_drivetrain`. Cited on pages 9,10 and 11.

[13] Manuele Bertoluzzo and Giuseppe Buja. Road electric vehicles course. Cited on pages 9 and 13, 2015.

[14] T Gerrits. *Dynamic drive concept using speed dependent power electronics reconfiguration: applied to electrical machines for automotive traction.* Technische Universiteit Eindhoven, 2015. Cited on pages 22, 26, 29, 32, 33, 34, 35, 36 and 37.

[15] Motion and dynamic equations for vehicles. `https://nptel.ac.in/courses/108103009/module2/lec3/1.html`. Cited on page 12.

[16] RC Hibbeler. Engineering mechanics: Statics and dynamics 13/e, 2013. Cited on pag 12.

[17] Mehrdad Ehsani, Yimin Gao, Stefano Longo, and Kambiz Ebrahimi. *Modern electric, hybrid electric, and fuel cell vehicles.* CRC press, 2018. Cited on pages 9, 13 and 14.

[18] Andreas Dinger, Ripley Martin, Xavier Mosquet, Maximilian Rabl, Dimitrios Rizoulis, Massimo Russo, and Georg Sticher. Batteries for electric cars: Challenges, opportunities, and the outlook to 2020. *The Boston Consulting Group*, 7:2017, 2010. Cited on pages 15, 17, 17, and 18.

[19] Michael Tse-Gene Chang. *Performance targets for electric vehicle batteries.* PhD thesis, Massachusetts Institute of Technology, 2015. Cited on pages 17 and 18.

[20] Daniel Küpper, Kristian Kuhlmann, Sebastian Wolf, Cornelius Pieper, Gang Xu, and Justin Ahmad. The future of battery production for electric vehicles. urlhttps://www.bcg.com/publications/2018/future-battery-production-electric-vehicles.aspx, 11 Set 2018. Cited on page 18.

[21] Manuele Bertoluzzo, Giuseppe Buja, Giovanni Pede, and Angelo Puccetti. Hybrid battery-supercapacitor storage system for electric city cars. *EEVC Brussels, Belgium*, 2011. Cited on pag 21.

[22] Ivan Spina. Tecniche di controllo ottimizzate, monitoraggio parametrico e diagnostica per azionamenti pm brushless mono e pluri motore. 2011. Cited on page 29.

[23] Silverio Bolognani. Electric drive course. C, 2008.

[24] Giancarlo Rini. *Analysis and design of high performance multiphase electric drives for vehicle and aircraft applications.* PhD thesis, alma, 2015. Cited on page 26.

[25] E. Levi, R. Bojoi, F. Profumo, H.A. Toliyat, and S. Williamson. Multiphase induction motor drives – a technology status review. *IET Electric Power Applications*, 1(4):489, 2007.

[26] Gianmario Pellegrino and Simone Adamo. Progettazione di motori elettrici multifase con software open source.

[27] R. Bojoi, S. Rubino, A. Tenconi, and S. Vaschetto. Multiphase electrical machines and drives: A viable solution for energy generation and transportation electrification. In *2016 International Conference and Exposition on Electrical and Power Engineering (EPE)*, pages 632–639, Oct 2016.

[28] Henk Huisman, Jorge Duarte, Elena Lomonova, and Bram Daniels. Multi-phase motor control algorithm. *ModulED*, 01-11-2018. Cited on pages 26, 37 and 38.

[29] Ching-Tsai Pan and Jenn-Horng Liaw. A robust field-weakening control strategy for surface-mounted permanent-magnet motor drives. *IEEE Transactions on Energy Conversion*, 20(4):701–709, 2005.

[30] Thomas Gerrits, Cornelis GE Wijnands, Johannes JH Paulides, and Jorge L Duarte. Fault-tolerant operation of a fully electric gearbox equivalent. *IEEE Transactions on Industry Applications*, 48(6):1855–1865, 2012.

[31] Ramu Krishnan. *Switched reluctance motor drives: modeling, simulation, analysis, design, and applications*. CRC press, 2001. CIted on page 33.

[32] Phillip W Rowland. Low impact motor control with star-delta starting. In *1998 IEEE Annual Textile, Fiber and Film Industry Technical Conference (Cat. No. 98CH36246)*, pages 10–1. IEEE, 1998. Cited on page 35.

[33] J. W. Kolar. Envision on future power electronics. In *Joint Annual Meeting of Italian Researchers of the Groups of Electrical Systems, Converters, Drives and Machines*, July 4-5, 2013. Cited on page 36.

[34] Rainer Marquardt. Modular multilevel converter: An universal concept for hvdc-networks and extended dc-bus-applications. In *The 2010 International Power Electronics Conference-ECCE ASIA-*, pages 502–507. IEEE, 2010. Cited on page 37.

[35] Francois Forest, Eric Laboure, Thierry A Meynard, and Jean-Jacques Huselstein. Multicell interleaved flyback using intercell transformers. *IEEE Transactions on Power Electronics*, 22(5):1662–1671, 2007. Cited on page 37.

[36] `http://www.delta-elektronika.nl`. Cited on page 37.

[37] The Free Encyclopedia Wikipedia. Accessed march 24, 2019. `https://en.wikipedia.org/wiki/Space_vector_modulation`. Cited on pages 44 and 45.

[38] MLA Caris, H Huisman, and JL Duarte. Implementation of various balancing control methods for flying-capacitor power amplifiers. In *2015 IEEE International Symposium on Predictive Control of Electrical Drives and Power Electronics (PRECEDE)*, pages 115–120. IEEE, 2015. Cited on pages 46 and 47.

[39] Henk Huisman, Maurice Roes, and Elena Lomonova. Continuous control set space vector modulation for the 3× 3 direct matrix converter. In *2016 18th European Conference on Power Electronics and Applications (EPE'16 ECCE Europe)*, pages 1–10. IEEE, 2016.

[40] T Gerrits, JL Duarte, CGE Wijnands, EA Lomonova, JJH Paulides, and L Encica. Twelve-phase open-winding spmsm development for speed dependent

reconfigurable traction drive. In *2015 Tenth International Conference on Ecological Vehicles and Renewable Energies (EVER)*, pages 1–7. IEEE, 2015. Cited on page 39.

[41] The Free Encyclopedia Wikipedia. Accessed march 22, 2019. `https://en.wikipedia.org/wiki/PLECS`. Cited on page 41.

[42] Thom T.W.M.C. Overhof. Design, analysis and verification of on-the-fly winding reconfiguration for a pm motor drive. Master's thesis, 2019. Cited on pag 43.

[43] Jose Rodriguez and Patricio Cortes. *Predictive control of Power Converters and Electrical Drives*. 2012.